

AM
SK1

NASA Contractor Report 3403

Design and Fabrication of a Stringer Stiffened Discrete- Tube Actively Cooled Panel for a Hypersonic Aircraft

Frank M. Anthony and Robert G. Helenbrook

DEPARTMENT OF DEFENSE
PLASTICS TECHNICAL EVALUATION CENTER
CONTRACT NAS1-12806 AFMRCOM, DOVER, N. J. 07801
FEBRUARY 1981

DISTRIBUTION STATEMENT A DTIC QUALITY INSPECTED
Approved for public release;
Distribution Unlimited

NASA

19960312 078

19950312

NASA Contractor Report 3403

**Design and Fabrication of a
Stringer Stiffened Discrete-
Tube Actively Cooled Panel
for a Hypersonic Aircraft**

Frank M. Anthony and Robert G. Helenbrook

Bell Aerospace Textron

Buffalo, New York

Prepared for
Langley Research Center
under Contract NAS1-12806



National Aeronautics
and Space Administration

**Scientific and Technical
Information Branch**

1981

CONTENTS

Section	Page
TABLE OF CONTENTS	iii
LIST OF ILLUSTRATIONS	v
LIST OF TABLES	vi
LIST OF SYMBOLS	vii
SUMMARY	1
INTRODUCTION	2
DESIGN REQUIREMENTS	3
General	3
Specific Requirements	4
DESIGN STUDIES	4
Thermal Structural Optimization	5
Parametric Thermal Analyses	7
Parametric Structural Analyses	9
Mass Summary	12
EXPERIMENTAL STUDIES	13
Test Specimens	13
Results	16
FINAL DESIGN	16
Description	16
Performance Characteristics	18
Mass	21
TEST PANEL	22
Design	22
Fabrication	25
Future Improvements	27
Inspection	28
Mass	30
Load Adapters	31
CONCLUDING REMARKS	32

CONTENTS

Section		Page
APPENDIX A	MATERIALS SELECTION AND PROPERTIES	34
APPENDIX B	THERMAL ANALYSIS METHODS	37
APPENDIX C	STRUCTURAL ANALYSIS METHODS	44
APPENDIX D	THERMAL STRUCTURAL ANALYSES RESULTS	47
APPENDIX E	EXPERIMENTAL RESULTS	58
APPENDIX F	FABRICATION OF TEST HARDWARE	66
APPENDIX G	INSPECTION OF TEST HARDWARE	70
APPENDIX H	CRACK ARRESTOR TEST DATA	74
REFERENCES	78

LIST OF ILLUSTRATIONS

		Page
Figure		Page
1	Actively Cooled Structural Panel	2
2	Many Parameters Influence Panel Optimization	5
3	Repetition of Design Process Relates Skin Temperature and Panel Mass	6
4	Two Coolant Circuits were Compared	7
5	Counterflow of Coolant Minimizes Axial Temperature Differences	8
6	Maximum Panel Temperature Increases with Passage Spacing	10
7	Optimum Passage Width Increases with Passage Spacing	10
8	Coolant Temperature Has a Greater Influence on Pressure Drop than Passage Spacing	10
9	Mass of Coolant Inventory Plus APS Power Insensitive to Passage Spacing	10
10	Temperature and Stress Trends	11
11	Panel Stability Characteristics	12
12	Minimum Weight is Influenced by Practical Considerations	12
13	Unstiffened Fatigue Specimens	14
14	Stiffened Fatigue Specimens	15
15	Details of Panel Design	17
16	Temperature Distribution at Mid-Length	20
17	Stress Distribution at Mid-Length	20
18	Test Panel Assembly	23
19	Test Panel Details	24
20	Tubing Installation Details	25
21	Application of Silver Filled Epoxy	26
22	Rework of Plugged Interconnect Holes	27
23	Infrared Scan Results After Rework	29
24	Load Adapter	31
25	Tensile Lap Shear Strength of Various Adhesives	36
26	Peel Strength of Various Adhesives	36
27	Panel and Discrete Passage Thermal Models	37
28	Manifold/Splice Thermal Model	42
29	Axial Temperature Distribution, Flow in Half the Coolant Passages	48
30	Temperature Distribution at Inlet and Outlet, Flow in Half the Coolant Passages	49
31	Effect of Bondline Conductivity on Maximum Skin Temperature	50
32	Manifold Finite Element Idealization	53
33	Fatigue and Pressure Test Specimens Were Cut from a Cooled Skin Panel	58
34	Manifold End Plug Test Specimens 2024-T3 Aluminum Alloy	60
35	Coolant Passage Tubing End Plug (Test Specimens Do Not Have Holes to Match Manifolding)	61
36	Joint Fatigue Test Specimens	62
37	Coolant Tubing Anomalies	72
38	Crack Propagation Specimen, Center Notch	75
39	Crack Growth Behavior of Flat 2024-T3 Sheet 92.3 ± 55.8 kPa ($13,400 \pm 8100$ psi)	76
40	Crack Growth Behavior of Cooled Panel Specimens, Third Set/Second Series 92.3 ± 55.8 kPa ($13,400 \pm 8100$ psi) Neglecting Load Inconsistencies	77

LIST OF TABLES

Number		Page
I	Design Requirements	4
II	Panel Fatigue Characteristics	9
III	Experimental Studies	14
IV	Experimental Results	16
V	Manifold and Outer Splice Temperature	19
VI	Mass Summary of 0.61 x 6.1m Cooled Panel	21
VII	Mass Summary of 0.61 x 1.22m Test Panel	30
VIII	Adjustable Fatigue Allowables for 20×10^3 Cycles	34
IX	Normal Operating Temperature Stresses	54
X	Hot End-Emergency Condition Temperature Stresses	56
XI	Cold End-Emergency Condition Temperature Stresses	57
XII	Description of Developmental Test Specimens	59
XIII	Summary of Development Test Results	63
XIV	Tension-Tension Fatigue Tests of Riveted Specimens Load Range All Specimens 45 to 4464N, Mean Load 2232N Cyclic Rate 2 - 4 Cycles per Pound Second	65

SYMBOLS AND PARAMETERS

Customary units were used for the principal measurements and calculations. Results were converted to the International System of Units (SI) for this final report.

APS	Auxiliary power system
Btu	British thermal units
b	Height of coolant passage, mm (in.)
C_p	Material specific heat, J/kg K (Btu/lbm °F)
d	Width of coolant passage, mm (in.)
E	Young's modulus of elasticity, Pa (psi)
F	Pumping power conversion factor, g/kWs (lbm fuel/Hp-hr)
F_{cc}	Crippling stress, Pa (psi)
F_{cy}	Compression yield stress, Pa (psi)
F_{tu}	Tensile ultimate stress, Pa (psi)
F_{ty}	Tensile yield stress, Pa (psi)
F_w	Face wrinkling stress, Pa (psi)
FWD	Forward
f	Fanning friction factor
H_b	Beaded skin height, cm (in.)
H_D	Hydraulic diameter, cm (in.)
HP	Horsepower
h	Heat transfer coefficient, w/m ² K (Btu/ft ² hr °F)
Hr	Hour
I	Moment of Inertia, m ⁴ (inch ⁴)
in.	Inch
K	Panel buckling coefficient
K_T	Loss coefficient, or stress concentration factor, dimensionless
k	Thermal conductivity, W/m·K (Btu·in./hr·ft ² °F)
ksi	Thousand pound force per square inch
l	Length, m (in.)
lbf	Pounds force
lbm	Pounds mass
M	Mach
\dot{m}	Coolant mass flow rate, kg/hr (lbm/hr)
n	Number of coolant passages
N/A	Not available
N	Compression load per unit length, N/m (lb/in.); or number of cycles or Newton
N_x	Axial load per unit length, N/m (lbf/in.)

SYMBOLS AND PARAMETERS (CONT)

N_{xy}	Shear load per unit length, N/m (lbf/in.)
N_y	Axial load per unit length, N/m (lbf/in.)
O.D.	Outside diameter, cm (in.)
psi	Pounds force per square inch
psf	Pounds force per square foot
P	Pressure, Pa (psi)
Pr	Prandtl number
q	Dynamic pressure, total heat load
\dot{q}	Heat flux, kW/m ² (Btu/ft ² sec)
R	Stress ratio - minimum stress divided by maximum stress ; or radius, cm (in.)
RT	Room temperature, K (°F)
Re	Reynolds number
S	Coolant passage spacing, mm (in.)
T	Temperature, K (°F)
T_{in}	Coolant temperature at inlet, K (°F)
T_{out}	Coolant temperature at outlet, K (°F)
t	Thickness, cm (in.)
V	Velocity of fluid, m/s (ft/s)
W	Mass, g (lbm)
α	Coefficient of thermal expansion
Δ	Delta; or difference
ΔT_f	Temperature difference across coolant film, K (°F)
ΔT_s	Temperature difference in outer skin from center of coolant passage to centerline between two passages, K (°F)
ϵ	Surface emissivity
μ	Poisson's ratio ; or fluid viscosity, kg/ms (lbm/ft s)
ρ	Density, kg/m ³ (lbm/ft ³)
σ	Stress, kN/m ² (lbf/in ²)
σ_i	Stress/induced by external loading, kN/m ² (lbf/in ²)
σ_{th}	Stress induced by temperature difference, kN/m ² (lbf/in ²)
θ	Time, hour

SUBSCRIPTS

c	Coolant
f	Film
s	Skin
fw	Wall

SI UNITS

g	Gram (mass)
K	Kelvin (temperature)
m	Meter (length)
N	Newton (force)
Pa	Pascal (pressure and stress)
W	Watt (power)
s	Second (time)

SI PREFIXES

m	Milli (10^{-3})
c	Centi (10^{-2})
k	Kilo (10^3)
M	Mega (10^6)

SUMMARY

This report presents the results of a program which optimized the design of a full-scale $0.61 \times 6.1 \text{ m}$ ($2 \times 20 \text{ ft}$) actively cooled panel for minimum panel mass. Design conditions and requirements were representative of those for a hypersonic transport. Details of the panel design were finalized on the basis of results from static and fatigue test specimens which incorporated major design features. Six large fatigue specimens, $0.1 \times 0.2 \text{ m}$ ($4 \times 8 \text{ in.}$) were tested by the Langley Research Center of NASA. A $0.61 \times 1.22 \text{ m}$ ($2 \times 4 \text{ ft}$) test panel was fabricated and delivered to the Langley Research Center for assessment of the thermal and structural features of the optimized panel design. The panel concept incorporated an unshielded skin actively cooled by a network of discrete, redundant, counterflow passages interconnected with appropriate manifolding, and assembled by adhesive bonding. The cooled skin was stiffened with a mechanically fastened conventional substructure of stringers and frames. The cooling passages were parallel to the stringers. A 40 water/60 glycol solution was the coolant.

An iterative optimization procedure was used to define the minimum mass configuration. The optimization procedure was applied to only the panel and its cooling system. The distribution system (pumps, lines, etc.) were not included. Structural considerations dominated, an in-plane loading of $\pm 210 \text{ kN/m}$ ($\pm 1200 \text{ lb/in.}$), a pressure loading of $\pm 6.9 \text{ kPa}$ ($\pm 1.0 \text{ psi}$) and a design life of 5000 cycles. The minimum equivalent panel thickness was defined by structural/life requirements. Skin and stiffening elements were proportioned to maximize buckling resistance. Coolant passage characteristics were defined to limit panel operating temperature to 390 K (240°F) which provided minimum equivalent thickness within practical design constraints. A unit mass of 10.27 kg/m^2 (2.10 psf) was calculated for the full-scale panel which included the skin, stringers, coolant inventory, tubing, adhesives and crack stoppers but not the manifolding, clips or fasteners.

Adhesive bonding permitted the use of an efficient structural alloy, 2024-T3, for the skin and substructure while a corrosion resistant alloy, 3003-H14, was used for the coolant passages. The high design heat flux 136 kW/m^2 ($12 \text{ Btu/ft}^2 \text{ sec}$) required the use of thin bondlines of high thermal conductance. Fabrication procedures were developed to permit the use of thin bondlines at critical locations despite the tolerances associated with machining and with sheet metal forming. High thermal conductance and structural strength were achieved by using alternate stripes of silver-filled epoxy paste adhesive and epoxy film adhesive.

Low pressure leak testing, radiography, holography and infrared scanning were applied at various stages of fabrication to assess integrity and uniformity. By nondestructively inspecting selected specimens which were subsequently tested to destruction, it was possible to refine inspection standards as applied to this cooled panel design.

INTRODUCTION

Cooling requirements for advanced hydrogen-fueled air-breathing engines may be less than the heat sink capability of the engine fuel flow, Reference 1. The potential availability of fuel cooling in excess of that required to cool advanced hydrogen fueled engines makes cooling of the airframe structure an intriguing design option. To provide valid comparative data, information is needed for the actively cooled surface panel subjected to high heating intensity. Even if some heat shielding is required because the available heat sink is insufficient to cool unshielded structure, References 2 through 6 indicate a significant reduction in structural mass and a corresponding increase in payload results from the use of actively cooled structure for hypersonic transports. References 1 and 7 indicate that such heat shielded arrangements can be lighter than the base actively cooled surface approach. A number of prior studies, References 8, 9 and 10, discuss a variety of external thermal protection concepts which incorporate active cooling. In general, heat shields and insulation tend to increase initial and operating costs. Trades must be made between the mass reduction and the increased cost associated with the use of heat shielding to attenuate the thermal load to a cooled structure.

An actively cooled surface panel must satisfy thermal and structural requirements imposed by the severe operating environments associated with a hypersonic transport during its frequent long duration flights. Figure 1, defines the main elements of the present cooled panel assembly, the major functions of each element, and the primary construction materials. The unshielded actively cooled skin contains two counterflow circuits for the water/glycol coolant to achieve a redundant design. When this project was initiated there was relatively little experimental technology base for bare, actively cooled structures subjected to high heating intensities. An important aspect of the present investigation was to identify the interaction among the thermal and structural functions so that the relative importance of the design parameters could be identified.

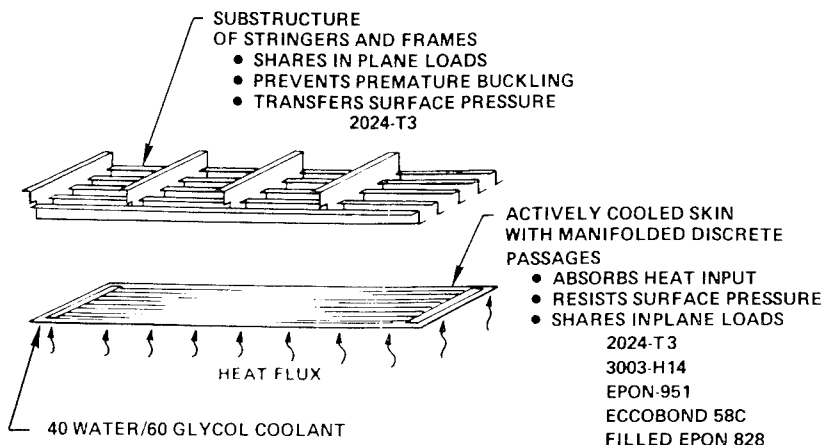


Figure 1. Actively Cooled Structural Panel

The program plan emphasized optimization of the design of a $0.61 \times 6.1 \text{ m}$ ($2 \times 20 \text{ ft}$) full-scale panel. The use of conventional structural materials, specifically aluminum alloys, imposed a structural temperature limit of about 442 K (300°F). As part of the optimization process, major features of the design were checked by fatigue tests of specimens at NASA/Langley. Using the results

of analytical trade studies and fatigue tests, the panel design was finalized. A test panel was fabricated and delivered to NASA for experimental evaluation of the fully-integrated thermal structural features of the actively cooled structure.

The main body of the report summarizes the studies and tests performed to identify the optimum configurational features of the actively cooled structural panel concept. The thermal structural optimization process is described and results of parametric studies are presented. The results of fatigue tests of specimens which incorporated such details, and of other types of tests found to be desirable, permitted finalization of the design for the full-scale panel and the definition of fabrication and inspection procedures to be used for the test panel. The test panel design, fabrication, and inspection are described. Details of the various efforts are presented in appendices.

The purpose of this program was to optimize the design of an actively cooled structural panel, to experimentally verify major design features by using small test specimens, and to provide a test panel for experimental verification of the thermal structural integrity of the design at the Langley Research Center. The cooled panel was fabricated from conventional aluminum alloys. The program was conducted with the requirements and instructions of NASA RFP 1-15-3785.

The use of names of commercial products or of manufacturers in this report does not constitute official endorsement of such products or manufacturers, either expressed or implied, by the National Aeronautics and Space Administration.

Major contributors at Bell, in addition to the authors, included J. D. Witsil, Jr. - thermal analysis; W. N. Meholick - structural analysis; A. L. Mistretta - coordination of manufacturing, inspection, and in-house testing activities; A. L. Peterson - manufacturing; and L. Vecchies - quality assurance.

DESIGN REQUIREMENTS

The problems of designing and verifying the performance of an actively cooled structural panel are identified here in terms of general and specific requirements. The manner in which these requirements influence the design process is described in subsequent sections of the report.

General

The actively cooled structural panel must be designed for convective cooling by a liquid which is pumped through a closed loop system such that heat is rejected to the hydrogen fuel via a heat exchanger. Long life without catastrophic failure is a design objective. The selected coolant must be compatible with the material of construction; and failure due to corrosion, cracks and fatigue must be avoided. Proper manifolding of coolant flow through the panel is necessary. The consequences of cooling system malfunctions should be assessed and the relative merits of redundant coolant passages considered. In addition to achieving a long life the cooled panel must be structurally sound so that no failures are induced by buckling or high thermal stresses even when loads are applied eccentrically. The interactions of in-plane loads and lateral pressures, and the presence of manufacturing imperfections must be considered when assessing buckling resistance.

Because of the large number of considerations involved in the design of an actively cooled structural panel, and the lack of a significant data base for this structural concept, the program proceeded from design to verification of design features using fatigue testing, to finalization of the design, and to fabrication of a test panel. Experimental evaluation of this test panel by NASA/Langley Research Center will be reported separately.

Specific Requirements

The actively cooled structural panel was designed for minimum mass while meeting design requirements considered representative of a hypersonic transport. Local environmental conditions, design life, size, materials, factors of safety, and material strength were considered. The specific design requirements are listed in Table I; the primary design considerations were specified by NASA; supplementary requirements were defined by Bell.

TABLE I
DESIGN REQUIREMENTS

<u>NASA</u>	
Heat Flux	136 kW/m ² (12 Btu/ft ² sec)
In Plane Loading	± 210 kN/m (± 1200 lb/in.)
Pressure Loading	± 6.89 kPa (± 1.0 psi)
Design Life	5000 Cycles
Aluminum Alloy Materials	Compatible with Coolant
Length and Width	6.1 x 0.61 m (20 x 2 ft)
Frame Spacing	0.61 m (2 ft)
Outlet Pressure	345 kPa (50 psi)
Edge Joints	Of Realistic Design
<u>BELL</u>	
Life Scatter Factor	4.0
Factors of Safety	Loads 1.0 Limit/1.5 Ultimate
	Temperature 1.0 Limit/1.0 Ultimate
	Pressure Only 1.5 Proof/2.0 Ultimate
Strength Allowables	Based on 10,000 Hours of Exposure
Initial Imperfection	0.001 x Frame Spacing
Redundant Coolant Circuits	

DESIGN STUDIES

The incorporation of active cooling into a load carrying structural panel requires the integration of thermal design features along with those normally associated with primary load carrying airframe structure. The many design variables are investigated through an iterative optimization procedure. Parametric thermal and structural analyses provide the information needed to define optimum proportions for meeting design requirements. The features of a particular panel concept influence the specifics of the optimization process. This cooled panel concept employs stringer and frame

stiffening of an actively cooled airframe skin. The cooled skin incorporates manifolds and discrete passages for distribution of the coolant. Structural loads are supported by the combination of the skin and the substructure, but cooling is incorporated only in the skin.

The design problem is one of minimizing the mass of the actively cooled structural panel. This requires definition of the geometric proportions of the panel and its operating characteristics in such a way as to satisfy loads, life, and temperature criteria as influenced by the construction material and coolant choices.

Thermal Structural Optimization

Major elements of the optimization process are shown in Figure 2. The operating requirements, usually derived from environmental considerations were defined in the DESIGN REQUIREMENTS section, and serve as the forcing functions for design efforts. The circular interlinking of thermal and structural parameters depicts the iterative nature of the design process which develops the optimized design parameters located in the overlap of the thermal and structural domains. For the more general case, thermal and structural limits may impose restrictions on the environmental aspects, hence, their interlinking. For this program, cooling system mass and many of the environmental factors were not considered because they are related to a specific vehicle configuration whereas the panel was not for a particular vehicle.

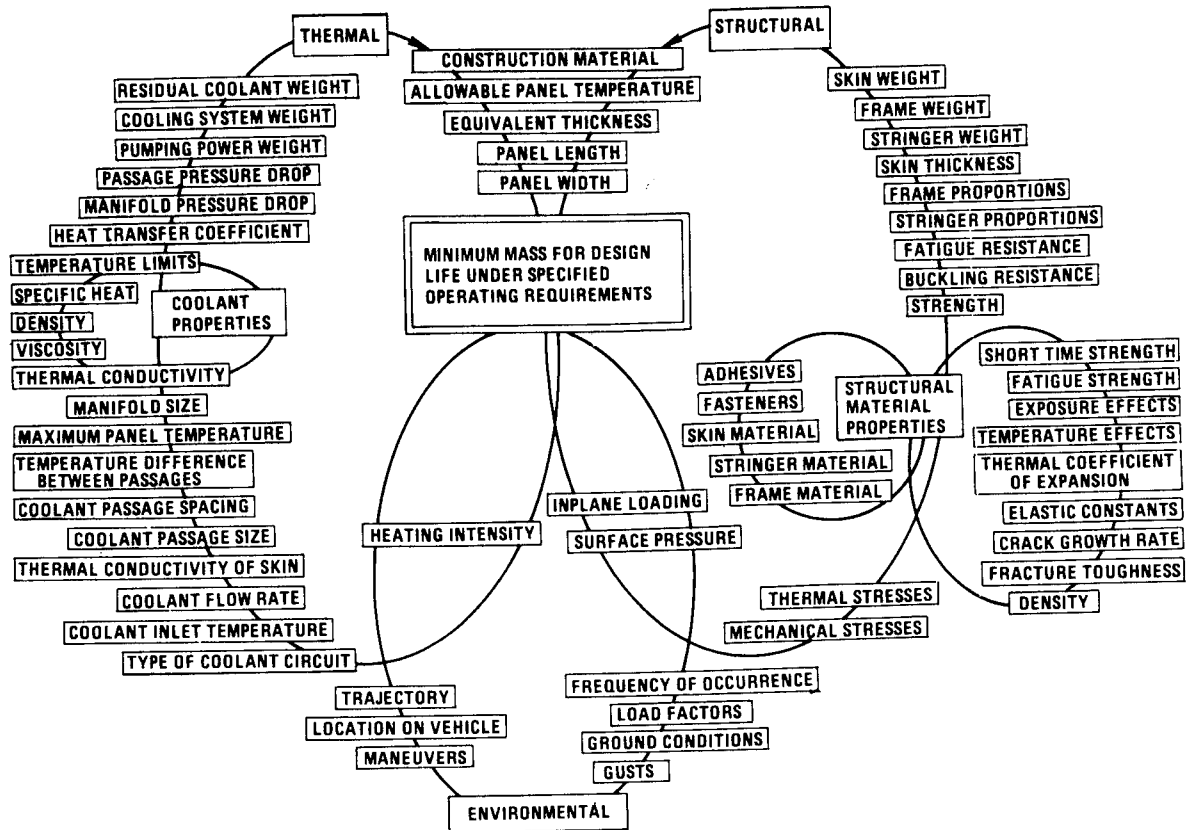


Figure 2. Many Parameters Influence Panel Optimization

Because of the large number of parameters, a starting point must be assumed. Reference 3 indicated that minimum mass is achieved when skin thickness is minimized and when a large temperature rise is permitted for the coolant. This suggests an initial design point with a high maximum temperature relative to mechanical property characteristics of the construction material and a thickness based on the design life requirement under the specified loading and the assumed maximum temperature. Analyses are conducted to define other parameters which establish a particular design and its mass. A different maximum temperature is assumed and the procedure presented in Figure 3 is repeated. After several iterations a relationship is developed between panel mass and maximum operating temperature. From this it is possible to select a design of minimum mass.

The rectangular boxes of Figure 3 define the operations in the design process; the oval boxes identify inputs. Beginning at the left with the selection of a maximum skin temperature, the design effort proceeds along separate thermal and structural paths after the material is proportioned between the skin and the stiffening elements. The thermal and structural efforts converge to allow computation of the mass of the cooled panel.

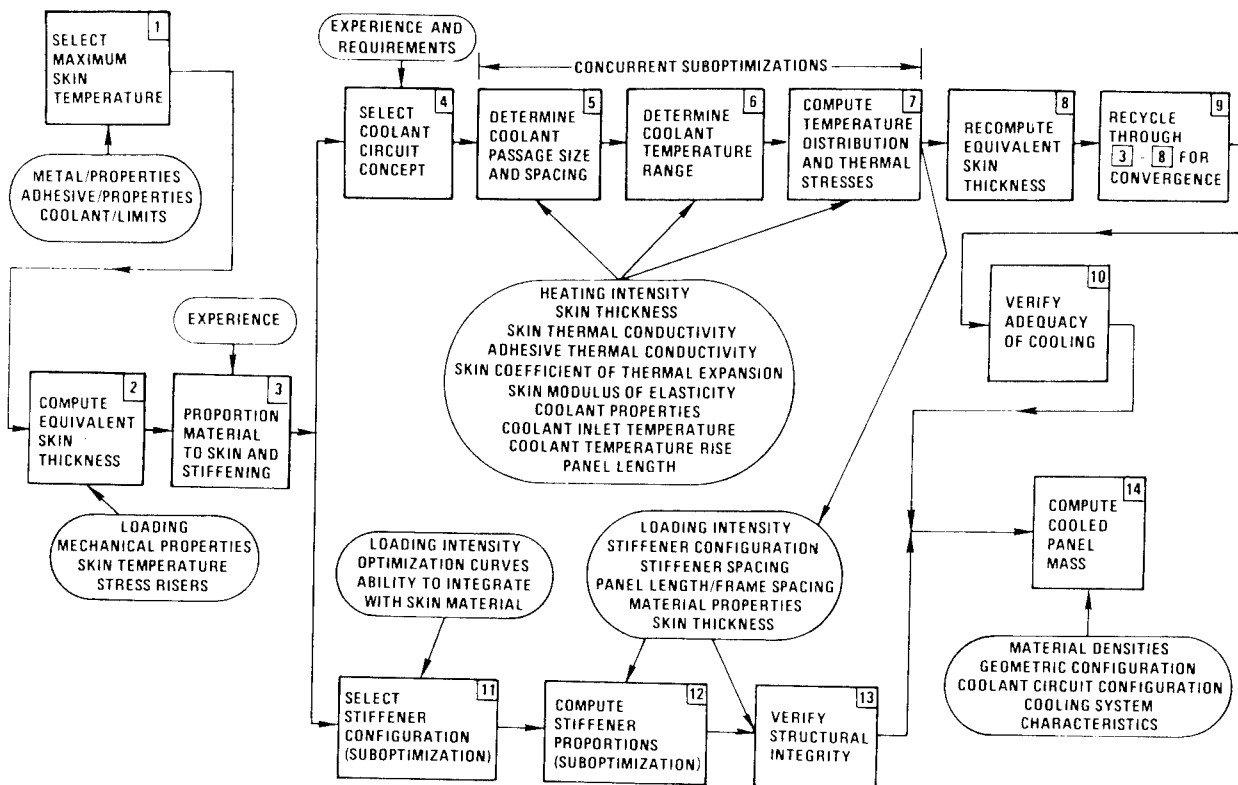


Figure 3. Repetition of Design Process Relates Skin Temperature and Panel Mass

As the design procedure is implemented, several suboptimizations are performed. Along the line of thermal analysis effort the suboptimizations relate the coolant passage cross-sectional characteristics, passage spacing, and coolant temperature range. Passage cross section and panel length influence the mass of coolant within the panel and the pressure drop through the panel which is related to

the mass of the Auxiliary Power System (APS) penalty, the mass of fuel required to circulate the coolant as adjusted for turbine and pump efficiencies. Suboptimization of the coolant passage spacing is related to the number of coolant passages, the mass flow through each passage and the passage cross-sectional area. Closer spacings reduce thermal stresses, and are beneficial from a structural point of view. The structural suboptimizations select the proper type of stiffener and the stiffener proportions. Structural efficiency charts for compressively loaded panels, such as Reference 11, permit rapid choice of the stiffening concept by relating equivalent thickness and loading intensity for a variety of stiffener types. Unless the design for minimum mass leads to unrealistic proportions, such a chart is most useful and is easily applied. Having selected the most desirable stiffener arrangement, the proportions can be found by referring either to the design charts or available computer programs derived from established structural theory in Reference 14. Basically, the stiffeners are proportioned to provide maximum load carrying capability prior to buckling for a given panel mass.

Adequacy of cooling (temperature limit) and structural integrity are verified before the mass of a particular design is computed. The results of this process are presented later, in the Mass Summary portion of this section.

Parametric Thermal Analyses

The thermal analyses begin with Box 4 of Figure 3 and proceed through Box 10. Materials aspects are discussed in Appendix A and the analysis methods are presented in Appendix B. The actively cooled structural panel incorporates discrete coolant passages. Both single and redundant coolant circuits, incorporating semielliptical and quarter elliptical coolant passages as shown in Figure 4 were compared. Through the use of redundant cooling passages supplied by separate coolant distribution systems, loss of a vehicle would be avoided in the event of a serious malfunction of one system.

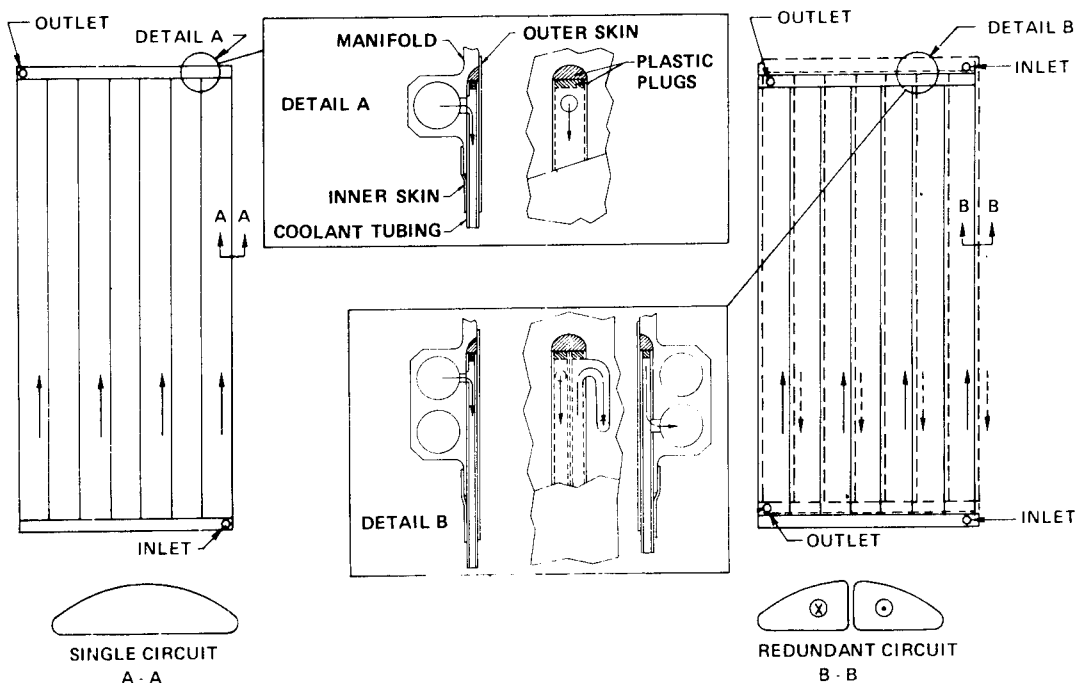


Figure 4. Two Coolant Circuits Were Compared

Although panel temperature rises when the coolant flowrate is halved, the structure retains limit load strength capability for at least one hour (sufficient time to permit a safe landing). Coolant flow in the redundant system can be parallel or counterflow as shown in Figure 4. The semi and quarter elliptical tube configurations are preferred to circular segments because of better flow conditions in the outer corners which lead to more uniform heat removal and a slightly lower pressure drop. Within the cooled panel only a small mass price is paid for redundancy, the mass of the short tube wall section and a slight increase in pressure drop. Reference 6 indicated that the mass of two independent coolant distribution systems, each of half capability, is only $1.23 \times$ the mass of one full-capacity system. Temperature distributions for the two coolant circuit concepts are shown in Figure 5; the right hand plot is the temperature distribution for the optimized panel of the selected design. For the same increase in coolant temperature down the length of the panel, the counterflow arrangement of redundancy provides more axial uniformity and was selected for the panel design. This eliminates complications caused by integrating panels that expand more in the transverse direction at one end than at the other.

Because the total coolant flow rate is the same for the single circuit and redundant counterflow designs, the coolant temperature rise is the same, 56K (100°F). For the single flow direction, the very low coolant inlet temperature results in a low heat transfer coefficient and a large temperature difference between the tube wall and the coolant bulk. Therefore, the maximum panel temperature occurs near the inlet rather than near the outlet as might be expected. When a counterflow arrangement is used the low heat transfer coefficient near the inlet of one coolant passage is offset by the much higher heat transfer coefficient near the outlet of the adjacent passage.

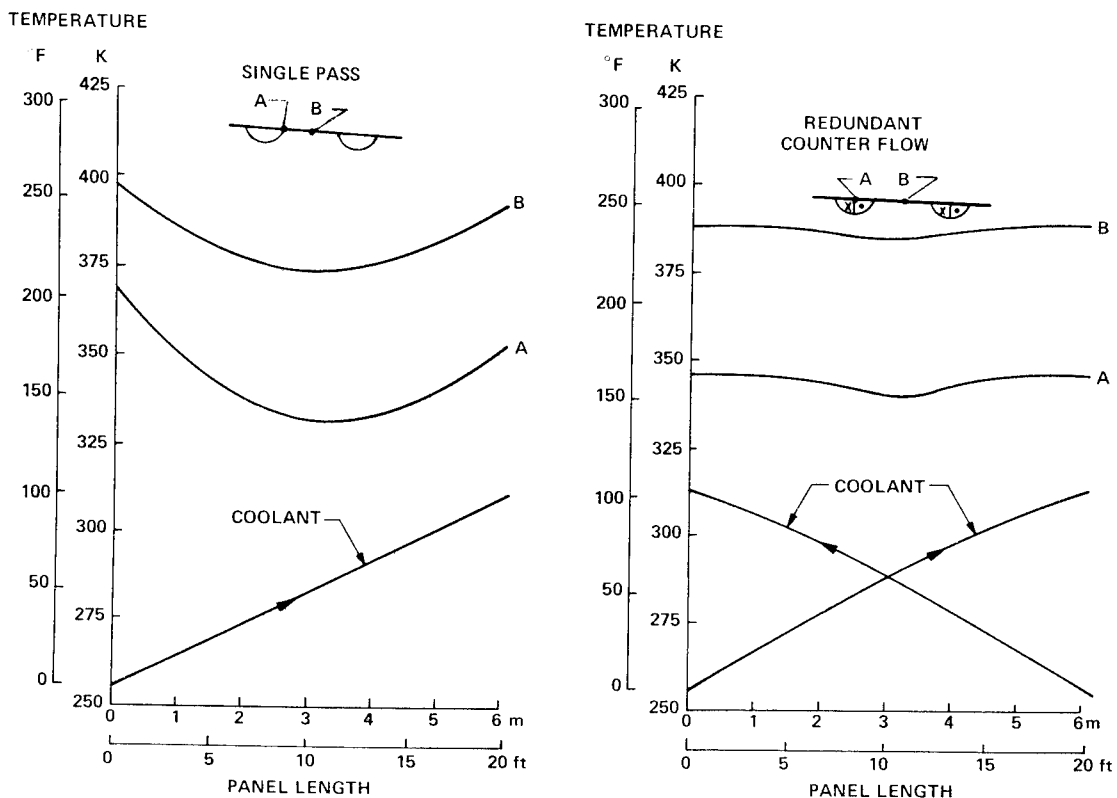


Figure 5. Counterflow of Coolant Minimizes Axial Temperature Differences

Concurrent suboptimizations are performed to relate coolant passage spacing, passage size, maximum panel temperature, inlet and outlet temperatures of the coolant, pressure drop, mass of the cooling elements, temperature distributions in the panel designs, and the resultant thermal stresses. Figures 6 through 10 illustrate the relationships obtained. As the passages are spaced further apart, the maximum panel temperature increases (Figure 6). The panel temperature increases as the temperature rise of the coolant is allowed to increase (equivalent to a decrease in coolant flow rate). For designs which minimize the mass of the cooling elements, passage spacing has a definite effect on passage size as illustrated in Figure 7. As the passage spacing is increased, the quantity of heat to be absorbed by a single cooling passage is greater. For a selected rise in coolant temperature down the length of the panel, it is necessary to increase the coolant flow per passage as the number of passages is reduced. Minimum combined mass of the coolant inventory and the auxiliary power system is obtained by increasing the flow area of each passage. The trend in the coolant passage size with increasing passage spacing is such that the pressure drop down the length of the panel decreases slightly as passage spacing is increased, Figure 8. The net result is to decrease the combined mass of the coolant inventory and APS as coolant passage spacing is increased, Figure 9.

In addition to the mass aspects derived from the parametric thermal analyses, the resultant temperature distributions give rise to thermal stresses. Figure 10 summarizes maximum and minimum panel temperatures as well as resulting tensile and compressive thermal stresses parallel to the coolant passages as functions of coolant passage spacing. The thermal stresses are combined with the load induced stresses as will be discussed in the next subsection.

Parametric Structural Analyses

The structural analyses identified in Figure 3 as part of the thermal structural optimization begin with the determination of an equivalent skin thickness for an assumed operating temperature. The equivalent skin thickness is determined by dividing the loading by the allowable stress. When a life objective is defined the allowable stress may include both steady and alternating components. As specified in the design requirements an in-plane loading of ± 210 kN/m (1200 lb/in.) must be sustained for 5000 simulated flight cycles. But actively cooled panels experience both thermal and mechanical loadings. Therefore, after the first thermal iteration the magnitude of thermally induced loads can be estimated. The stress experienced by an equivalent thickness of cooled panel is then defined as shown in Table II which also defines the manner in which the fatigue allowable is established. Design stress levels were 51.0 ± 133.4 MPa (7400 \pm 18,500 psi); see Appendix D for details.

TABLE II
PANEL FATIGUE CHARACTERISTICS

$\sigma = \frac{1}{2} \sigma_{th} \pm \left(\frac{1}{2} \sigma_{th} + \sigma_i \right)$
Fatigue Allowable Reduced by:
Factor for 10,000 Hours of Exposure
Temperature
Stress Concentration of 2.0 and 4.5
Design Life of 20,000 Cycles (5000 \times 4.0)
Equivalent Thickness Required = 2.75 mm (0.11 in.)

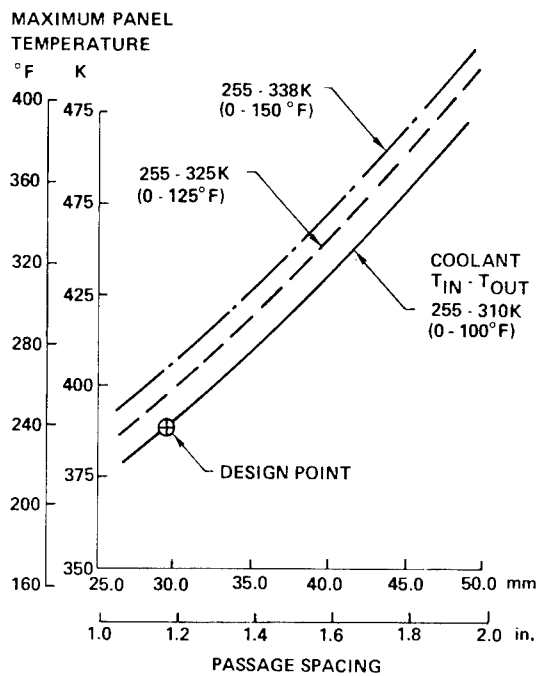


Figure 6. Maximum Panel Temperature Increases with Passage Spacing

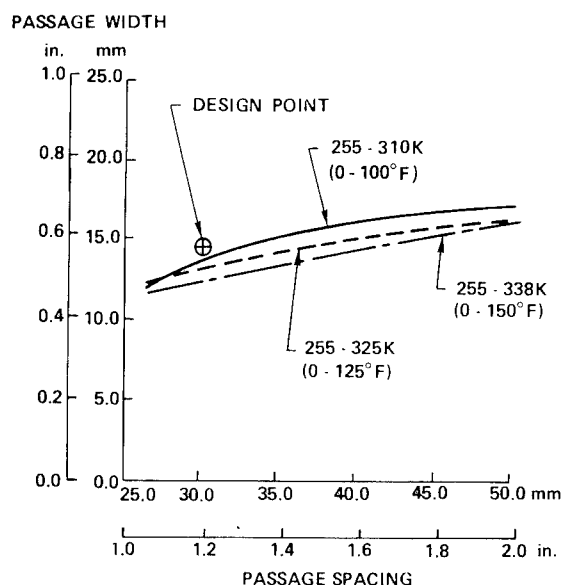


Figure 7. Optimum Passage Width Increases with Passage Spacing

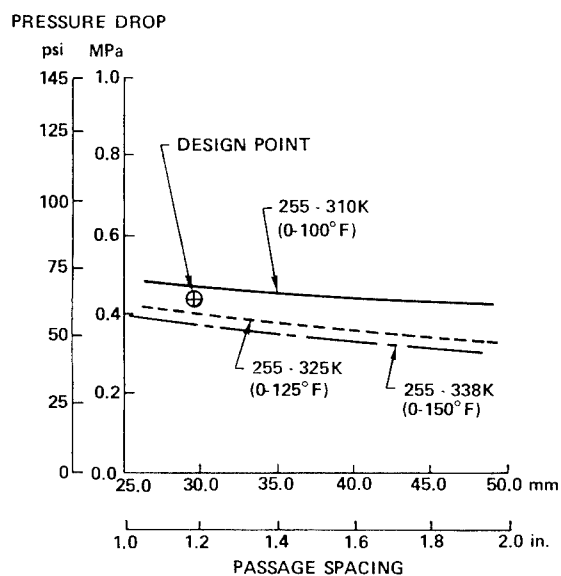
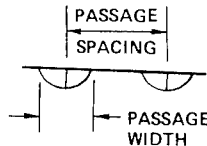


Figure 8. Coolant Temperature Has a Greater Influence on Pressure Drop than Passage Spacing

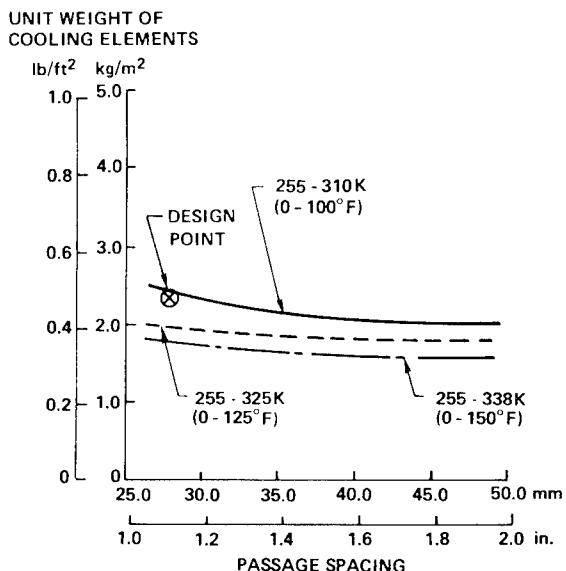


Figure 9. Mass of Coolant Inventory Plus APS Power Insensitive to Passage Spacing

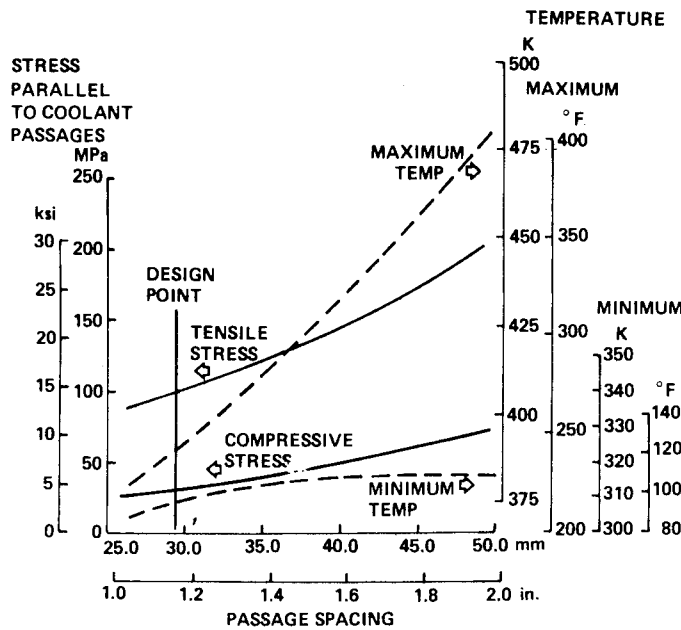


Figure 10. Temperature and Stress Trends

The rationale for combining the thermally induced load as steady and alternating components is based on the fact that, during each ground-air-ground cycle, thermal stresses reach a maximum and then decrease to zero. Such a variation in thermal stress can be represented by a steady component equal to one-half of the maximum value and an alternating component of equal magnitude. When the steady component is combined with the positive half-amplitude, the total thermal stress is equal to the maximum value and when it is combined with the negative half-amplitude the sum is zero.

Using the procedure described above and design allowable fatigue strengths based on Reference 15, as corrected for temperature in accordance with Reference 16, the equivalent thickness at the panel temperature corresponding to minimum total mass is 2.75 mm (0.11 in.). Structural Analysis Methods are discussed in Appendix C.

This equivalent thickness of 2.75 mm (0.11 in.) was proportioned using two computer codes based on Reference 14 to maximize the in-plane load that could be supported in combination with a normal surface pressure of ± 6.89 kPa (± 1.0 psi) and an initial out of plane imperfection of 0.001 times the panel length between frames, 0.6 m (24 in.), Reference 17. The Zee section stringer was selected because it is one of the most effective stiffening configurations, can be produced at low cost, and is easily integrated between discrete coolant passages of the panel design. The two computer codes were used to obtain predictions of the in-plane loading which will not initiate buckling and the in-plane loading which will cause buckling. The proportioning of the equivalent skin thickness was constrained by the use of standard sheet thicknesses. These allowable loadings are shown in Figure 11 as a function of equivalent skin thickness; the design point is identified. The past experience of Reference 8 indicates that buckling can induce changes in the cross-sectional shape of coolant passages. Therefore, up to limit load conditions the panel should not be permitted to buckle. Based on the design selected, an axial loading of approximately 470 kN/m (2700 lb/in.) can be carried without buckling, more than twice the specified alternating in-plane load.

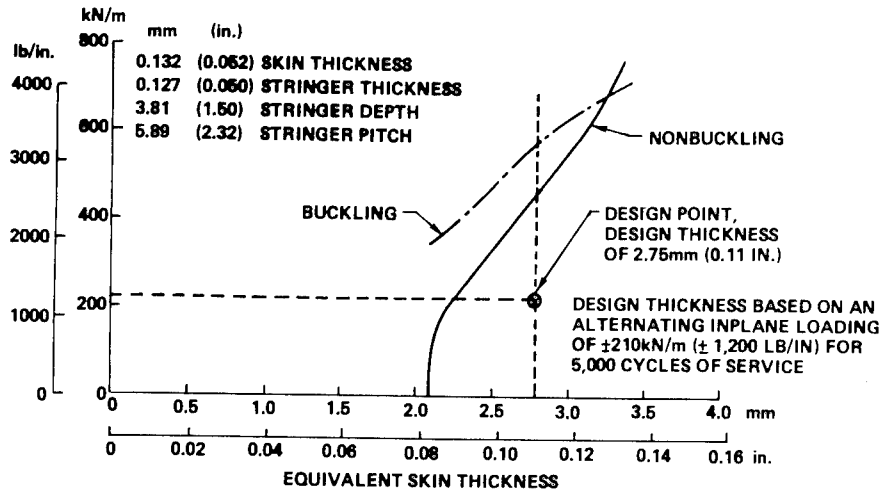


Figure 11. Panel Stability Characteristics

Mass Summary

After the mass of structural and cooling system elements are defined as functions of maximum panel operating temperature it is possible to select a design of minimum mass which meets the thermal and structural design requirements. Results of the parametric thermal and structural analyses are summarized in Figure 12. The mass of the structure is greater than the mass of all other elements combined; it increases as operating temperature increases and the design allowable strength decreases. The mass of the cooling system elements decreases slightly as panel temperature increases. The combined mass of the adhesive, coolant passage tubing, and crack arrestors shows a slight decrease with temperature increase. The net result is a decrease of panel mass as temperature decreases. However,

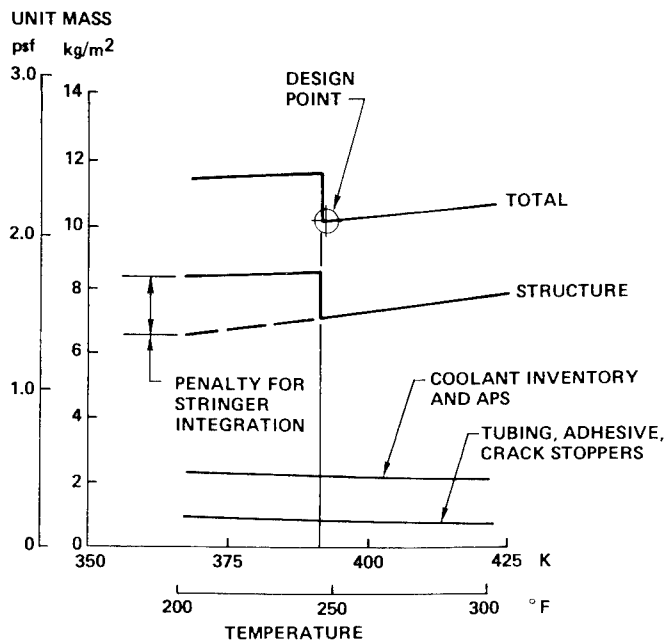


Figure 12. Minimum Weight is Influenced by Practical Considerations

because of the discrete coolant passages, a point is reached where it is no longer possible to incorporate stiffeners on the portion of the skin between coolant passages. Spacers are needed to avoid interference between the stiffener flange and the coolant passages. The spacers introduce a step in the mass trend. The design point selected for the panel, therefore, was where stiffener flanges could be incorporated between coolant passages; the unit mass of the panel design is 10.3 kg/m^2 (2.1 psf) and the maximum operating temperature under nominal design conditions is 390K (240°F). The manifolds, frames, clips and fasteners were not included in the optimization. Therefore, the mass of the final panel designs, 12.23 kg/m^2 (2.5 psf), was greater than the optimized value. The comparison in Reference 13 showed the stringer/frame stiffened, discrete tube actively cooled panel to be the lightest of three unshielded concepts considered.

EXPERIMENTAL STUDIES

When developing a new design concept, experimental verification of its main features is a desirable prelude to prototype fabrication. NASA requirements dictated fabrication of certain test specimens for evaluation of major characteristics at the Langley Research Center. The NASA test specimens, and others tested at Bell, were cut from a single $0.61 \times 1.22 \text{ m}$ (2 x 4 ft) panel which closely resembled the cooled skin of the delivered test panel. In addition to providing test material, this panel offered the opportunity of gaining experience with the fabrication techniques. Because other aspects of the cooled panel design could not be totally defined by parametric studies and analyses, additional tests were conducted at Bell. The Bell tests focused primarily on the choice of adhesives and in the verification of design changes and certain fabrication techniques. Details of the experimental evaluations are provided in Appendix E; a summary is provided here.

Test Specimens

The initial plan for validation of panel design details involved the testing of six fatigue specimens at the Langley Research Center. During the fabrication of these specimens, areas in need of process refinement were identified; the NASA tests identified some areas of deficiency. Therefore, the experimental studies were expanded to include five additional types of specimens, four of which involved aspects of adhesive utilization. Table III summarizes the types of experimental studies, the number of each type of specimen and the purpose of each test series.

The specimens for the Langley investigations were the largest and the most complex. Duplicates of three configurations were involved. The first $0.17 \times 0.27 \text{ m}$ (6.5 x 10.5 in.) configuration consisted of two sheets of aluminum bonded together with alternate stripes of Epon 951 and Ecco-bond 58C adhesives, upper photo of Figure 13. The second $0.13 \times 0.27 \text{ m}$ (5.13 x 10.5 in.) configuration, lower photo of Figure 13, was more complex; the transition from the manifold to the inboard portion of the cooled panel was incorporated along with the actual coolant passage installation. The third, $0.13 \times 0.38 \text{ m}$ (5.13 x 11.2 in.), configuration was most complex, Figure 14; it incorporated an actual manifold section, coolant passages, stiffeners that were notched to pass over the manifold and reinforced, and the panel edge attachment.

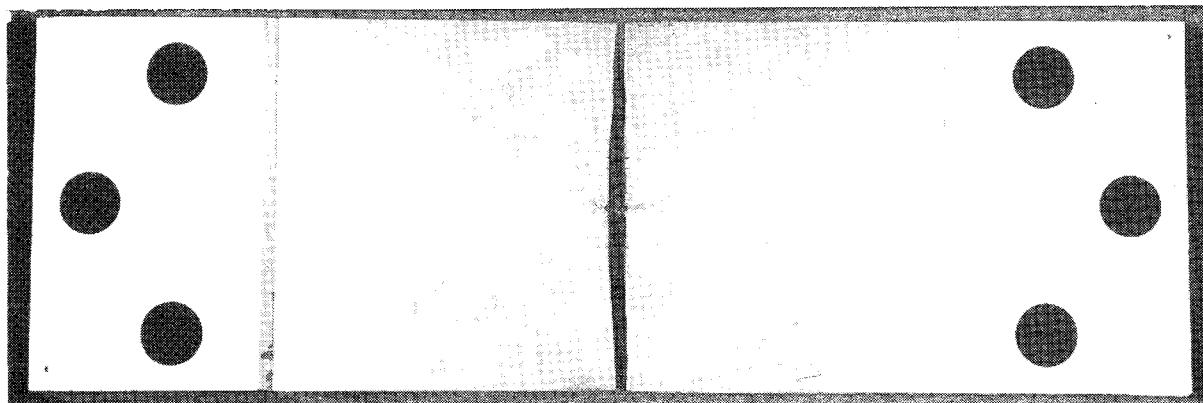
Except for the pressure panels which were of similar size and complexity, all of the specimens tested at Bell were less complex and of smaller size. In addition to serving their purpose in establishing failure pressure levels, the pressure panels provided an opportunity to assess nondestructive inspection records with post-test examination of failed assemblies.

TABLE III
EXPERIMENTAL STUDIES *

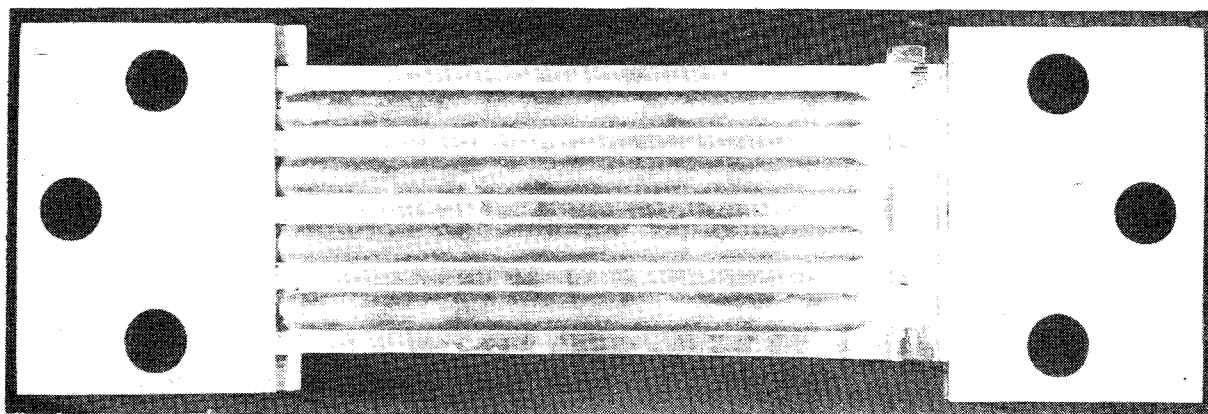
Specimen Type	Purpose
● NASA Fatigue (6)**	Validate Panel Details
● Manifold End Plug (13)	Select Adhesive
● Coolant Passage Plug (10)	Select Potting Compound
● Pressure Panel (4)	Validate Pressure Integrity
● Edge Attachment (15)	Validate Design Change
● Manifold Repair (1)	Validate Repair Technique

*See Appendix E for details

**Number of Specimens

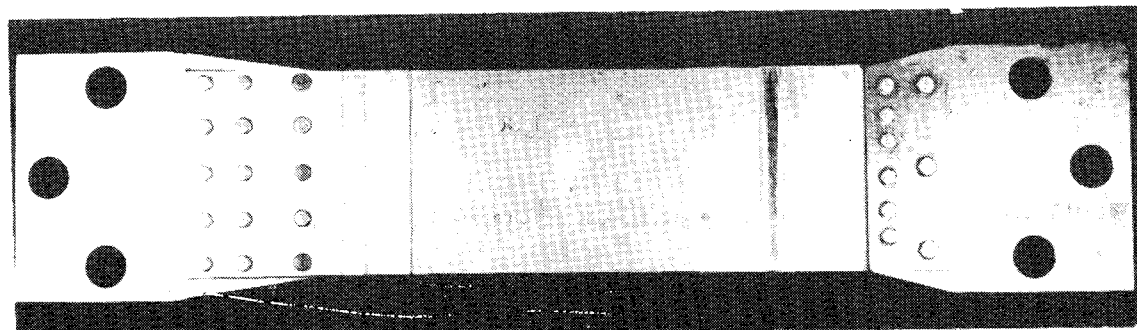


a. BONDED SKIN
0.27m (10.5 IN.) TEST ZONE

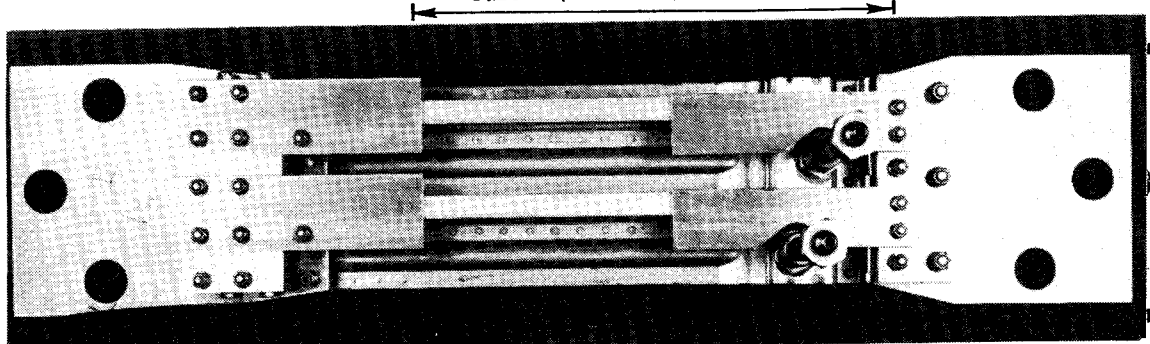


b. COOLANT PASSAGE/RAMP

Figure 13. Unstiffened Fatigue Specimens

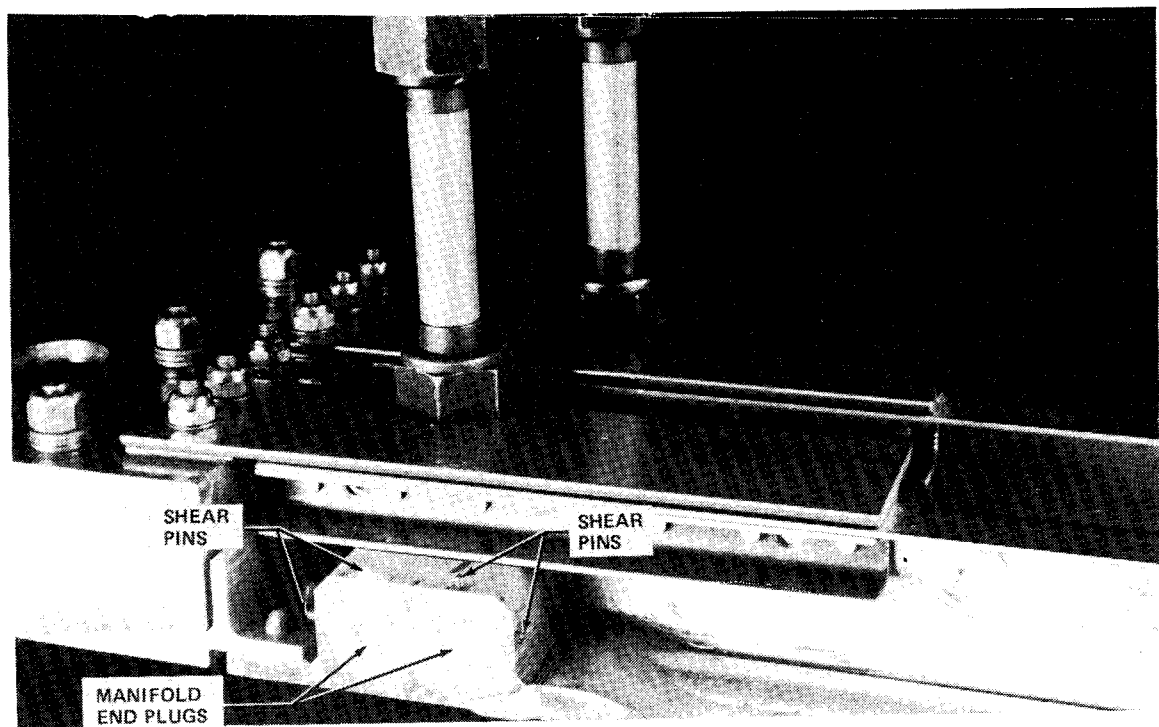


TOP VIEW



0.28m (11.2 IN.) TEST ZONE

BOTTOM VIEW



SPLICE/MANIFOLD END

Figure 14. Stiffened Cooled Skin Fatigue Specimen

Results

Details of the cooled panel design and the associated fabrication procedures were assessed by the various experimental evaluations. The effort required to validate manufacturing procedures was significantly greater than anticipated. As is often the case, the design concept was relatively straightforward but its successful implementation required great attention to details. The manufacturing details which required refinement were associated primarily with the use of adhesives. Problem areas included sealing the ends of the tubing, preventing leaks at manifold end plugs and precluding leaks at the interface of the tubing and manifold. While it was not necessary to develop new materials, it was necessary to compare alternate approaches before selections could be made for specific functions. The experimental results of Table IV verified that adhesive bonding could be used even when the most critical bond line thicknesses were small compared to manufacturing tolerances associated with machining and sheet metal forming. The techniques developed appear to be suitable for production application.

TABLE IV
EXPERIMENTAL RESULTS *

<ul style="list-style-type: none">● NASA Fatigue● Bonded Skin● Transition● Stiffened● Manifold End Plug● Coolant Passage Plug● Pressure Panel● Edge Attachment● Manifold Repair	<p>Similar to Single Thickness Adequate Fatigue Life, Leakage Inadequate Splice Design, Leakage Alumina Filled Epon 828 Selected Alumina Filled Epon 828 Selected Tighter Tolerances Needed on Tubing, Improved Manufacturing Techniques Developed Cherrybuck Rivets Used in Double Shear Blind Rivets Sealed with Scotch Weld 1838</p>
---	---

*See Appendix E for details

FINAL DESIGN

Based on the analytical trade studies and the experimental evaluations, design details for the actively cooled structural panel were finalized. Particular attention was given to design features which minimized the likelihood of leakage at bonded joints. The description of the design is followed by discussions of performance and mass characteristics. The design features described incorporate knowledge gained during the fabrication of the test panel.

Description

The full sized panel is 0.61 x 6.1 m (2 x 20 ft) in planform. As shown in Figure 1, it consists of an actively cooled skin with multiple discrete coolant passages manifolded as two redundant counterflow circuits, and a conventional substructure of Z-section stringers and frames on 0.61 m (2 ft) centers. The primary construction material is 2024-T3 aluminum alloy, chosen because of its attractive strength-to-weight ratio and its widespread usage in the aerospace industry. The coolant passage tubing is 3003-H14 aluminum alloy selected because of its corrosion resistance and formability.

Details of the design are illustrated in Figure 15. The enlarged view at the lower right shows the redundant counterflow coolant passages nested between a flat outer skin and a beaded inner skin. Crack arrestors are located at the edges of each tube and between the two tubes; as indicated in Appendix H, hard drawn stainless steel wires were most effective. (Due to fabrication difficulties, crack arrestors were not included in the test panel.) The adhesive bond between the coolant passage tubing and the formed inner skin is made with a silver-filled epoxy. The adhesive bond between the outer skin and the inner subassembly (manifolds, formed skin, tubes, and crack arrestors) is made with alternate stripes of epoxy film adhesive and silver-filled epoxy paste adhesive. The upper left hand view illustrates the manner in which the coolant passages merge with the edge manifold and the integration of the substructure and edge splices. Each coolant passage tube is connected to its appropriate manifold plenum by a hole drilled from the inner surface of the manifold. This prevents the interconnecting holes from becoming plugged with adhesive during bonding. The unwanted holes through the diametrically opposite side of each manifold plenum are plugged with adhesive coated blind rivets. The seal sheet over the manifold region provides redundancy to the seals formed between the manifold and the coolant passages by the adhesive bond and at the ends of the coolant passages by potting material.

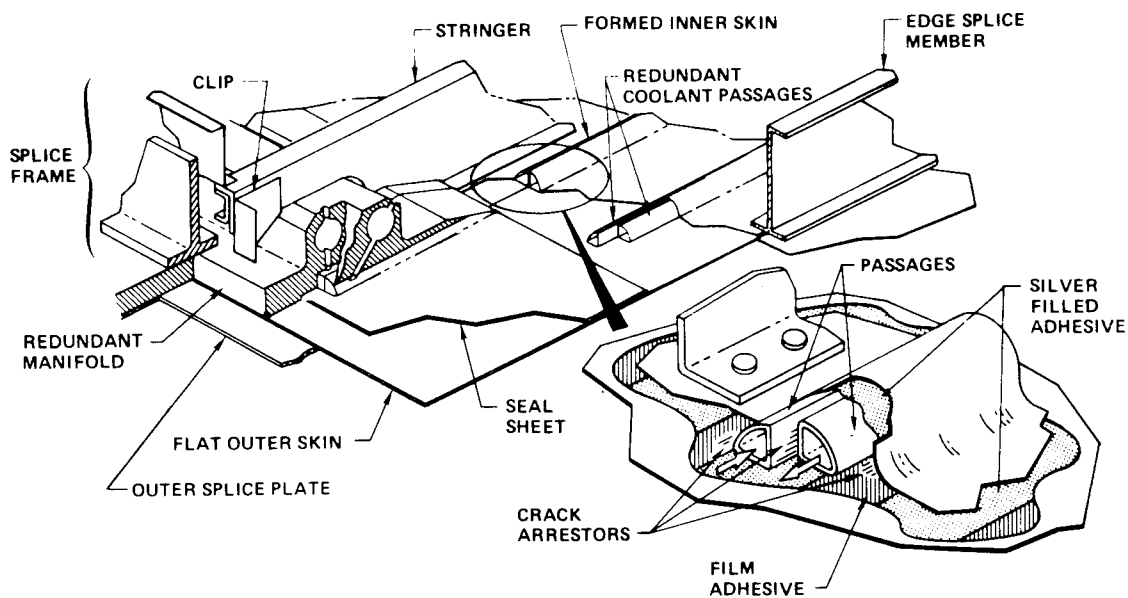


Figure 15. Details of Panel Design

The primary elements of the substructure are Z-section stringers joined to the cooled skin at every other land between coolant passages by countersunk aluminum alloy rivets. In the region of the manifold the stringer is joggled and notched. The strength removed by the notch is replaced by a small channel riveted to the basic stringer and the end clip which attaches the stringer to the transverse splice frame, see Figure 14. The splice frame consists of an extruded tee and formed sheet metal details. The flange of the tee forms the inner splice plate; the outer splice plate is titanium. Experimental evaluations indicated a double shear splice joint was necessary, see Appendix E. A single shear joint is used along the longitudinal edge because no in-plane load was specified transverse to the coolant passages.

Further illustrations of design details are presented in Figures 18, 19 and 20, which describe the test panel. Figure 11 and Appendix F provide material and thickness details.

Performance Characteristics

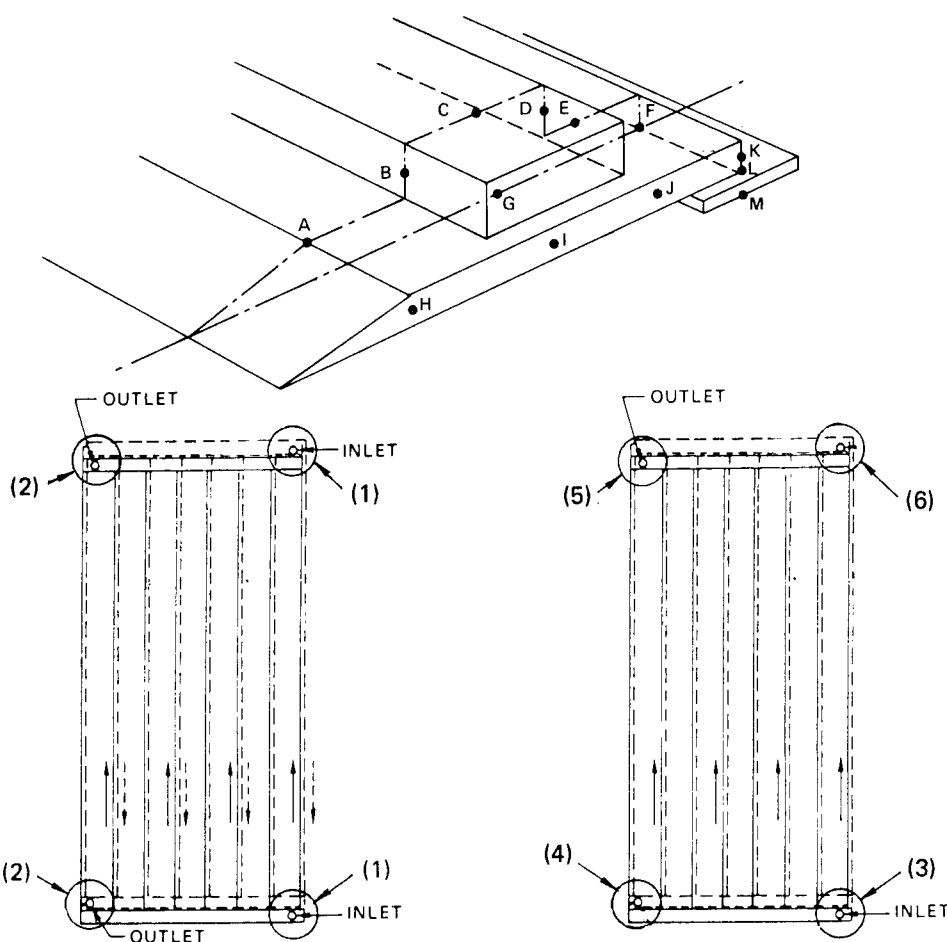
Under the design heating conditions of 136 kW/m^2 (12 Btu/ft² sec) and total water/glycol flow rate of 11,000 kg/hr (24,250 lb/hr), the axial temperature distribution is shown in Figure 5. The pressure drop through the panel is 758 kPa (110 psi).

The highest temperatures on the panel assembly are experienced along the transverse splices because the coolant passage cannot extend to the end of the panel; space must be provided for a row of rivets. Table V lists temperatures in the manifold region for normal and emergency conditions. The emergency condition assumes that one of the two independent coolant circuits is inoperative so that the coolant flow is reduced to one-half of the design value. The higher temperatures in this region can be tolerated structurally because of the 4.0 mm (0.157 in.) thickness of the manifold block as compared to a skin thickness of 1.3 mm (0.052 in.), and the use of titanium for the outer splice, location M. Under normal operating conditions the maximum temperatures on the manifold and titanium splice are 442 and 653K (335 and 715°F), respectively, while for the emergency situation they increase to 494 and 689K (430 and 780°F).

The temperature distribution transverse to the coolant passages at the mid length is illustrated in Figure 16. In the region of the coolant passage the temperature is low, between cooling passages the temperature is noticeably higher. The dashed line depicts the temperature along the formed inner skin. Although this temperature is much lower than that of the outer skin it is still quite effective in transferring heat to the coolant because at this axial station the coolant temperature is 285K (55°F). Under an emergency condition the coolant temperature rise increases from 311 to 361K (100 to 190°F), and the maximum panel temperature inboard of the manifolds increases to 389 to 444K (240 to 340°F). Additional results of thermal and structural analyses are provided in Appendix D.

The transverse temperature distribution gives rise to axial thermal stresses as indicated in Figure 17. The temperature of the stiffener was assumed to be 383K (225°F). The line coding of the stress distribution corresponds to the elements illustrated in the cross-sectional view of a coolant passage/stiffener zone. The maximum tensile thermal stress occurs on the inner beaded skin and has a magnitude of approximately 100 MPa (14 ksi); the tensile stress in the outer skin is only about half that magnitude. Along the land between the coolant passages, where the stringers are riveted to the skin, compressive thermal stresses are induced; a maximum level of 35 MPa (5 ksi) is experienced. Thermal stresses in the stiffener are quite small. The nature of the thermal stress distribution is significant with regard to the fatigue life of the panel. Where there are stress risers (rivets), the thermal stresses are compressive; where high tensile thermal stresses are experienced there are no stress risers. In computing the design life of the panel a stress concentration factor of 4.5 was applied at the rivet locations and a factor of 2.0 was applied in regions that did not contain any particular stress risers. This latter assumption was to account for the difference between production hardware and laboratory test specimens from which the fatigue data of Reference 15 was obtained. Therefore, the predicted life of 20,000 cycles (5,000 cycle design life x 4.0 scatter factor) is considered conservative.

TABLE V
MANIFOLD AND OUTER SPLICE TEMPERATURES



Location	Temperature Ratio, Local Value/389 K (700°R)					
	Normal Operation* (Redundant Cooling Circuits)		Emergency Operations (Single Circuit)			
			Inlet End		Outlet End	
Location	(1)	(2)	(3)	(4)	(5)	(6)
A	0.82	0.82	0.89	0.95	0.99	0.99
B	0.80	0.81	0.85	1.03	0.93	0.97
C	0.80	0.71	0.72	0.99	0.94	1.01
D	0.81	0.68	0.68	0.92	1.02	1.09
E	1.04	0.92	1.00	1.18	1.14	1.17
F	1.14	1.08	1.12	1.27	1.23	1.27
G	0.89	0.85	0.89	1.06	1.01	1.08
H	0.99	0.98	1.04	1.12	1.11	1.14
I	1.01	0.97	1.02	1.17	1.14	1.17
J	1.06	1.03	1.06	1.21	1.17	1.21
K	1.11	1.06	1.07	1.23	1.19	1.23
L	1.13	1.06	1.10	1.25	1.21	1.25
M ⁺	1.68 ⁺	1.61 ⁺	1.65 ⁺	1.77 ⁺	1.73 ⁺	1.77 ⁺

* Because of counterflow design both ends are the same.
+ Titanium

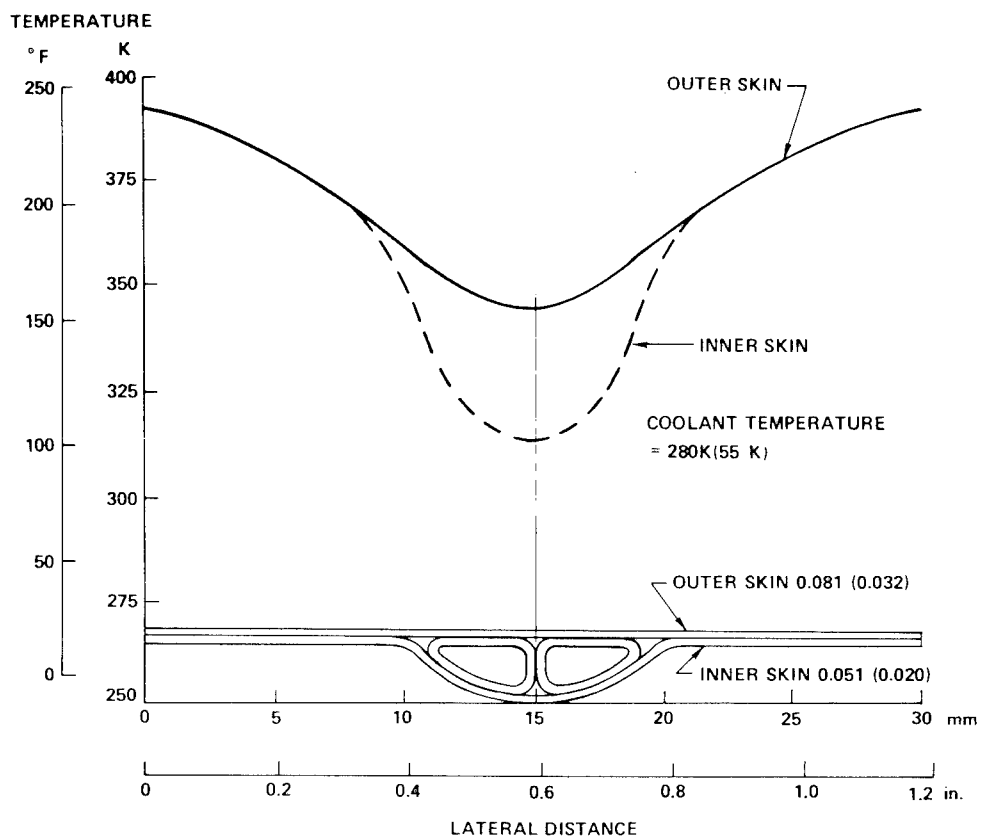


Figure 16. Temperature Distribution at Mid-Length
(Stiffener not Included)

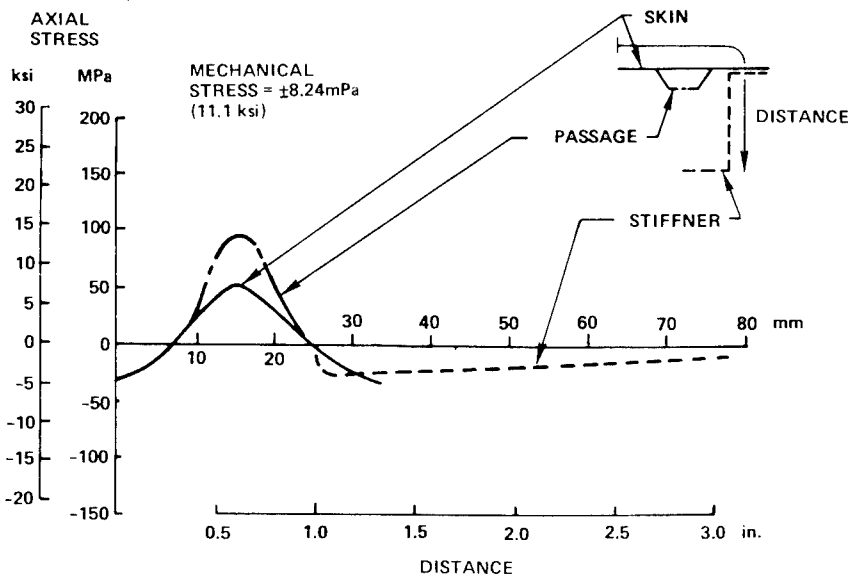


Figure 17. Thermal Stress Distribution at Mid-Length

Mass

The mass of the major elements of the 0.61 x 6.1 m (2 x 20 ft) actively cooled structural panel are summarized and totaled in Table VI. Major items of the dry mass are the skins and the stiffening elements. The major element of wet mass is the coolant inventory in the passages. Dry mass entries are based on actual measurements of detailed parts fabricated for the test panel as reported in Appendix F. Elements of wet mass are calculated. On a unit area basis, the dry, wet, and total mass values are 10.44, 1.75 and 12.19 kg/m² (2.14, 0.36 and 2.50 psf) respectively. This compares with a unit mass of 10.27 kg/m² (2.10 psf) computed on the basis of the optimization trade studies. About 35% of the discrepancy, 0.67 kg/m² (0.14 psf), is due to the greater quantity of silver-filled adhesive needed between the beaded inner skin and the coolant passages because of sheet metal forming tolerances; and 65%, 1.29 kg/m² (0.26 psf), is due to the fact that during the optimization trade studies manifolds, clips, and fasteners are not included.

TABLE VI
MASS SUMMARY OF 0.61 x 6.1M COOLED PANEL

	Mass kg (lbm)	Mass kg/m ² (lbm/ft ²)
<u>Dry Structure</u>		
1. Skin(s)	13.55 (29.88)	3.647 (0.747)
2. Cooling Passages	3.38 (7.45)	0.908 (0.186)
3. Manifolds - includes all that is integral with panel; includes end flange(s); includes metal necessary to direct coolant into passages	2.06 (4.54)	0.557 (0.114)
4. Stiffening (does not include longitudinal edge stiffening)	14.50 (31.98)	3.91 (0.800)
5. Longitudinal edge stiffening and closeouts	3.17 (6.99)	0.840 (0.172)
6. Adhesives, braze alloy, solder	0.82 (1.81)	0.220 (0.045)
7. Fasteners, inserts, clips	1.15 (2.53)	0.313 (0.064)
8. Crack stoppers	0.15 (0.33)	0.049 (0.010)
Dry Structure Total	38.78 (85.56)	10.444 (2.139)
<u>Coolant</u>		
1. Coolant inventory in passages	4.88 (10.75)	1.313 (0.269)
2. Coolant inventory in manifolds	0.51 (1.12)	0.137 (0.028)
3. Passages' coolant pumping penalty*	1.02 (2.24)	0.273 (0.056)
4. Manifolds' coolant pumping penalty*	0.10 (0.21)	0.024 (0.005)
Coolant Total	6.51 (14.32)	1.747 (0.358)
Total	45.29 (99.88)	12.191 (2.497)

* (at 2 lb/hp=hr)

TEST PANEL

An actively cooled test panel was fabricated and delivered to NASA for evaluation of thermal and structural integrity of the panel design. The 0.61 x 1.22 m (2 x 4 ft) test panel was a shortened version of the 0.61 x 6.1 m (2 x 20 ft) full-scale panel design. Figure 18 shows the conventional appearance of the test panel. It consisted of a cooled skin with integrated manifolding at both ends for the redundant counterflow coolant passage networks, and a substructure of Z-stringers and frames. Realistic edge attachments were incorporated. End adapters were provided for the application of alternating tensile and compressive in-plane loadings, and extended the assembly length to 1.88 m (74 in.).

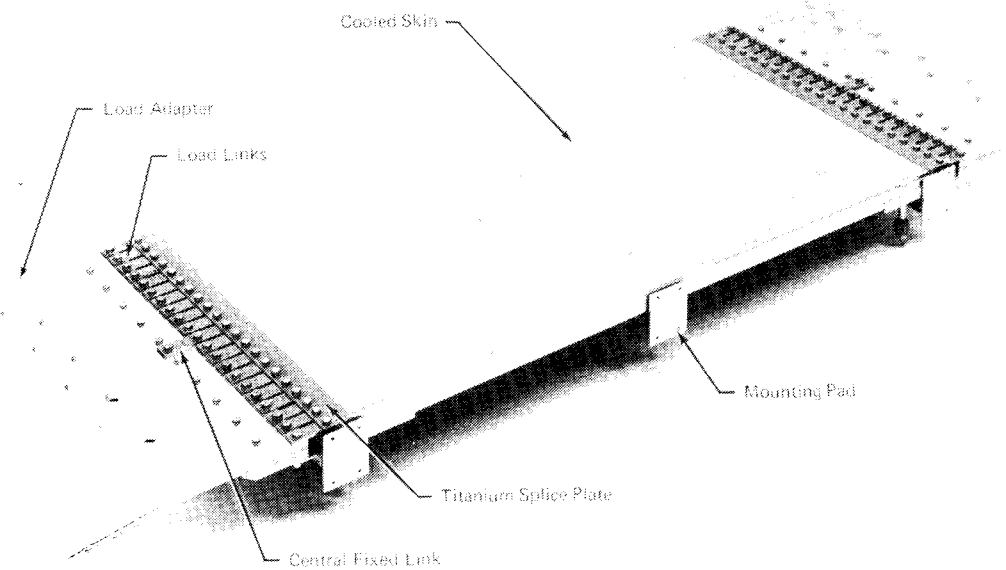
Design

While the panel has a conventional appearance, Figure 18, integration of the coolant circuits makes it unconventional in nature. Flush riveting is apparent on the external surface. The outer titanium splice plate can be identified by its different coloring as compared to the cooled aluminum skin. At each end of each frame a mounting pad is provided for a linear ball bearing which is part of the NASA test apparatus. The stringers and frames are conventional except for the rather large extruded T-sections riveted at the ends of the stringers and the extruded C-channel (not visible, but see Figure 19) installed outboard of the end frames. These particular elements were introduced to distribute loads from the end adapters into the test panel. At the near end of the panel, inlet and outlet fittings can be seen. Two of the fittings are for the installation of pressure gages for testing purposes and would not be incorporated in a panel design for an actual aircraft.

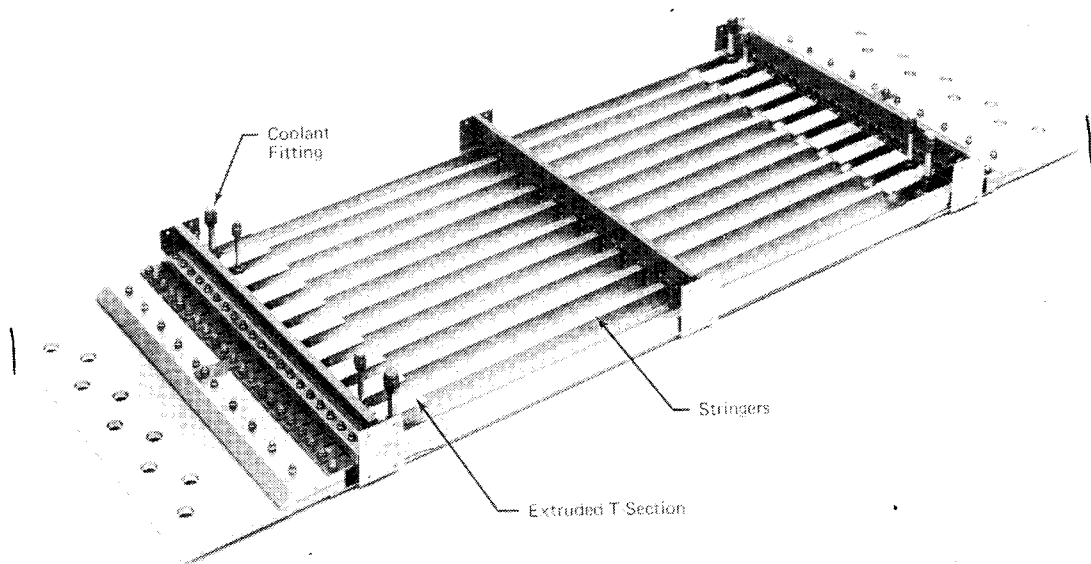
Structural details of the assembly are illustrated in Figure 19. The conventional center frame is a notched Z-section which is attached to the stringers by shear slips and a long angle. Rivets attach the stringers to the cooled skin. The height of the coolant passage prevents the frame flange from attaching directly to the skin; small spacer blocks are used at these riveted joints. The lower photo provides details of the splice and end frame. The splice is seen more clearly at the upper right of this photo where the outer titanium splice plate and the inner extruded aluminum T-section are seen to be spaced by the edge of the cooled panel manifold. The center of the picture shows the extruded T-section reinforcements, the flange of the stringer, and a formed C-channel that reinforces the stringer where it is notched to accommodate the coolant manifold block.

Details of the notched stringer and manifold block are indicated more clearly in the lower photo of Figure 14, which also shows the bonded manifold end caps. The load on the end cap bond line is minimized by the use of two shear pins. A male fitting is adhesively bonded and shear pinned to the manifold at each inlet and outlet location.

There were some differences between the full-scale panel design and the test panel. The test panel: (1) did not incorporate crack arrestors, (2) did not have the titanium splice recessed within the outer mold line, and (3) used an L-shaped slot to connect one end of each coolant tube to the inboard manifold. Crack arrestors were eliminated because installation difficulties were encountered during fabrication of the cooled skin from which the NASA fatigue specimens were cut. The titanium splice was not recessed because the need for a double shear attachment was not determined until after all of the manifolds were machined; recessing of the machined parts would have reduced the strength of the edge joint in the cooled skin by about 25%. The interface between the L-shaped slot (see the lowest tube installation on Figure 20) and the coolant passage tubing, was found to be a source of leakage and plugging, therefore it was eliminated from the final design, which incorporated all changes resulting from experiences in fabricating the fatigue and test panels.

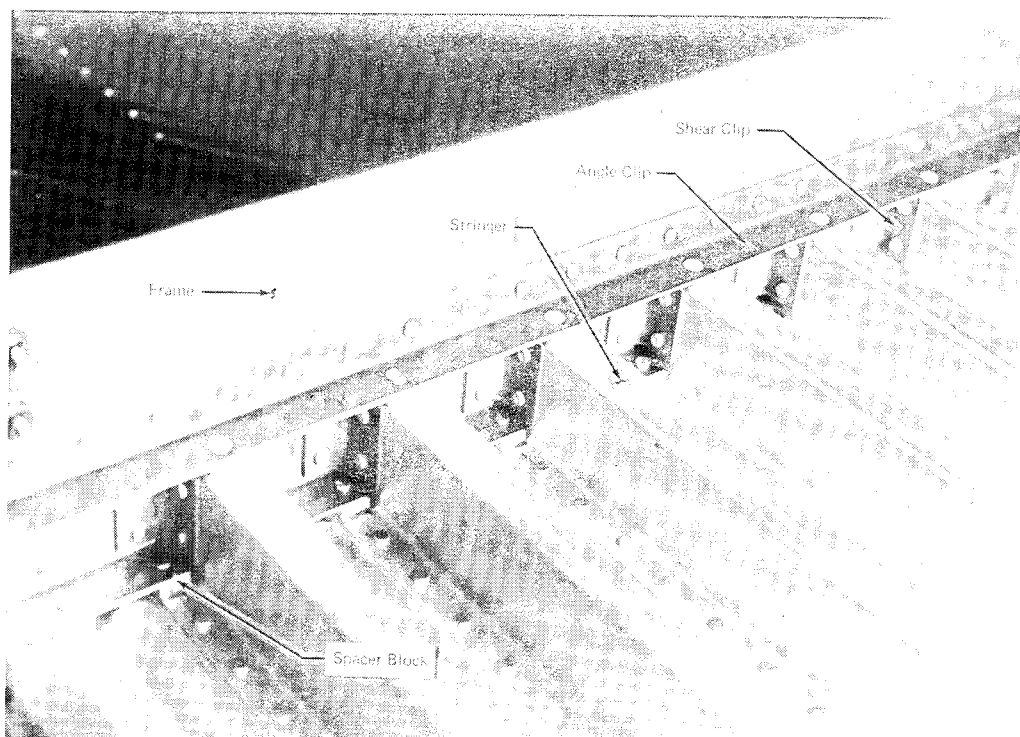


TOP VIEW

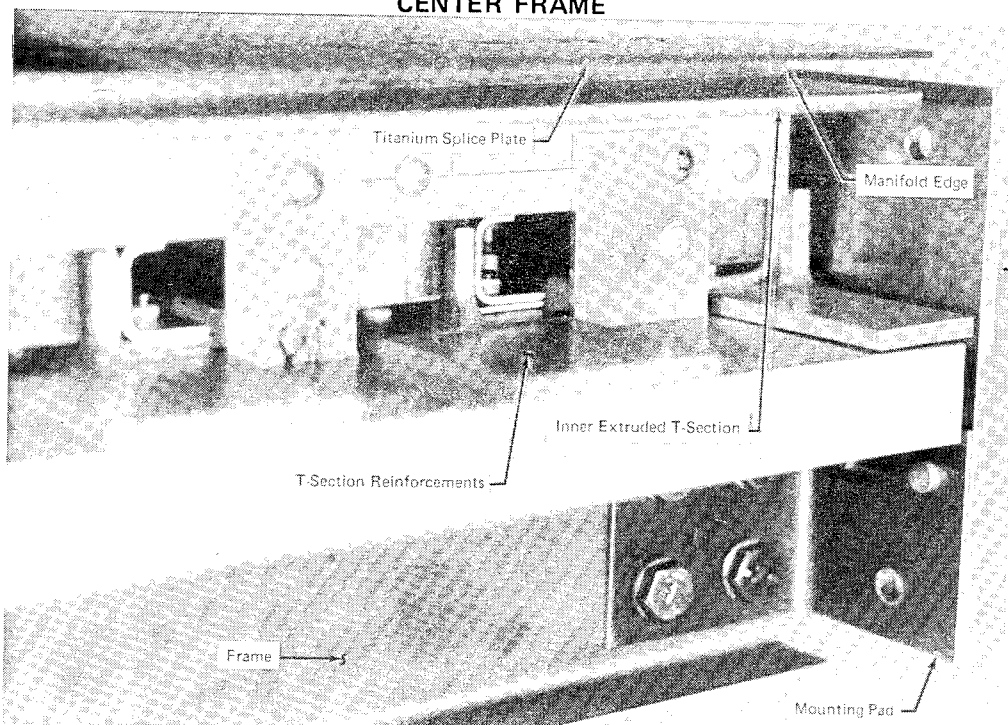


BOTTOM VIEW

Figure 18. Test Panel Assembly



CENTER FRAME



SPLICE AND END FRAME

Figure 19. Test Panel Details

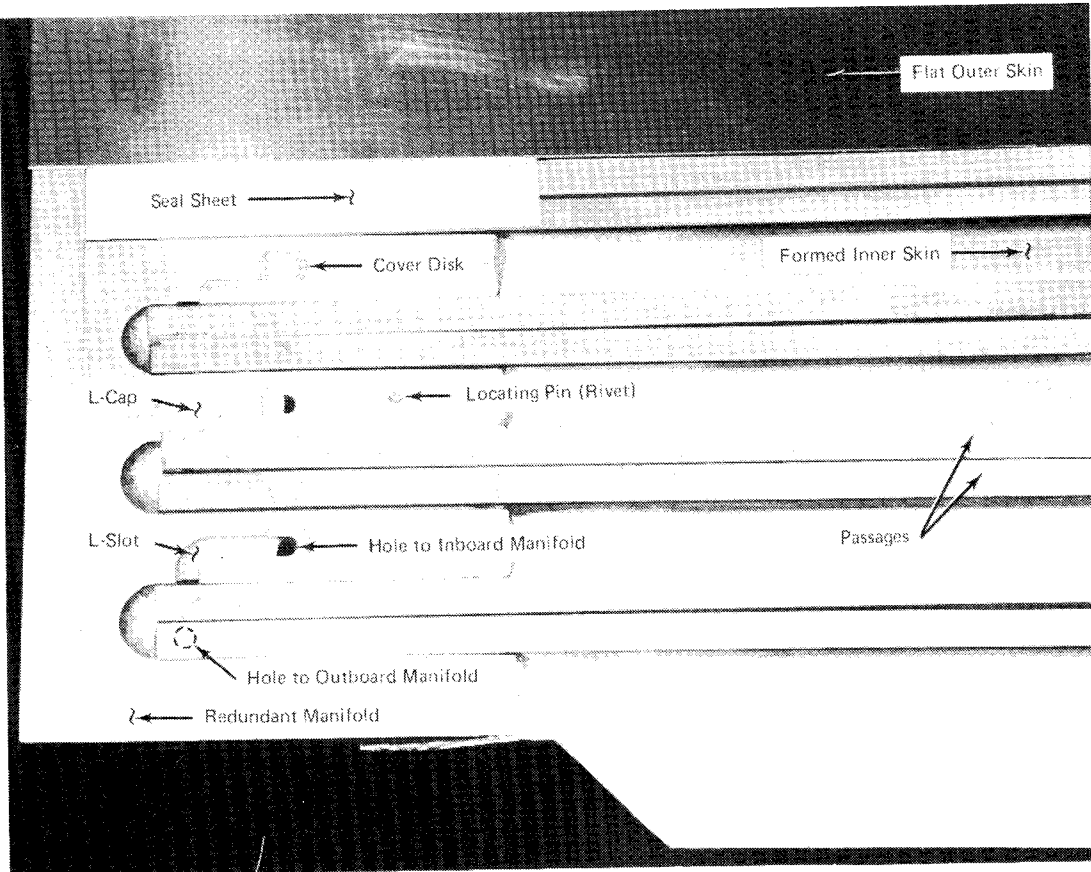


Figure 20. Tubing Installation Details

Fabrication

Fabrication activities consisted of making detailed metallic parts and assembling them into a cooled structural test panel. Conventional airframe practices were used to produce the detailed parts and to join the cooled skin to the stiffening substructure which together formed the test panel. The detailed parts of the cooled skin were adhesively bonded. Numerous difficulties were encountered and resolved before the cooled skin was fabricated successfully. Procedures are summarized here, details are provided in Appendix F.

The manifold blocks were machined with milling and gun drilling tools. Manifold end plugs, Figures 14 and 34, and fittings were turned on a lathe. The formed inner skin was produced on a female die in an hydraulic press. The substructure was produced by a combination of brake forming and machining. Standard extrusions were used for some of the stiffening elements. Because of the stringent tolerance required for the coolant passage tubing, flat on one side to ± 0.012 mm (0.0005 in.) and ± 0.05 mm (0.002 in.) wall thickness, only one supplier out of the 20 contacted offered to meet requirements on a fixed price basis. Stringers, frames and clips were assembled to the adhesively bonded cooled skin by riveting. Titanium cherrybuck rivets were used for the transverse splice joints, aluminum alloy rivets were used at all other locations.

The need for unconventional adhesive bonding procedures was dictated by four considerations. First, the high design heat flux for which the panel was designed requires the outermost bondline to be thin and of high thermal conductivity. Second, thin bondlines are inconsistent with the tolerances associated with formed sheet metal parts, 0.7 mm (0.03 in.) and machined parts, 0.2 mm (0.01 in.). Third, structural adhesives have low thermal conductivities. Fourth, the adhesive joints must be leak tight to water/glycol. A silver-filled epoxy paste adhesive was used to bond the coolant passage tubes to the formed inner skin; Figure 21 shows the method of application. A sequence of debulking and cleaning steps was used prior to autoclave cure to set the tubes flush with the surface of the inner skin, thereby cancelling tolerance effects related to the dimensions of the tubing, the manifolds and the formed inner skin. A flat surface was achieved onto which the outer skin could be bonded by a thin adhesive layer. The high thermal conductivity requirement of the bondline could be met by the silver-filled epoxy paste adhesive, but its shear and peel strengths are low. Therefore, narrow alternate stripes of high strength film adhesive and high conductivity paste adhesive were used to bond the flat outer skin to the subassembly of the manifolds, tubes and inner skin, see Figure 15.

Several leak tight joint configurations were required by the panel design. The ends of the coolant passage tubes were potted using a room temperature curing adhesive which allowed clean-up of excess of adhesive before it was fully cured; an oven cure prevented flow during subsequent autoclave cures of the cooled skin. The same adhesive was used to bond the manifold end caps and to seal the slight gap between the coolant passage tube and the L-cap, see the upper tubes in Figure 20. The interface between the coolant passage tubing and the manifold was a particularly difficult joint to seal.

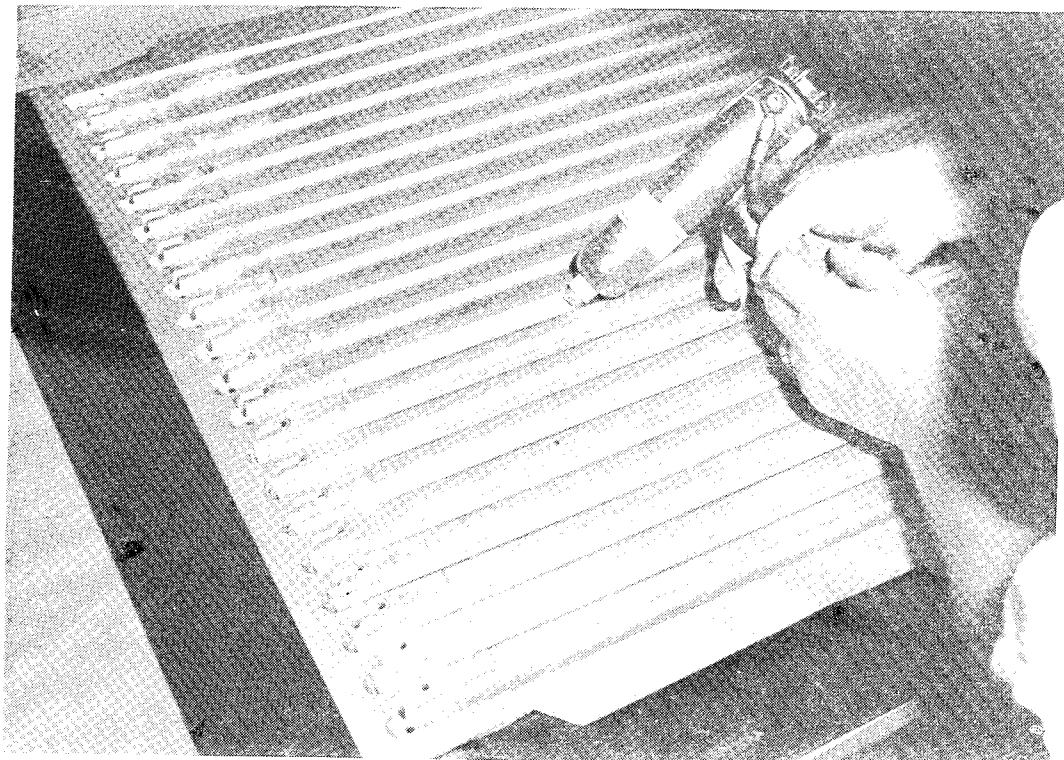


Figure 21. Application of Silver Filled Epoxy

A film adhesive was chosen for this location because low flow was necessary to preclude plugging of the holes that connect the tubes to the manifold plenums. If not enough adhesive is used there may be leakage between the coolant circuits and out around the manifold/tube interface. Both types of leaks were found in test specimens. An excessive amount of adhesive could cause flow which could plug the interconnect holes. During inspection of the test panel, plugging was found and corrected.

To remedy the blockage problem in the test panel, holes were drilled through the manifold plenums into the coolant passage tubing. In the outboard manifold plenum these holes were moved inboard 2 mm (0.08 in.) from the plenum centerline, see Figure 22. In order to connect the other coolant tube to the inboard manifold it was necessary to drill directly through the plenum about 2 mm (0.08 in.) outboard of the plenum centerline. This effectively short circuited the L-slots, see Figures 4 and 22.

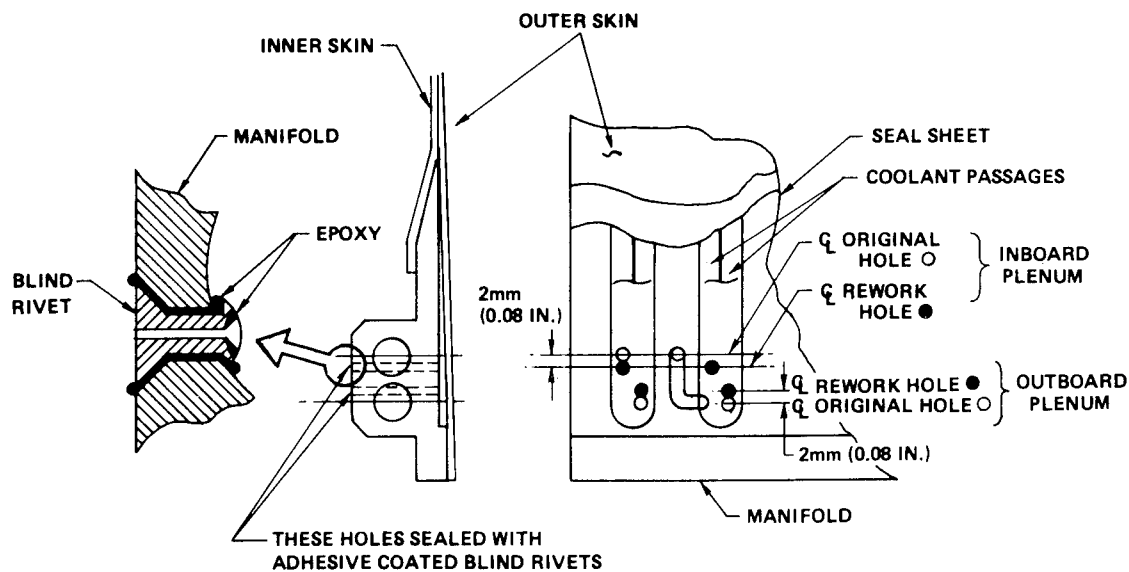


Figure 22. Rework of Plugged Interconnect Holes

Future Improvements

During fabrication of the test panel, certain difficulties were encountered that could be avoided by relatively simple design improvements. Adhesive flow caused blockage of the predrilled interconnecting holes in the manifold and coolant tubes. The L-caps were tedious to install; some of the joints were not leak tight and had to be repaired. The mass of silver-filled adhesive needed was greater than anticipated because of variations of the depth of the beads formed on the inner skin. Proper positioning of the crack arrestors could not be maintained. Subsequent paragraphs describe improvements that should eliminate such difficulties for future panels based on this concept.

Blockage of the interconnecting holes by adhesive can be avoided by drilling the holes after the cooled skin is bonded rather than drilling the detailed parts prior to assembly. Figure 15 shows the improved configuration. The holes between the outboard manifolds and the coolant passage tubing are oriented perpendicular to the panel surface. By using a diagonal orientation for the holes between the inboard manifolds and the coolant passage tubing it is possible to flow coolant to the outboard end of the tubing and to eliminate the L-slots in the manifolds, the L-caps, and the cover disks shown

in Figure 20. As compared to the L-slot configuration used for the test panel, the center rib between the outboard and inboard manifolds must be thicker. From a design point of view, the panel mass is increased by 0.5 kg (1.2 lb), about 0.15 kg/m^2 (0.03 lb/ft^2). From a manufacturing point of view, the drilling of the interconnecting holes after bonding simplifies the assembly and enhances reliability.

Another refinement in the fabrication of the panel that appears to be desirable is concerned with achieving better dimensional control of the beads in the inner skin. With the low cost tools used for this project and the limited tooling trials, it was not possible to achieve good control of bead depth. Beads in the center of the inner skin were approximately 0.17 mm (0.007 in.) deeper than the beads near the edges. Gradual reworking of the form die sequenced with repeated tool trials would permit bead depth to be controlled to a closer tolerance. This would reduce the amount of silver-filled epoxy needed to bond the coolant passages into the beaded skin such that the mating surface for the flat outer skin is truly flat, see Figure 15.

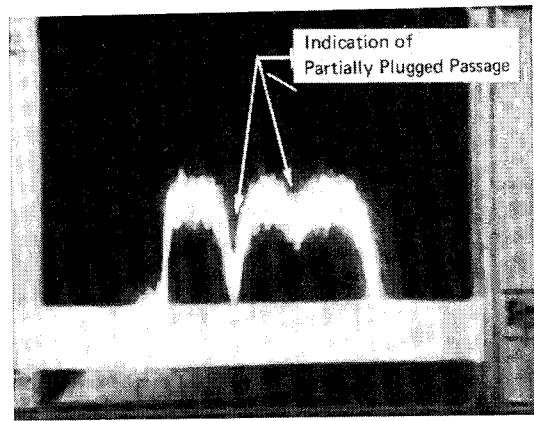
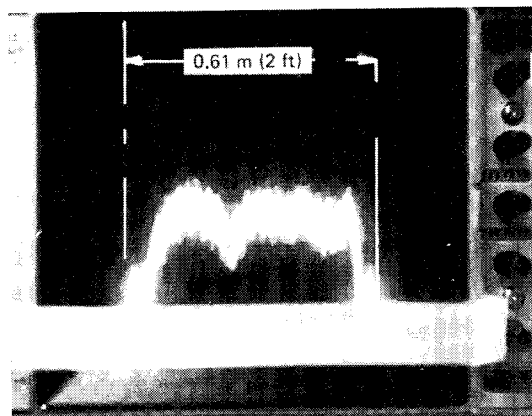
A final fabrication process improvement is needed with regard to the installation of the crack arrestors. When small samples were made for evaluating the concept, see Appendix H, it was possible to maintain proper positioning of the crack arrestors. During fabrication of the $0.61 \times 1.22 \text{ m}$ (2 x 4 ft) skin, which was cut into fatigue and pressure test specimens, considerable difficulty was encountered in maintaining proper position of these crack arresting wires. Therefore, the crack arrestors were not incorporated in the test panel. As the length of the panel increased, it was more difficult to locate the crack arrestors. Proper tensioning tools or specially straightened long lengths of wire would be required to control locations.

Inspection

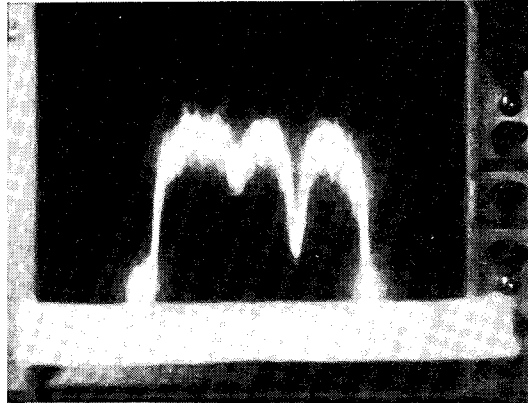
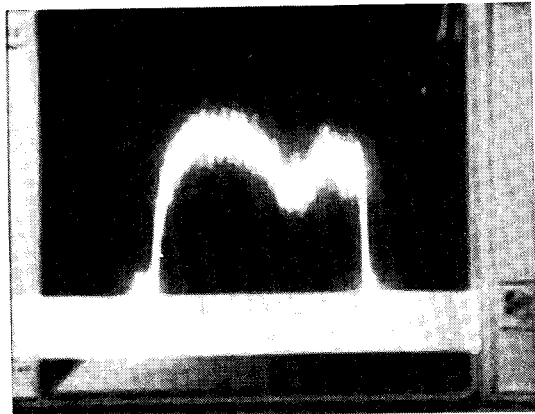
A series of inspections was necessary to ensure proper fabrication of the cooled skin. Assembly required sequencing the fabrication and inspection steps so that remedial action could be taken, if necessary, before subsequent assembly steps precluded suitable repairs. Detail parts were given conventional inspections. The potted end plugs of the coolant passage tubing were checked for leak tightness with GN_2 before assembly into the panel. After bonding the coolant passage tubes, L-caps, and disks into the beaded skin/manifold subassembly, pressure tests with GN_2 were conducted with the panel submerged in water to identify sources of leaks. Holographic inspections showed uniformity of fringe patterns for all coolant passages; this is indicative of good bonding of the tubing to the inner skin and manifold. Radiographic inspection indicated good uniformity of paste adhesive distribution between the beaded skin and coolant passages. One relatively long void region, $1.5 \times 38 \text{ mm}$ (0.06 x 1.5 in.) was found. Its presence will decrease the heat transfer effectiveness of this region by less than 5%. There were some indications of small pores and rivulet patterns indicative of resin/toluene flow. Their effect on thermal conductance is negligible. Details of the inspection procedures are given in Appendix G.

During installation of pressure fittings for the cure of the seal skins, adhesive blockage was noted in some of the holes between the manifold and the coolant passages in the outboard manifolds. Infrared scans of the completed skin confirmed the seriousness of the blockage. After the rework described in the proceeding subsection the IR scans indicated a significant improvement in the uniformity of coolant flow, see Figure 23. Radiographic inspection indicated good filling of the high conductivity paste adhesive between the alternate stripes of the structural film adhesive. An internal proof pressure of 1654 kPa (240 psig) was sustained successfully by the cooled skin.

After installation of the substructure and the load adapters the proof pressure test of 1654 kPa (240 psig) was repeated successfully.



FLOW TO INBOARD MANIFOLD



FLOW TO OUTBOARD MANIFOLD

FIRST CIRCUIT

SECOND CIRCUIT

Figure 23. Infrared Scan Results After Rework

Mass

The calculated mass of the cooled skin and substructure is compared to the measured mass of the panel in Table VII. The higher measured mass is due primarily to the additional adhesive required to compensate for the tolerances associated with sheet metal forming.

TABLE VII
MASS SUMMARY OF 0.61 x 1.22M TEST PANEL

	Mass, kg (lbm)		Measured Unit Mass (kg/m ² (lbm/ft ²))
	Calculated	Measured	
Cooled Skin			
Manifold (2)	2.06 (4.54)	2.15 (4.74)	2.89 (0.59)
Outer Skin	1.68 (3.69)	1.72 (3.82)	2.31 (0.48)
Inner Skin	1.15 (2.54)	1.03 (2.26)	1.38 (0.28)
Seal Sheet (2)	0.08 (0.18)	0.07 (0.16)	0.09 (0.02)
Tube (40)	0.29 (0.64)	0.28 (0.68)	0.38 (0.09)
Adhesive	0.89 (1.96)*	1.08 (2.38)**	1.45 (0.30)
Fittings	0.08 (0.18)	0.12 (0.26)	0.16 (0.03)
Subtotal	6.23 (13.75)	6.46 (14.25)	8.68 (1.78)
Substructure			
Stringers (9)	2.65 (5.85)	2.49 (5.49)	3.35 (0.69)
Channels (2)	0.65 (1.42)	0.64 (1.40)	0.86 (0.18)
Frames (3)	1.06 (2.31)	1.09 (2.40)	1.46 (0.30)
Clips	0.07 (0.16)	0.08 (0.17)	0.11 (0.02)
Spacers	0.06 (0.14)	0.08 (0.18)	0.11 (0.02)
Titanium Splice (2)	0.17 (0.38)	0.19 (0.42)	0.26 (0.05)
Rivets	0.32 (0.71)	0.32 (0.71) [†]	0.43 (0.09)
Subtotal	4.98 (10.97)	4.89 (10.77)	6.57 (1.35)
Panel Assembly	11.21 (24.70)	11.35 (25.02)	15.25 (3.13)
Interface hardware with load adapters is excluded.			
* Computed based on measurements of skin beads			
** Obtained by subtracting weight of details from weight of assembly			
† Calculated not measured			

Load Adapters

The proposed NASA thermal structural evaluation of the actively cooled test panel will involve thermal and mechanical loadings applied simultaneously. Radiant quartz lamps will apply the thermal loading; a tensile/compression load frame will apply the mechanical loading. The load adapters provide the path between the load frame and the test panel. They are designed to apply the in-plane loading through the neutral axis of the panel while the thermal expansion of the panel is accommodated. The design selected is illustrated in Figure 24. A total of 21 pairs of titanium alloy straps attach each large aluminum alloy plate to each end of the panel. Titanium was chosen for the load links to accommodate any temperature rise induced by the quartz lamp heater. The linkage assembly is stabilized during compressive loading by the center link which does not rotate. The bolt spacing for each link was established so that the angle of rotation caused by thermal expansion is small, 1.1° maximum. The change in axial length of a rotated link is less than the clearances between the bolt and bolt hole. Close tolerance bolts are used in carefully bored holes to minimize any pounding action as the in-plane loading is reversed from tension to compression.

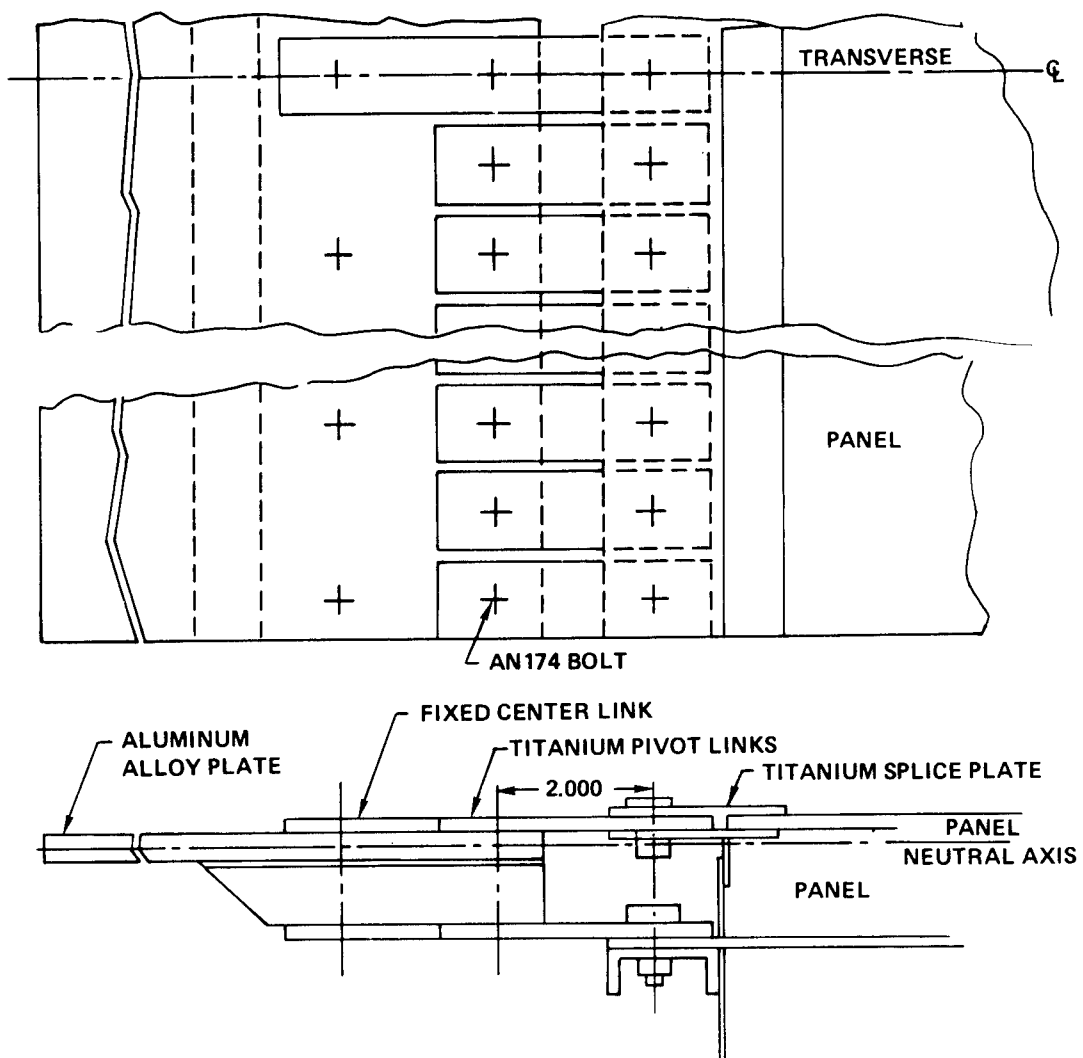


Figure 24. Load Adapter

CONCLUDING REMARKS

This report presents the results of a program which optimized the design of a full scale 0.61×6.1 m (2×20 ft) actively cooled panel for minimum panel mass. The design conditions and requirements were representative of an hypersonic transport. Details of the panel design were finalized on the basis of results from various static and fatigue tests conducted by Langley Research Center and Bell Aerospace; the specimens incorporated major design features of the panel. A 0.61×1.22 m (2×4 ft) test panel was fabricated and delivered to the Langley Research Center of NASA for assessment of the thermal and structural design features of the optimized panel design. The concept incorporated an unshielded surface panel actively cooled by a network of discrete, redundant, counterflow passages interconnected with appropriate manifolding, and assembled by adhesive bonding. This cooled skin was stiffened with a mechanically fastened conventional substructure of stringers and frames. The cooling passages were parallel to the stringers.

Until the test panel is evaluated experimentally, conclusions cannot be drawn as to its thermal and structural adequacy. Nevertheless, some conclusions can be drawn with regard to the methodology used for developing the panel design and the procedures for fabricating and inspecting the test panel:

1. The most demanding of the design and fabrication aspects of the actively cooled panel were associated with integration of the cooling system into the panel skin. The use of redundant (dual) coolant passages greatly complicated interfacing of the passages with the manifolds.
2. The redundant cooling passages keep panel temperatures down to 445 K (340°F) and provide structural limit load strength capability for one hour if one of the distribution systems suffer a loss of coolant.
3. The full scale aluminum alloy panel was optimized for a minimum mass of 10.27 kg/m^2 (2.10 lbm/ft^2). This mass was only 25 % greater than an uncooled panel operating at the same 377 K (245°F) maximum temperature. At the design flux of 136 kW/m^2 ($12 \text{ BTU/ft}^2 \text{ sec}$), an uncooled aluminum alloy panel would melt.
4. Because of the many thermal and structural design variables involved, a relatively complex iterative optimization procedure was required to define the panel configuration of minimum mass.
5. Fatigue life was the dominant aspect of the structural considerations. Structural aspects accounted for 75% of the stiffened panel mass.
6. Thermal stresses were approximately equal to mechanical stresses.
7. The counterflow panel cooling circuitry used in the panel skin provides a more uniform axial panel temperature than a single pass cooling system. This should minimize differential expansion problems when the counterflow panels are integrated into a complete aircraft structure.

8. Adhesive bonding and mechanical fastening assembly techniques permitted maximum flexibility in material selection. However, obtaining bonded leak-free coolant passage/manifold joints was difficult.
9. Despite the obvious fabrication difficulties, the one-quarter, 2:1 elliptical cooling passages were bonded between inner and outer skins for two reasons. Peeling stresses are minimized in the passage to skin joints. Better heat transfer is obtained from the portion of the coolant passage not in direct contact with the heated outer skin because the formed inner skin conducts heat to the curved portion of the coolant passage tubing.
10. The high design heat flux, 136 kW/m^2 ($12 \text{ Btu/ft}^2\text{sec}$) required thin bondlines of high thermal conductivity and high structural integrity. Alternate stripes of silver filled epoxy paste and epoxy film adhesives were used to satisfy performance requirements.
11. Attainment of the necessary dimensional control on the thin-walled cooling passage tubing of asymmetric shape as dictated by the thin bondline requirement, represented a state of the art advance in tube drawing.
12. A careful assembly sequence was required for the cooled skin to accommodate machining and formed sheet metal tolerances which ordinarily would not permit thin bondlines.
13. Small test specimens proved the ability of crack arrestors (wires located next to coolant passages) to retard crack growth into the coolant passages. However, incorporation of the crack arrestors into the larger test panel proved difficult and they were not incorporated.
14. Holographic and infrared scanning techniques were adapted successfully to the unique nondestructive inspection requirements of an actively cooled structural panel.

APPENDIX A MATERIALS SELECTION AND PROPERTIES

Design of the actively cooled structural panel required consideration of the basic materials of construction, the coolant, and adhesives for assembly of the panel elements and material for crack stoppers. A requirement of the effort was to utilize conventional aircraft construction materials such as aluminum alloys. This is an excellent choice because of the favorable strength to density ratio of the aluminum alloys and their high thermal conductivities. In addition, fabrication procedures are well established and production costs for these alloys tend to be lower than for other structural airframe materials. An extensive review of candidate aluminum alloys for hypersonic cooled aircraft applications was conducted in Reference 6. For this particular project, consideration was given to 2024, 2048, and 2219 alloys. The 2024 alloy was selected because of its good thermal and structural properties, availability, good fatigue characteristics, reasonably good resistance to corrosion and crack growth, and its relatively good fracture toughness. The 2048 alloy was of interest because of its better process and compositional controls which resulted in improved fracture toughness and somewhat superior mechanical properties. The 2219 alloy was considered because of its weldability and brazability. The 2048 and 2219 alloys were not selected because of their limited availability as compared to the 2024 material.

Properties for the 2024-T3 alloy selected for the sheetmetal elements of the actively cooled panel were obtained primarily from Reference 15. Fatigue properties are not provided in this reference as a function of temperature, therefore, the temperature effects defined in Reference 16 were used. Because the primary failure mode during panel test is expected to be fatigue, the design allowables used for the panel are provided in Table VIII.

TABLE VIII
ADJUSTED FATIGUE ALLOWABLES FOR 20×10^3 CYCLES*

K (°F)	Alternating Stress for Steady Stress and K_T Indicated, kPa (ksi)							
	$K_T = 2.0$				$K_T = 4.5$			
	69 (10)	104 (15)	138 (20)	0 (0)	69 (10)	138 (20)	0 (0)	69 (10)
300 (81)	± 145 (21)	± 142 (20.6)	± 138 (20)	± 103 (15)	± 69 (10)	± 56 (8.2)		
325 (126)	± 138 (20)	± 135 (19.6)	± 131 (19)	± 96 (13.9)	± 65 (9.4)	± 52 (7.6)		
350 (171)	± 124 (18)	± 121 (17.6)	± 117 (17)	± 88 (12.8)	± 60 (8.7)	± 47 (6.8)		
375 (216)	± 114 (16.5)	± 111 (16.1)	± 107 (15.5)	± 83 (12)	± 54 (7.9)	± 41 (5.9)		
400 (261)	± 105 (15.2)	± 102 (14.8)	± 98 (14.2)	± 76 (11)	± 48 (6.0)	± 35 (5.1)		
425 (300)	± 96 (14)	± 93 (13.5)	± 90 (13)	± 72 (10.5)	± 43 (6.2)	± 30 (4.3)		

*Values from Reference 14 corrected for 10,000 hours exposure and for temperature.

Desirable properties for the coolant include a relatively wide operating temperature range, low viscosity, high thermal conductivity, high specific sheet. A high flash point is desirable along with low chemical reactivity and nontoxicity. References 2 and 9 compared more than 20 candidate coolants for the hypersonic aircraft application. The methanol/water combination was rejected because of its toxicity and the volatility of the alcohol constituent. The composition of the selected

ethylene glycol/water combinations was 60/40 which provided properties having good flow characteristics over the temperature range from 344 K (160°F) to 262 K (-65°F) required for all weather operation. Property data was obtained from Reference 19.

The basic design of this actively cooled panel relies heavily on the use of nonmetallics primarily as adhesives but also as potting compounds. Structural and thermal requirements tend to be contradictory. A number of structural adhesives were considered, their structural properties were compared on the basis of vendor literature. All have low thermal conductivities and relatively high thermal expansions. To achieve good control of bond lines, an essential aspect of product uniformity and fit, only film adhesives were considered. The choice of Epon 951 as the structural adhesive was based primarily on its availability in a thin unsupported film with a thickness ranging between 0.05 and 0.06 mm (0.002 and 0.0025 in.). The other adhesives had minimum thicknesses of 0.08 mm (0.003 in.) or greater. As seen in Figures 25 and 26, the shear and peel strengths of the selected adhesive are comparable to the best in the group and the retention of these strengths is high as a function of temperature.

Even with a structural adhesive thickness of only 0.05 mm (0.002 in.) the low thermal conductivity of the structural adhesive causes a large thermal resistance between elements of the cooled panel. To increase the thermal conductance between the outer skin and the inner elements (the coolant passage tubing and inner skin) alternate stripes of highly conductive adhesive were used in conjunction with the structural film adhesive, see Figure 15. The conductive adhesive was not used over the entire panel because of inferior structural characteristics, particularly peel strength. On the basis of vendor literature Eccobond 58C was chosen, primarily because of its high thermal conductivity but also because of its fairly good mechanical properties and the compatibility of its cure cycle with the one for the Epon 951. Inasmuch as thermal conductivity was of prime importance and structural characteristics were of lesser importance, thermal conductivity measurements were the only tests conducted on the adhesive in a quantitative sense. Measurements made, by the Wyle Laboratories of Hampton, Va. for NASA, on samples of adhesive bonds between 6.35 mm (0.25 in.) aluminum alloy plates gave thermal conductivity values of 0.85 ± 0.50 W/m K (5.9 ± 3.5 Btu-in./ft² hr°F) for a 0.08 mm (0.003 in.) bond line and 2.17 ± 0.78 W/m K (15.1 ± 5.4 Btu-in./ft² hr°F) for a bond line thickness of 3.0 mm (0.12 in.). The analysis performed during the design of the cooled panel used the manufacturer data for all properties including thermal conductivity of 8.6 W/m K (60 Btu-in./ft² hr°F), Reference 20, which appears to be optimistically high. A value of 2.9 W/m K (20 Btu/ft² hr°F) as used in Reference 7 agrees with this high end of the Wyle data although the experimental data of Reference 7 is somewhat lower. The effect of thermal conductivity on the maximum panel temperature under normal operating conditions was defined subsequently, see Appendix D, Figure 31; the effect is small for k values above 2 W/m K.

The cooled panel design concept incorporated crack stoppers in the vicinity of the coolant passages to provide an increase in time for the detection of any skin cracks prior to loss of coolant. Hard drawn stainless steel wire of 0.15 mm (0.006 in.) diameter was selected on the basis of tests reported in Appendix H and was located as shown in Figure 15. No properties were measured specifically for the crack stoppers. The load carrying capability of these wires was not included in the basic design of the panel. During preparation of the early test specimens, considerable difficulty was encountered in installing the crack stoppers. Therefore, they were eliminated from the test panel. The merits of their incorporation (assuming improved installation techniques are developed) are indicated by the results of Appendix H.

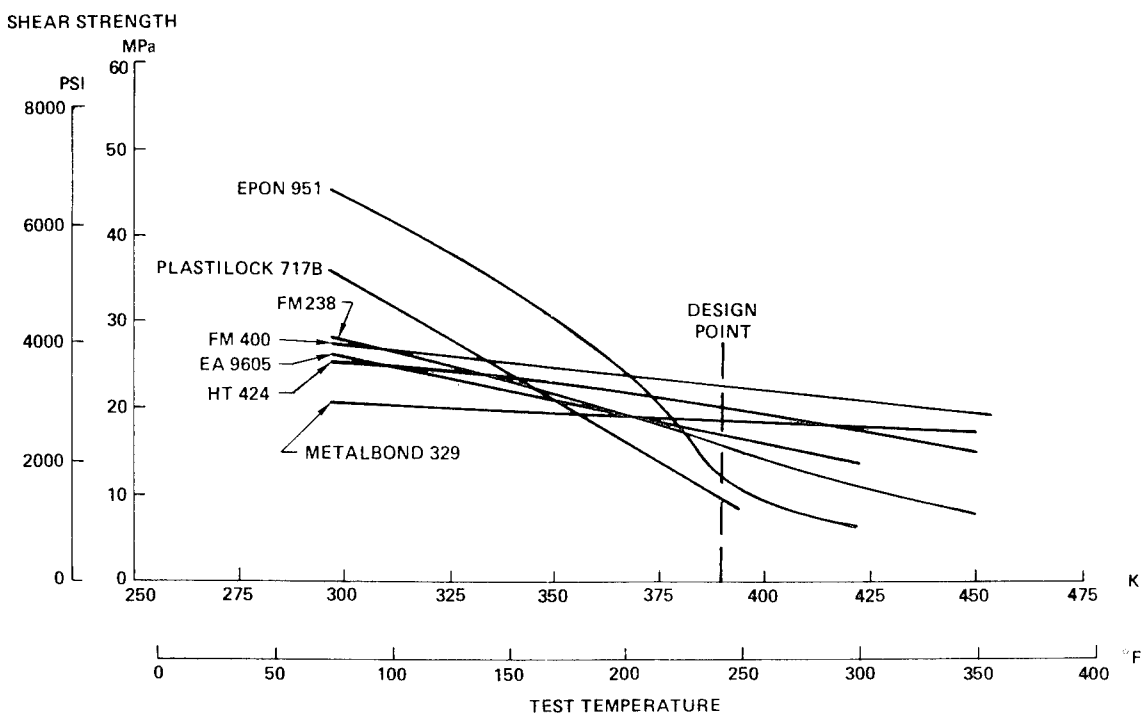


Figure 25. Tensile Lap Shear Strength of Various Adhesives

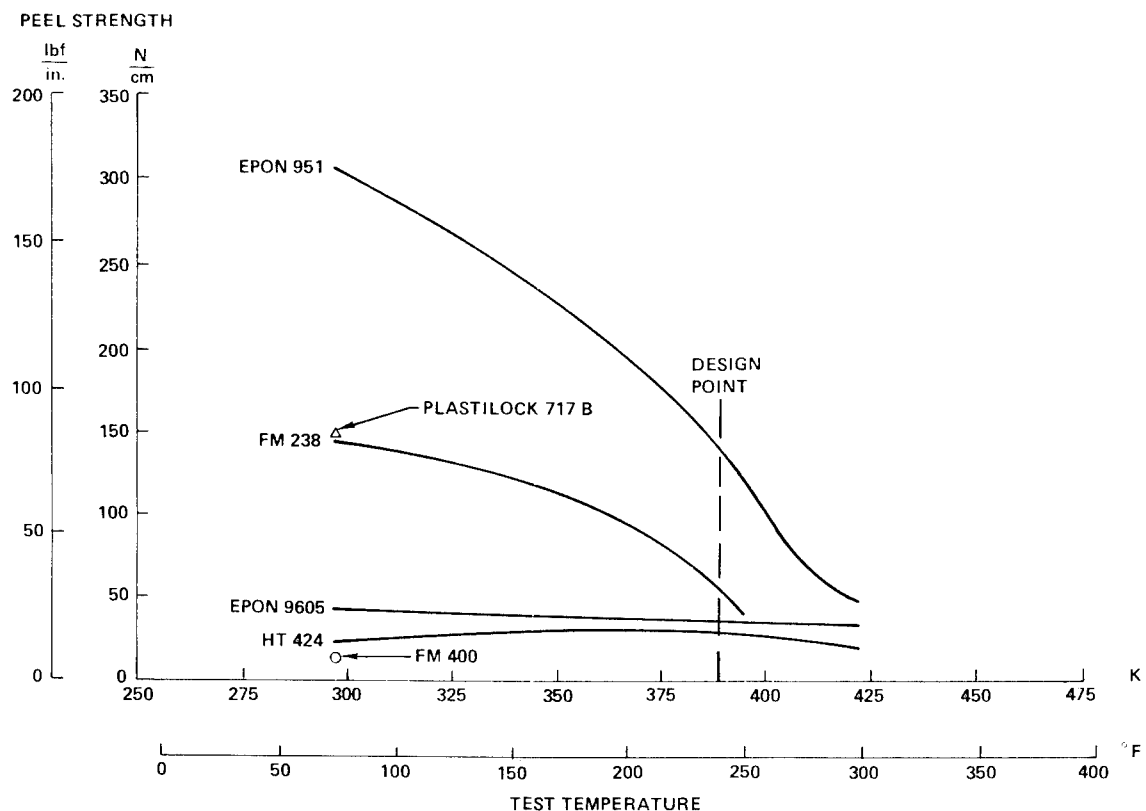


Figure 26. Peel Strength of Various Adhesives

APPENDIX B

THERMAL ANALYSIS METHODS

The parametric and final analyses for the actively cooled panel were performed using existing Bell Aerospace Textron thermal analyzer codes. One code determined the optimum passage size for a specified external heat flux, wall temperature, coolant temperature rise, passage shape and material properties. Upon completion of the passage sizing, more refined analyses were performed to define the temperature levels and distributions in the passage manifold and splice regions, including counterflow within the two redundant circuits. In this section, a brief description of the panel sizing program is provided; the thermal idealizations of the manifold and splice regions are presented; and the method used for assessing rivet temperature is described. Results are provided in the text of the report and in Appendix D.

Panel Sizing Procedure

The thermal suboptimizations, boxes 5, 6 and 7 of Figure 3, and the verification of cooling adequacy, Box 10 of Figure 3, were performed using the passage sizing computer code. An axial slice of the panel, containing one passage between isothermal lateral boundaries was analyzed; longitudinal conduction is not included. The analytical model is shown in Figure 27. Panel planform dimensions and applied heat flux specified in design requirements were held constant for all analyses. Other parameters that were kept constant included: sheet material (2024-T3), coolant (60% ethylene glycol/40% water), and coolant passage configuration (two quarter ellipses with combined width to height ratio of 4:1). Material choices are discussed in Appendix A. The elliptical passage configuration provides 90° corners which are desirable from a heat transfer point of view. In order to develop trade-off relationships the coolant inlet and outlet temperatures and the coolant passage spacing (number of passages) were varied.

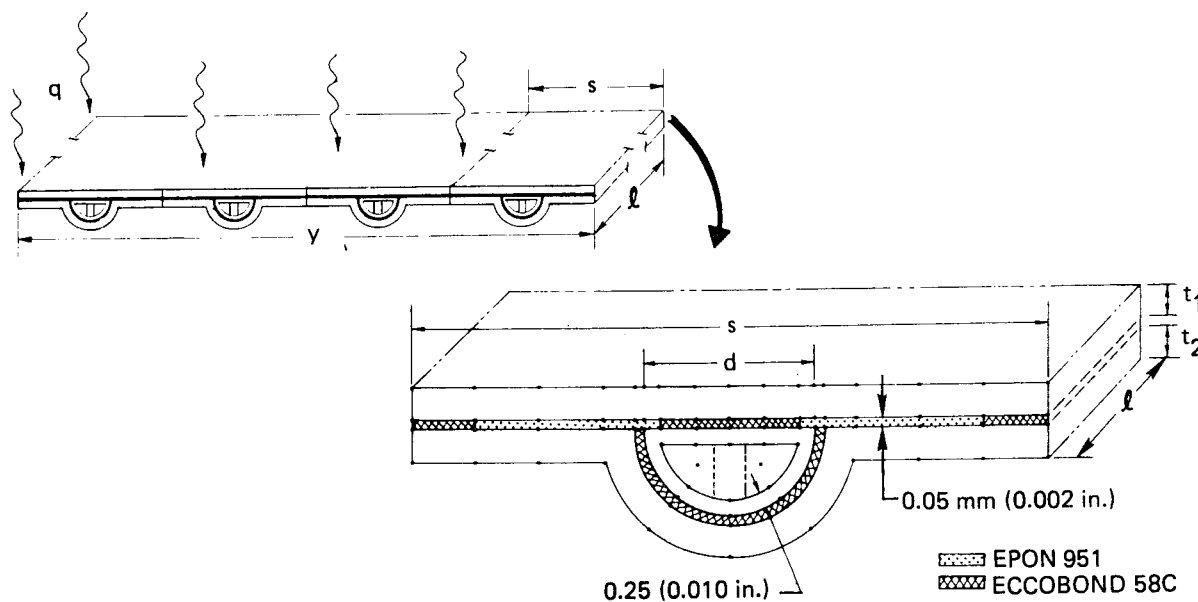


Figure 27. Panel and Discrete Passage Thermal Models

Input data includes incident heat flux, panel dimensional characteristics, material properties, inlet and outlet temperatures of the coolant, allowable panel temperatures, and a friction factor/ Reynolds number relationship. With this the code computes the total heat load and required coolant flow rate to the panel using the incident heat flux, panel width and panel length.

$$Q = q \cdot y \cdot l$$

$$\dot{m} = Q/C_p(T_o - T_I)$$

The following steps outline the sizing procedures and equations used for determining the final passage size and spacing.

1. On the basis of an assumed starting value for the optimization parameter, the passage size at the inlet is computed.
2. Employing this value for the passage size, the initial value passage spacing for the outlet station is computed from the following equation:

$$S - d = \sqrt{\frac{8k_s \cdot t (T_{max} - T_o)}{q}}$$

3. The flow rate in each passage is computed from the following equation:
$$\dot{m}_p = \dot{m} \frac{S}{y}$$
4. The Reynolds number in the passage is computed at each axial segment from the equation

$$Re_i = \frac{\dot{m}_p \cdot d_h}{A_p \cdot \mu_i}$$

where the *i* denotes the segment being analyzed.

5. At each segment, the heat transfer coefficient in the passage is computed employing one of the following equations:

If $Re < 2100$

$$h = 1.86 \frac{k_f}{d_h} Re_f^{0.33} Pr_f^{0.33} \left(\frac{d_h}{X} \right)^{0.33} \left(\frac{\mu_f}{\mu_s} \right)^{0.14}$$

If $2100 < Re < 10000$

$$h = 0.0000426 \frac{k_f}{d_h} Re_f^{1.5} Pr^{0.33} \left(\frac{\mu_f}{\mu_s} \right)^{0.14}$$

If $Re > 10000$

$$h = 0.027 \frac{k_f}{d_h} Re^{0.8} Pr^{0.33} \left(\frac{\mu_f}{\mu_s} \right)^{0.14}$$

6. The film temperature drop at each segment is computed from the equation

$$\Delta T_{f,i} = q/h_i$$

7. The wall temperature in the passage is computed as

$$T_{w,i} = T_{b,i} + \Delta T_{f,i}$$

If this value exceeds the saturation temperature of the coolant, subcooled boiling exists and an iteration technique is used for purposes of computing the actual wall temperature. The equation used for accounting for subcooled nucleate boiling was obtained from Reference 25 and is written as:

$$\frac{C_{pi} \Delta T_{f,i}}{h_{fg} Pr_l^{1/7}} = 0.013 \left[\frac{q_b/A}{\mu_f h_{fg}} \sqrt{\frac{g_c \sigma}{g (P_l - P_v)}} \right]^{0.33}$$

where

$$q_b = q_t \cdot h A_s (T_s - T_b)$$

8. The skin temperature at each segment is computed from the relationship:

$$T_{s,i} = T_{w,i} + \Delta T_{s,i}$$

where

$$\Delta T_{s,i} = \frac{(s - d)^2 q}{8k_s t}$$

9. If any of the wall temperatures along the panel exceed the maximum value specified in the input, the program increments the optimization parameter and recommences from Step 1 of the sizing procedure.
10. If all temperatures are more than 1K (2°F) below the desired maximum value, the passage spacing is refined on the basis of the most recent film temperature drops. The following equations are employed:

$$\Delta T_{s,i}^1 = T_{max} - T_{w,i}$$

$$(S - d)_i = \sqrt{\frac{8k_s t \Delta T_{s,i}}{q}}$$

The program selects the minimum of the (S-d) array and repeats steps 3 to 10 until the maximum temperature is achieved at some point on the panel.

11. After converging on the desired passage spacing and size (recalling that this is for only one value of the optimization parameter), the pressure drop through the passage is computed from the following relationship:

$$\Delta P_i = \frac{f_i l_i}{2g\rho_i d_h} \left(\frac{m_p}{A_p} \right)^2$$

where f_i is a function of Re_i and evaluated from the input table. The total pressure drop is:

$$\Delta P_t = \sum_{i=1}^n \Delta P_i$$

12. The pressure drop through the inlet and outlet are computed by the procedure outlined in Paragraph 3.4 of Reference 2 and because of its length, it will not be described in this report.
13. The manifold pressure drops are added to the passage pressure drop and this total is then used in the following equation to obtain the fuel requirements for the auxiliary power system.

$$W_{APS} = \frac{\dot{m}_v \cdot \Delta P \cdot \psi \cdot \eta}{550\rho A_v n}$$

where ψ is 2.0 lb/h-m for an oxygen-hydrogen system and η is the system efficiency which was selected as 80%.

14. The residual coolant weight in the panel is computed as

$$W_r = \frac{A_p \cdot l \cdot y}{S} \left(1 + \frac{y}{l} \right)$$

for a nonredundant system and may be the same or twice that amount for a redundant system depending on the details of the design.

15. The APS fuel weight and the residual weight are added to determine the total system weight.

16. The optimization parameter is then incremented by either a program input or by a programmed convergence procedure whichever the user prefers and steps 1 through 15 are repeated.

After sufficient data points are generated, the program then selects the passage size and spacing that yield the least weight panel.

Manifold Analysis

The passage sizing computer program considers the residual coolant mass and the pressure drop associated with the manifolds but does not analyze the heat transfer aspects. The temperature levels in the manifold region were computed with a general purpose thermal analyzer routine; the appropriate conduction and convection heat transfer equations are solved by a forward finite difference technique. The end of the manifold region was modelled by four longitudinal slices in the region illustrated in the figure of Table V. A total of 39 material nodes and four fluid nodes were used. Two of the four fluid nodes modelled the two plenums in the manifold and two modelled the two edge coolant passages.

By using the appropriate heat transfer coefficients in the manifold plenums it was possible to analyze the two different corners of the panel; diagonally opposite corners were identical because of the counterflow coolant circuitry. At two of the corners there is total inlet flow in the outboard plenum and only 1/20 of the outlet flow in the inboard plenum, see Figure 4. At the other two corners only 1/20 of the inlet flow is in the outboard plenum and total outlet flow is in the inboard plenum. As shown in Table V the corners with a low flow of the low temperature (inlet) coolant are hotter than those with high inlet flow.

Splice Analysis

After the fatigue tests at the Langley Research Center indicated the need for double shear splices along the transverse edges of the panel and tests at Bell indicated that an external titanium splice plate was desirable, it was necessary to analyze the design change. The same general purpose thermal analyzer code used for the manifold analysis was used for the splice region. The analytical model was based on the idealization of Figure 28 and represents the corner of the panel outboard of the centerline of the end rivet.

A uniform heat input of 136 kw/m^2 ($12 \text{ Btu/ft}^2 \text{ sec}$) was applied to the outer surface of the panel and was absorbed by the coolant flow in the manifold plenum. The heat incident on the manifold was conducted directly to the plenum wall. Heat incident on the titanium splice had to be transferred to the manifold through the contact resistance of the riveted joint. References 21 and 22 were used to determine the contact resistance for two different cases, one assumed a thermal conductance of $3123 \text{ W/m}^2 \text{ K}$ ($150 \text{ Btu/ft}^2 \text{ hr}^\circ\text{F}$) applied to the entire interface area, the other assumed a thermal conductance of $852 \text{ W/m}^2 \text{ K}$ ($550 \text{ Btu/ft}^2 \text{ hr}^\circ\text{F}$) applied to the projected area of the rivet head and no thermal conductance for the major portion of the interface. Results are discussed in Appendix D.

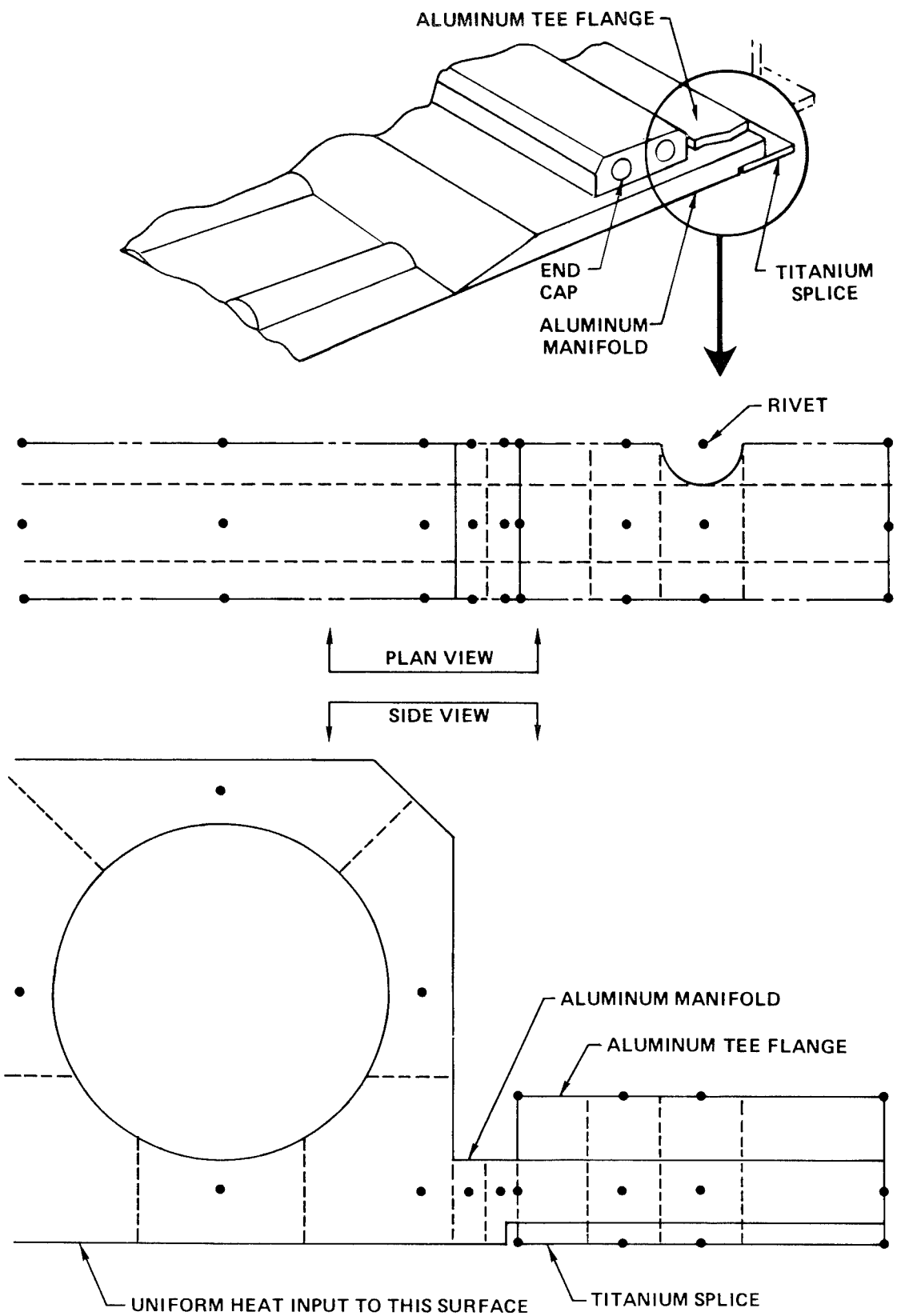


Figure 28. Manifold/Splice Thermal Model

Rivet Analysis

Because of the relatively high heat flux to which the panel will be subjected, rivets are of concern since they might constitute thermal discontinuities. Therefore, an analysis was conducted to estimate the temperature difference between a rivet and the panel structure. The analysis considered the aluminum alloy rivets used to join the skin panel to the substructure. Thermal conductance value was obtained from Reference 20. In this article, conductance is related to material parameters and pressure across the joint. The material parameters of thermal conductivity, density and Brinell hardness can be found in standard material data references. The pressure across the joint was estimated from the force required to yield the rivet shank thus setting the rivet. The thermal conductance of $11350 \text{ W/m}^2\text{K}$ ($2000 \text{ Btu/ft}^2\text{hr}^\circ\text{F}$) resulted in the rivet being 12K (22°F) hotter than the skin locally.

APPENDIX C

STRUCTURAL ANALYSIS METHODS

This appendix discusses the methods used to define the allowable strength of the construction material and to perform structural analyses of the cooled panel. Short time tensile, compressive and fatigue strengths were used to define dimensions of panel details and as measures against which structural integrity was assessed. Analyses were performed to check that the cross-sectional area of the panel provided the required life, to define the buckling strength of the panel, to compute thermal stresses in the central and manifold regions of the panel, to verify the adequacy of the stringer reinforcement in the manifold region, and to define the strength of the transverse joint.

Short Time Strength

All short time strength values were obtained from Reference 15. Room temperature strengths were degraded to account for 10,000 hours of prior exposure at 394K (250°F) and were degraded further to account for the local operating temperature. All degradation factors were obtained from Reference 15, and are summarized here.

<u>Mechanical Property</u>	<u>Factor* for 10,000 hrs at 394 K (250°F), Normal Operation</u>
F_{tu}	0.66
F_{ty}	0.77
F_{cy}	0.87
F_{su}	0.87
F_{bru}	0.87
E_c	0.90

*To obtain the allowable strength at 394 K (250°F) after 10,000 hours of exposure at 394 K (250°) multiply the room strength by the factor shown.

Fatigue Strength

Room temperature fatigue strength data from Reference 15 were degraded to account for 10,000 hours of prior exposure at 394 K (250°F), and to account for local temperatures using the temperature correction data of Reference 16. At 394 K (250°F) the reduction factor is 0.90. Stress concentration factors of 4.5 and 2.0 were used to rivet holes and on the unnotched surfaces. The latter factor was to account for the difference between laboratory specimens and as-fabricated structure. The results of the NASA fatigue tests suggest that this method of establishing fatigue allowables is conservative.

Verification of Fatigue Life

The thermal and mechanical loadings were combined as defined in Table II, and divided by the cross sectional areas of the panel at the mid length and through the rivets of the splice joint. The resultant stress distribution at each location was compared to local fatigue allowables. As long as the expected stresses were less than the appropriate allowables the design was deemed adequate.

Buckling Strength

The geometric proportions of the panel cross-section were selected from computer solutions which related the buckling strengths of optimized designs to the equivalent thicknesses of the designs. The optimization method is described in Reference 14. Only zee section stringers were evaluated. The designs were subjected to the constraints of available sheet thicknesses. Comparisons were made for 1 and 1.2 mm (0.04 and 0.05 in.) thicknesses. The equivalent thickness used for the design was defined by a fatigue analysis, see Figure 11. These analyses did not include the effect of the formed inner skin or the presence of the coolant passage tubing. Therefore, after the panel design was completed the cross-section was evaluated for buckling strength using the conventional column allowable method, Reference 14.

Thermal Stresses in Central Panel

Thermoelastic beam theory was used to compute thermal stresses in the central portion of the panel remote from the ends. The temperature distribution obtained from thermal analysis which did not include stringers, was multiplied by the αE product of the material for the appropriate local temperature. The resultant stress distribution was adjusted to equilibrate tensile and compressive thermal loadings over the panel cross-section including the stringers.

Thermal Stresses in Manifold Region

A finite element analysis was performed using the MAGIC code, Reference 24, to define thermal stresses in the manifold region. Only one quadrant of the panel was modelled, because of symmetry considerations, using 60 rectangular plate elements. The average local thickness was used for each element which was assumed to be at the average temperature of the area represented. Temperatures in the manifold region were obtained from the thermal analysis of the manifold. In the central portion of the panel the temperature variation perpendicular to the coolant passages was smeared across the element. The model is discussed along with results in Appendix D.

Stringer Reinforcement

Conventional analysis methods were used to compute the amount of area that had to be added to the stringer where it was cut away to clear the manifold. The inward displacement of the neutral axis was computed so that the local eccentric moment could be computed. Stress increments due to this eccentricity were added to the inplane loading.

Transverse Joint

The transverse splice joint was checked for rivet shear, shear tear-out, and bearing using conventional methods such as those given in Reference 15.

APPENDIX D

THERMAL AND STRUCTURAL ANALYSES RESULTS

This appendix summarizes results of thermal and structural analyses, performed in finalizing the details of the panel design. As such, they supplement the information provided in the text of the report.

Thermal

Emergency Operation – The body of the report presented the results of thermal analyses performed on the panel for the normal operating condition and on the manifold region for normal operating and emergency conditions. Panel temperatures for the emergency condition, one coolant loop inoperative, are presented in Figures 29 and 30 for longitudinal and transverse directions as related to the coolant tube. Because the coolant flow is halved from 3.4 kg/sec (7.4 lb/sec) to 1.7 kg/sec (3.7 lb/sec) when one loop is inoperative, the rise in coolant temperature is 106 K (190°F) rather than the 56 K (100°F) for the normal operating condition. Temperature dependent coolant specific heat prevents the temperature rise from doubling. As shown in Figure 29, the axial temperature variation in the panel material is essentially linear despite the somewhat nonlinear variation of coolant temperature. The temperature distribution perpendicular to the coolant passage at the inlet and outlet of the panel are shown in Figure 30. The maximum temperature difference is greatest at the inlet because of the relatively poor laminar heat transfer to the cold coolant, but the maximum temperature is not much higher than the design value for the panel. The 50 K (90°F) rise in coolant temperature is reflected in the temperature distribution at the outlet. The maximum panel temperature reaches 444 K (340°F) but the temperature difference is only 336 K (145°F), as compared to the maximum temperature of 400 K (260°F) and a temperature difference of 352 K (175°F) at the inlet.

Effect of Bondline Conductivity – The dual adhesive system in the outer-most bondline was dictated by the need for a high thermal conductivity. Figure 31 shows the relationship of panel temperature to thermal conductivity of the silver filled adhesive system. Vendor literature indicated a value of 8.65 W/m K (60 Btu-in./ft² hr°F) which was used for design purposes. Later measurements that NASA had performed on two bondline thicknesses of the silver filled epoxy indicated thermal conductivity values of between 0.43 and 2.88 W/m K (3 and 20 Btu-in./ft² hr°F). At the higher measured value panel temperatures would be very slightly higher than predicted. At the lower value there is a 78 K (50°F) increase but panel temperatures are still acceptable for aluminum.

Rivet Heating – Because there is a thermal contact resistance between the flush rivets and the outer skin, a thermal analysis was conducted to determine the temperature increase at the rivet head. Heat was assumed to flow only through the head of the rivet to the skin and not down the shank and through the upset head. The load across the interface was assumed to be the tensile yield strength of the aluminum rivet (this was assumed for the titanium Cherrybuck rivets also). The thermal conductance across the joint was conservatively estimated to be 11350 W/m² K (2000 Btu/ft² hr°F) using Ref. 22. The rivet heat was found to be 12 K (22°F) hotter than the panel skin. The decrease in rivet preload is less than 10%.

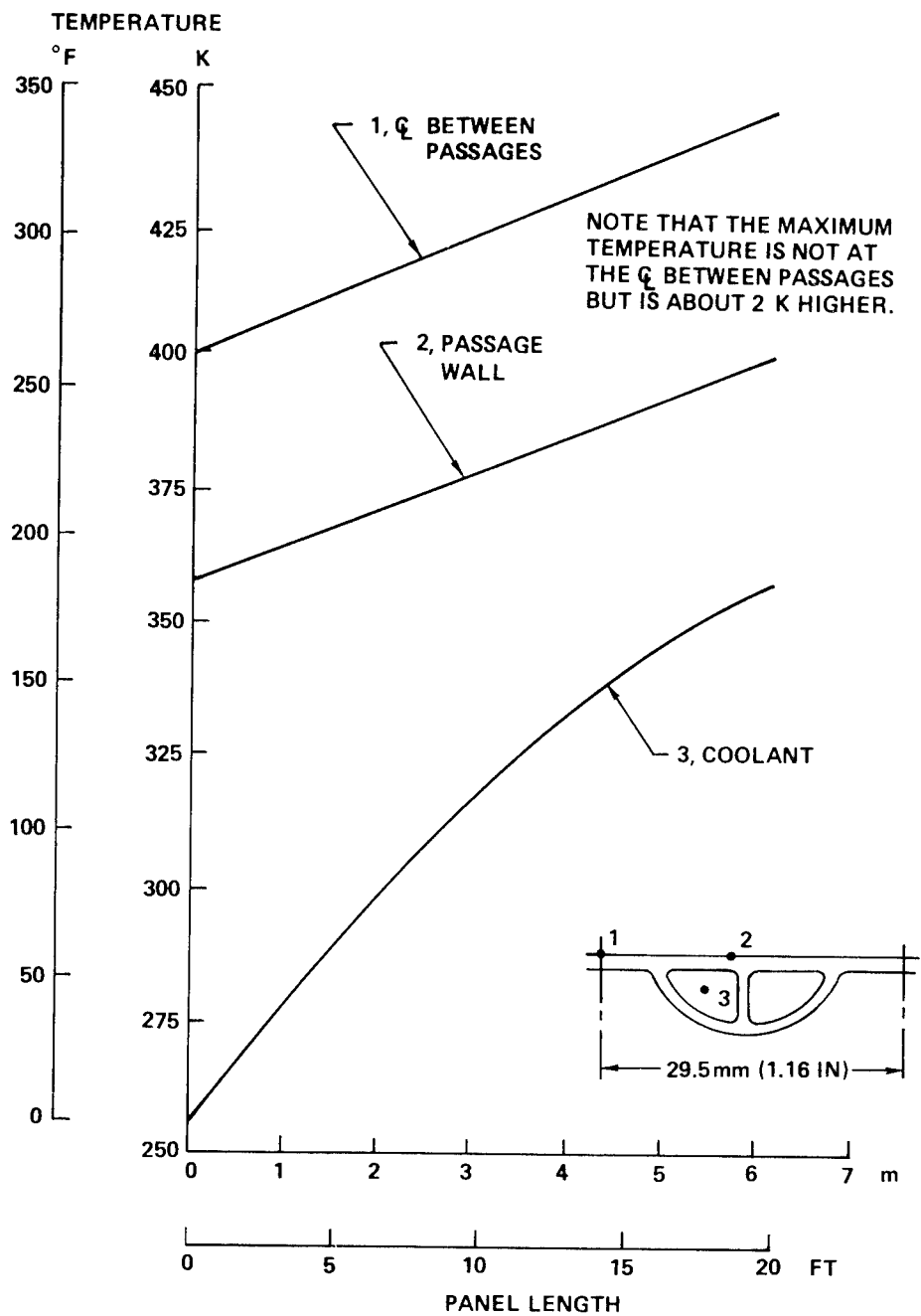


Figure 29. Axial Temperature Distribution, Flow in Half the Cooling Passages

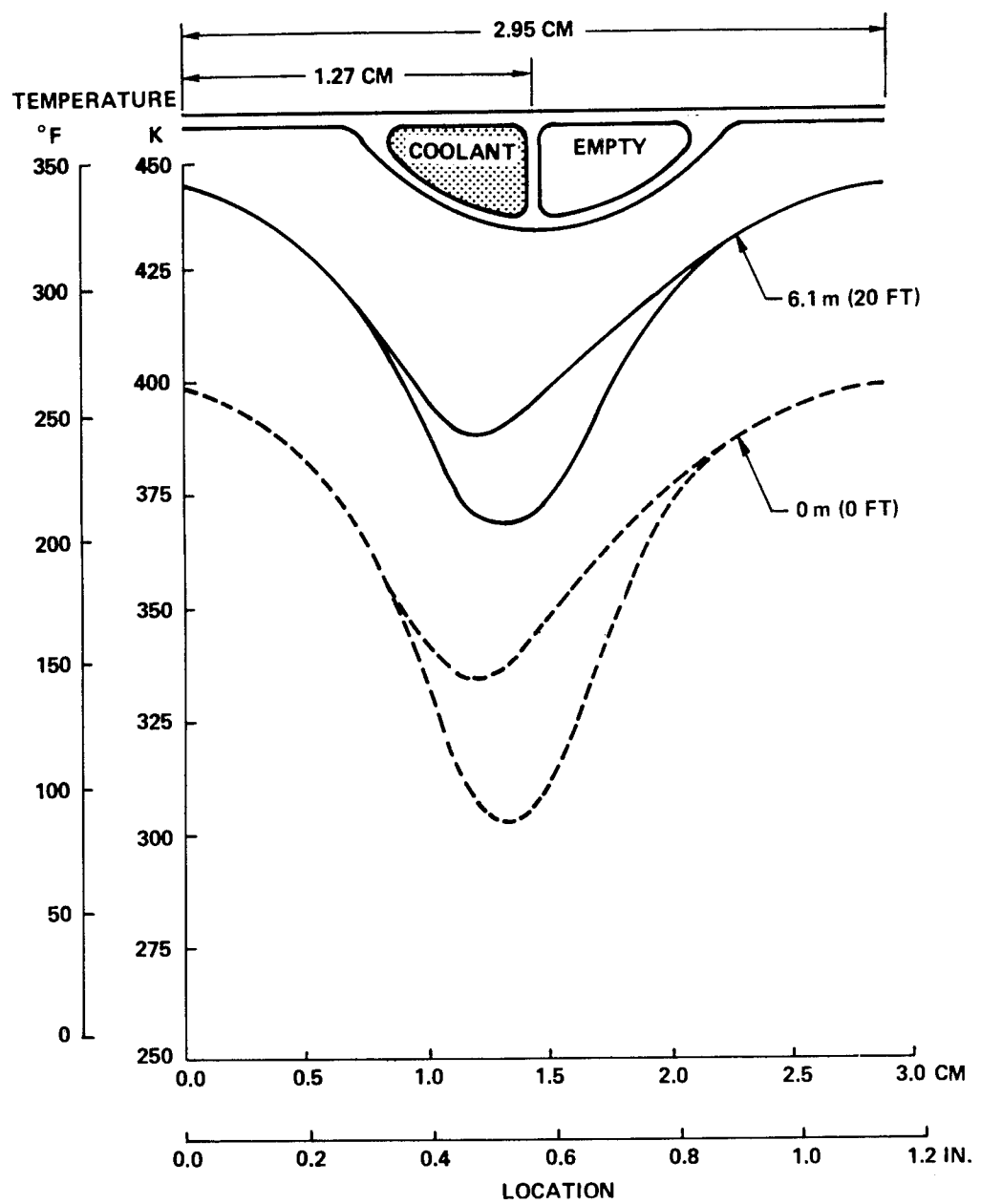


Figure 30. Temperature Distribution at Inlet and Outlet, Flow in Half the Coolant Passages

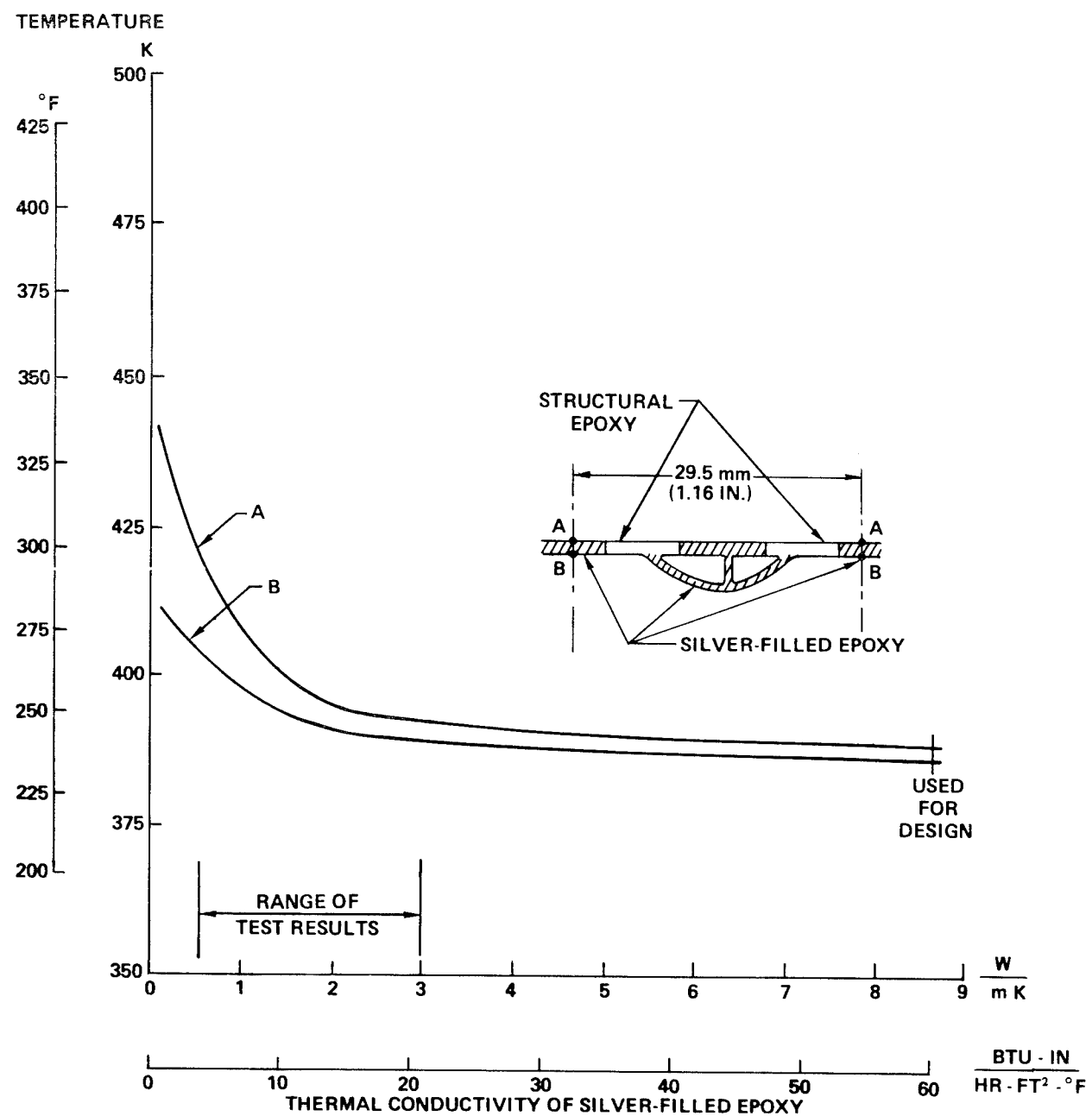


Figure 31. Effect of Bondline Conductivity on Maximum Skin Temperature

STRUCTURAL

After the equivalent thickness of the panel was determined by fatigue life and minimum mass considerations, the mass was proportioned between the skin and the stiffeners. Then it was necessary to conduct analyses to define various panel details. The latter analyses are reported here; they included: (1) the transverse joint, (2) cutout, (3) skin crippling, (4) manifold web, (5) manifold end cap joint, (6) coolant passage tubing, and (7) thermal stresses induced by the transverse manifolds.

Transverse Joint — This joint, as analyzed, was a single shear configuration. After the NASA/Langley fatigue specimen tests indicated the need for a double shear configuration the titanium strap was added and cherrybuck rivets were introduced. Their selection was based on fatigue test results, see Appendix E; no analysis was performed except for the titanium splice thickness which was selected to approximate the strength of the flange of the aluminum tee. This doubled the calculated static strength of the joint.

For the single shear design, HS47 fasteners were selected. At room temperature the 8080 N (1820 lb) shear strength and 15 mm (0.58 inch) spacing resulted in a joint strength of 611 kN/m (3510 lb/in.). The lower splice (across the stringer flanges) adds 85 kN/m (490 lb/in.) so that the total strength of the splice is 696 kN/m (4000 lb/in.). This is well above the ± 210 kN/m (± 1200 lb/in.) design level even when prior exposure, temperature and fatigue effects are considered. The basic problem of the single shear design was the moment introduced by the eccentricity of the shear forces in the panel edge and the inner splice plate (the flange of the tee that is the cap of the frame).

Under emergency operating conditions, it is not necessary to consider long life; the design allowable may be based on 1/2 hour exposure at temperature. For this analysis it was assumed that the manifold region had been operating for 10,000 hours at a temperature of 436°K (325°F) before the emergency condition was encountered. This led to the reduction of ultimate and yield strengths to levels that were between 60 and 72% of room temperature values for virgin material. Using the appropriate areas for tension, bearing, and shear tearout, stress levels were determined and compared with design allowable strengths. A comparison of the stress levels with the room temperature strength after exposure indicated ratios of 0.27, 0.48, and 0.59 for tension, bearing, and shear, respectively. If the 210 kN/m (1200 lb/in.) is considered to be a limit load, the joint can sustain that loading based on yield strength allowables (or 331 kN/m (1800 lb/in.) based on ultimate strength) at all temperatures up to 527 K (490°F). If a reduced load carrying capability is allowed, for example, considering the 210 kN/m (1200 lb/in.) to be the ultimate load, the allowable splice temperature would increase to 527 K (550°F). Reference to Table V indicates that the maximum temperature in the aluminum portion of the splice is 494 K (430°F).

The strength of the double shear joint is significantly higher than that of the single shear joint.

Cut-Out — In the region of the manifold plenums the outer flange of the stringer and part of the web must be cut away for clearance, see Figure 14. The inner flange was reinforced to stabilize the inner flange and cut web and to compensate for the loss in stringer area. The 46.5 mm² (0.072 in.²) of stringer that was removed was replaced with 56.8 mm² (0.088 in.²) as a small channel riveted to the stringer web and nested against the uncut flange of the stringer. Although the neutral axis was shifted by about 5.0 mm (0.20 in.) the induced moment produced an increase in local loading of 15% which was compensated by an increase of 42% in local moment of inertia.

Skin Crippling — Stability of the skin was checked using the moment of inertia of the outer skin, the beaded skin and the coolant passage tubing, 114 mm^2 ($27.4 \times 10^{-5} \text{ in.}^4$), to compute an effective skin thickness (2.8 mm (0.112 inch)). At the b/t ratio for the design, 28.2, the allowable was equal to the compressive strength of the material.

Manifold Web — The manifold web between the two counterflow plenums is loaded by the internal pressure in each. When both are pressurized to the ultimate level of 2.2 MPa (320 psig) and tolerances are taken into account to define the minimum web thickness, 1.6 mm (0.062 in.), an ultimate stress of 1380 kN/m^2 (13,200 psi) is generated. This is well within the strength limit of the 2024-T3 manifold. Other regions around the plenums are exposed to only half of this stress level.

Manifold End Cap — The manifold end caps close the plenums, are bonded in place and each joint is reinforced by two shear pins, see Figure 14. In assessing the adequacy of the joint the contribution of the shear pins was neglected. The ultimate pressure in the plenum of 2.2 MPa (320 psig) generates a force of 430 N (97 lb) and a bond shear stress of 1900 kN/m^2 (276 psi). This is well within the shear strength of the adhesive. Test results verified structural integrity.

Coolant Passage Tubing — When the coolant circuits are pressurized the long flat side coolant passage (which is bonded to the outer skin) tends to bulge. The maximum stress generated is $95,800 \text{ kN/m}^2$ (13,900 psi) ultimate. The corresponding local deflection is less than 0.018 mm (0.0007 inch). The stress in the webs between passages is $32,400 \text{ kN/m}^2$ (4700 psi).

When one of the coolant circuits is pressurized and the other is not the wall between them is subjected to a pressure loading. The resultant stress is $81,400 \text{ kN/m}^2$ (11,800 psi).

Thermal Stresses Due to Manifolds — Using the temperature distributions computed in the manifold region for normal and emergency operating conditions, see Table V, thermal stresses were computed using the structural idealization shown in Figure 32. Inasmuch as the temperature differences in the manifold region were of primary interest, the temperature distribution between coolant passages was smeared and relatively large elements were used. A finer grid was used in the manifold region where temperature variations were more severe. Reference to the manifold temperatures of Table V indicates a slight increase in temperature near the corner and long edges. Thus, the modeling near the edge is somewhat finer. It was assumed conservatively that the frames would prevent any out of plane distortion of the panel. Analysis conducted on a prior panel design had indicated a significant relief if such out of plane motion was allowed.

Thermal stresses are presented in Table IX for the temperature distribution experienced under normal operating conditions. Stresses parallel to the coolant passages (perpendicular to the manifolds) are quite low except near the long edge of the panel where very localized compressive stresses reach about $42,000 \text{ kN/m}^2$ (6100 psi) and are balanced by localized tensile stresses that are as high as $19,600 \text{ kN/m}^2$ (2840 psi). Note that all elements that have significant tensile thermal stresses in the direction parallel to the coolant passages (such that they would add to the in-plane loading stresses) are in the manifold region where the average equivalent thickness is in excess of 3.8 mm (0.15 inch) so that air load stresses here, 55000 kN/m^2 are about 40% lower than in the skin panel remote from the manifolding. Maximum thermal stresses are experienced parallel to the manifold (perpendicular to the coolant passages) with maximum compressive levels of $86,900 \text{ kN/m}^2$ (12,600 psi) and maximum tensile values of $111,900 \text{ kN/m}^2$ (16,230 psi). At the highest temperature in the splice region, the compressive yield allowable is estimated to be greater than $137,900 \text{ kN/m}^2$ (20,000 psi). The maximum tensile stresses are in regions of low temperature where yield allowables are equal to or greater than $275,800 \text{ kN/m}^2$ (40,000 psi).

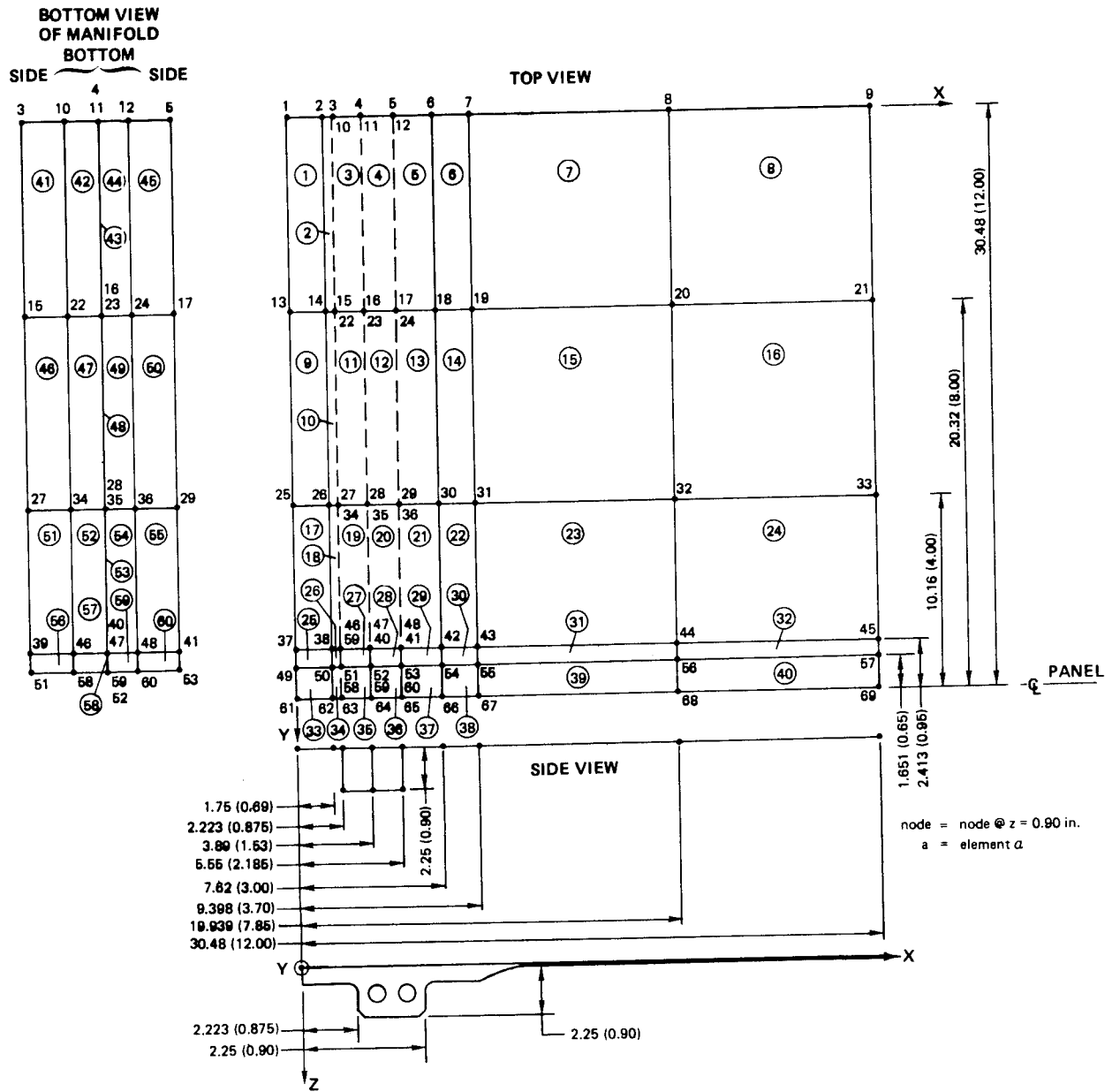


Figure 32. Manifold Finite Element Idealization. Dimensions are Given in cm (in.).

TABLE IX
NORMAL OPERATING THERMAL STRESSES*

Element	σ_x		σ_y		σ_z		Element	σ_x		σ_y		Element	σ_x	
	kN/m ²	psi	kN/m ²	psi	kN/m ²	psi		kN/m ²	psi	kN/m ²	psi		kN/m ²	psi
1	-1413	-205	-86736	-12580			31	-2641	-383	-7543	-1094			
2	-1724	-250	-42472	-6160			32	-3116	452	1193	173			
3	-951	-138	3178	461			33	14300	2074	-13286	-1927			
4	524	76	15044	2182			34	-4123	-598	7433	1078			
5	524	76	9142	1326			35	-27813	-4034	16244	2356			
6	-545	-79	-303	-44			36	-42292	-6134	46822	6791			
7	-1324	-192	-1882	-273			37	-33481	-4856	2365	343			
8	-186	-27	-896	-130			38	-41362	-5999	5502	-798			
9	-2372	-344	-85123	-12346			39	-34115	-4948	-3434	-498			
10	-4675	-678	-38176	-5537			40	-12673	-1838	1220	177			
11	-5150	-747	5943	862			41			5013	7979			
12	-4578	-664	14031	2035			42			111874	16226			
13	4468	648	5633	817			43			61101	8862			
14	-1344	-195	-4164	-604			44			94210	13664			
15	1565	227	3489	506			45			48600	7043			
16	-241	-35	-1427	-207			46			61749	8956			
17	1565	227	64535	9360			47			120782	17518			
18	7915	1148	-13576	-1969			48			64576	9366			
19	12004	1741	22429	3253			49			2117	307			
20	13817	2004	16361	2373			50			94279	13674			
21	11314	1641	5626	816			51			42782	6205			
22	10880	1578	9797	-1421			52			49511	7181			
23	7219	1047	-8088	-1173			53			71699	10399			
24	2951	428	-165	-24			54			41437	6010			
25	3627	526	-33895	-4916			55			45905	6658			
26	13838	2007	4937	716			56			16844	2443			
27	19547	2835	25676	3724			57			19967	-2896			
28	14189	2058	10942	1587			58			22180	3217			
29	10053	1458	3813	553			59			4540	31302			
30	4261	618	8943	-1297			60			4930	715			

Note: The subscripts (x, y, and z) refer to the system, not the local axis

x is the longitudinal direction

y is the latitudinal direction

z is normal to the panel

*Where there are no entries, stresses are less than 173 kN/m² (25 psi)

For the emergency operating conditions, the high temperature corner of the panel experiences the thermal stress of Table X. Maximum thermal stresses parallel to the coolant passages are $51,000 \text{ kN/m}^2$ (7400 psi) in compression and $27,400 \text{ kN/m}^2$ (3980 psi) in tension, while parallel to the manifold they are $75,000 \text{ kN/m}^2$ (10,875 psi) in compression and $84,700 \text{ kN/m}^2$ (12,280 psi) in tension. All were well within the range of 1/2 hour allowables. The larger temperature difference in the coolest corner results in higher thermal stresses, Table XI, $51,700 \text{ kN/m}^2$ (7500 psi) in compression and $20,700 \text{ kN/m}^2$ (3000 psi) in tension parallel to the coolant passages and $72,400 \text{ kN/m}^2$ (10,500 psi) in compression and $147,500 \text{ kN/m}^2$ (21,387 psi) in tension parallel to the manifold. Nevertheless, all are well below the 1/2 hour exposure strengths.

Because the thermal stresses change slowly no stress concentration factors were applied to them directly. As noted in Table II, the thermal stress was treated as a steady component and a cyclic component. The cyclic component was combined with the cyclic air loading and stress concentration factors of 2.0 and 4.5 were applied to the combination to account for rivet holes in the skin and splice, respectively.

Summary of Panel Stresses – Stresses at various points in the panel have been discussed in the body of the report and in this Appendix. It is appropriate here to summarize the major stresses in the skin and manifold regions of the panel as an aid in recognizing the realism of the levels as compared to current subsonic aircraft practice. Stresses are summarized parallel and perpendicular to the coolant passages for the normal operating and emergency conditions.

Normal Operation

Skin, Parallel to Passages	$51,000 \pm 127,000 \text{ kN/m}^2$ (7,400 \pm 18,500 psi)
Skin, Perpendicular to Passages	Essentially Zero
Manifold, Parallel to Passages	$9,800 \pm 63,500 \text{ kN/m}^2$ (1,420 \pm 9,220 psi)
Manifold, Perpendicular to Passages	$60,000 \pm 60,000 \text{ kN/m}^2$ (8,710 \pm 8,710 psi)

Emergency Condition, Hot End

Skin, Parallel to Passages	$52,700 \pm 129,000 \text{ kN/m}^2$ (7,650 \pm 18,750 psi)
Skin, Perpendicular to Passages	Essentially Zero
Manifold, Parallel to Passages	$13,700 \pm 67,500 \text{ kN/m}^2$ (1,990 \pm 9,790 psi)
Manifold, Perpendicular to Passages	$42,300 \pm 42,300 \text{ kN/m}^2$ (6,140 \pm 6,140 psi)

Emergency Condition, Cold End

Skin, Parallel to Passages	$66,900 \pm 143,000 \text{ kN/m}^2$ (9,700 \pm 20,800 psi)
Skin, Perpendicular to Passages	Essentially Zero
Manifold, Parallel to Passages	$10,100 \pm 63,900 \text{ kN/m}^2$ (1,470 \pm 9,270 psi)
Manifold, Perpendicular to Passages	$73,700 \pm 73,700 \text{ kN/m}^2$ (10,700 \pm 10,700 psi)

TABLE X
HOT END - EMERGENCY CONDITION THERMAL STRESSES*

Element	σ_x		σ_y		σ_z		Element	σ_x		σ_y		σ_z
	kN/m^2	psi	kN/m^2	psi	kN/m^2	psi		kN/m^2	psi	kN/m^2	psi	
1	386	56	-74980	-10875	-6191	-887	31	14451	2096	-1248	-181	
2	614	89	-42685	-6116			32	10790	1565	-490	-71	
3	993	144					33	27462	3983	-10315	-1496	
4	917	133	17919	2599			34	22587	3276	4054	588	
5	310	45	17168	2490			35	-1896	-275	8715	1264	
6	2344	340	6095	884			36	-21718	3150	5026	729	
7	3447	500	3978	577			37	-22277	3376	2261	328	
8							38	-37583	-5451	-1820	-264	
9	-5640	-818	-73829	-10708			39	-5014	-7399	-1793	-260	
10	9942	-1442	41975	6088			40	-25759	-3736	965	140	
11	-9529	-1382	-6522	-946			41			49746	7215	1172
12	7660	-1111	15637	2268			42	1034	150	49822	7226	170
13	-6302	-914	17830	2586			43			42258	6129	1379
14	-6874	-997	11218	1627			44	517	75	84419	12244	200
15	-6846	-993	6088	883			45			60040	8708	938
16	5757	-835	1731	251			46			2958	429	136
17	179	26	-53889	-7816			47	-945	-137	48739	7069	-459
18	5454	791	-17154	-2488			48			40782	5915	-2316
19	9370	1359	10866	1576			49	896	130	84668	12280	-336
20	11666	1692	15196	2204			50			60184	8729	-1455
21	11473	1664	11818	1714			51			5337	774	-211
22	18630	2702	3916	568			52	-1372	-199	21257	3083	73
23	22946	3328	2792	405			53			24373	3535	
24	12031	1745	-1207	-175			54	-1276	-185	45106	6542	
25	8791	1275	-26510	-3845			55			32449	4702	
26	20000	2900	3000	435			56			6957	1009	3106
27	22615	3280	17913	2598			57	12700	1842	-958	-139	
28	18402	2669	10921	1584			58			9384	1361	1680
29	13617	1975	3992	579			59	-862	-4737	687	11583	
30	14865	2156	-4654	-675			60			8508	1234	7295

*Where there are no entries stresses are less than 173 kN/m^2 (25 psi)

TABLE XI
COLD END - EMERGENCY CONDITION THERMAL STRESSES*

Element	σ_x		σ_y		σ_z		Element	σ_x		σ_y		σ_z
	kN/m^2	psi	kN/m^2	psi	kN/m^2	psi		kN/m^2	psi	kN/m^2	psi	
1	-1620	-235	-68313	-9908			31	6619	960	9473	-1374	
2	-1917	-278	-27055	-3924			32	14886	2159	1482	215	
3	-1910	-277	68888	999			33	3123	453	-12638	-1833	
4	-1331	-193	9522	1381			34	-20643	-2994	6674	968	
5	-172	-25	6143	891			35	-40672	-5899	16968	2461	
6	1379	200	-14810	-2148			36	-51566	-7479	3882	563	
7	2193	318	-24656	-3576			37	39921	-5790	3565	517	
8	1365	198	-400	-58			38	-53738	-7794	5778	-838	
9	290	42	-72285	-10484			39	-49553	-7187	5548	-809	
10	-200	-29	-26910	-3903			40	20195	2929	1848	268	
11	-1179	-171	9756	1415			41		73319	10634	-1924	-279
12	-1200	-174	10287	1492			42	-4158	-603	133145	19311	
13	-2654	-285	3123	453			43		67217	9749	-1917	-278
14	-3420	-496	-20333	-2949			44	-3192	-463	96644	14017	
15	-6846	-993	-25897	-3756			45		39293	5699	-979	-142
16	-7619	-1105	696	101			46		80993	11747	-2213	-321
17	1213	176	-59005	-8558			47	-4054	-588	147458	21387	
18	6653	965	-10756	-1560			48		73484	10658	-2296	-333
19	11445	1660	23215	3367			49	-2944	427	101250	14685	
20	13397	1943	12438	1804			50		35860	5201	-2413	-350
21	11466	1663	3771	547			51		60295	8745	414	60
22	13624	1976	-17099	-2480			52	-2889	419	89577	12992	
23	16017	2323	-17899	-2596			53		49422	7168	1448	210
24	11039	1601	903	131			54	1793	260	53303	7731	
25	-1282	-186	-32295	-4684			55		12424	1802	1289	187
26	5343	75	3351	486			56		35894	5206	50911	7384
27	13004	1886	24573	3564			57	-27986	-4059	24180	3507	
28	9560	1343	7543	1094			58		28675	4159	41472	6015
29	7660	1111	14755	2140			59	-14941	-2167		794	
30	5081	737	-8915	-1293			60		5474	32178	4667	

*Where there are no entries, stresses are less than 173 kN/m^2 (25 psi)

APPENDIX E EXPERIMENTAL RESULTS

When developing a new design concept, experimental verification of its main features is a desirable prelude to prototype fabrication. The NASA requirements dictated certain test specimens for evaluation of major characteristics at the Langley Research Center. These test specimens and others tests at Bell were cut from a single 0.61×1.22 m (2 x 4 ft) panel, Figure 33, which closely resembled the cooled skin of the deliverable test panel. Because other aspects of the cooled panel design could not be totally defined by parametric studies and analyses, additional tests were conducted at Bell. The Bell tests focused primarily on the choice of adhesives and in the verification of design changes and fabrication techniques. This Appendix summarizes the types of specimens used and the results obtained.

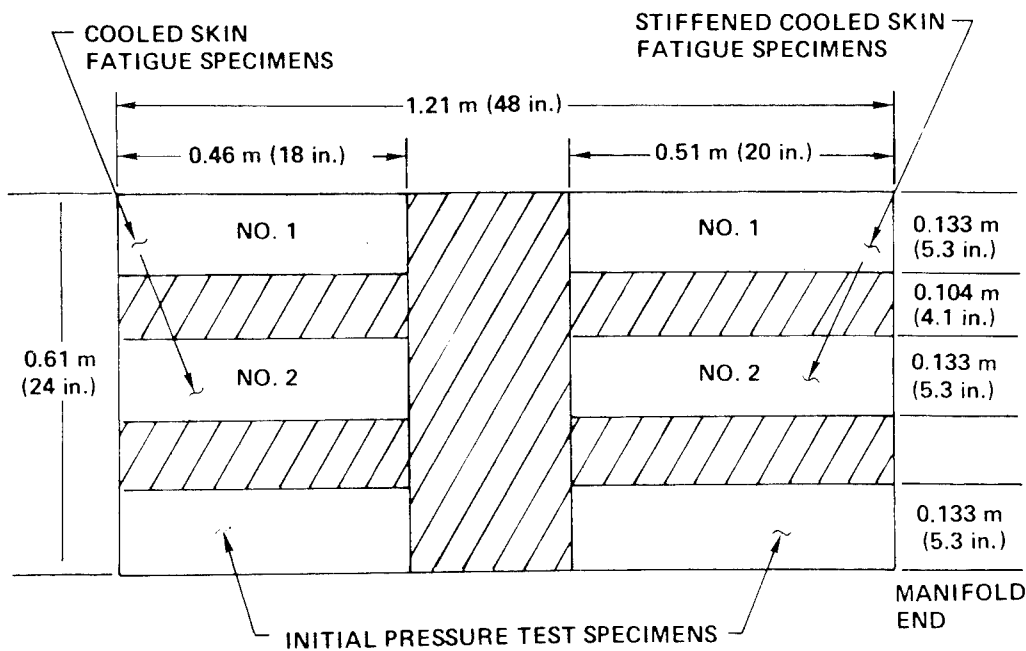


Figure 33. Fatigue and Pressure Test Specimens Were Cut From a Cooled Skin Panel

Test Specimens

Table XII provides summary descriptions of the developmental test specimens. Two categories are indicated, one for the specimens tested in the NASA Langley Research Center and another for those specimens tested at Bell. The purpose of the two bonded skin fatigue specimens, Figure 13, was to assess the suitability of the dual adhesive bonding technique with regard to fatigue life. The coolant passage/ramp specimens, Figure 13, investigated the fatigue behavior of the transition from the coolant distribution manifold to the individual coolant passages within the skin. In each specimen a 10×10 mm (0.4 x 0.4 in.) patch of Teflon replaced a similar area of adhesive on the sloping portion of the transition to simulate voids which could accentuate peeling of the inner skin from the manifold ramp. The purpose of the stiffened cooled skin fatigue specimens, Figure 14, was to verify the structural integrity of the edge attachment and stringer integration.

TABLE XII
DESCRIPTION OF DEVELOPMENTAL TEST SPECIMENS

Type	Quantity	Description	Purpose
1. Required for Preliminary Testing by NASA			
a. Bonded Skin Fatigue Specimens* (see Figure 13)	2	0.08 mm (0.032 in.) and 0.5 mm (0.020 inch) 2024-T3 Aluminum Alloy Skins bonded with alternate stripes of Epon 951 and Eccobond 58C adhesives; loading plates bonded to ends.	Establishment of the fatigue life of the basic bonded skin.
b. Cooled Skin Fatigue Specimens* (see Figure 13)	2	Selected cooled panel configuration and materials. Small teflon patches locally replaced adhesive on skin to manifold transition to simulate voids; loading plates bonded to ends.	Establishment of the fatigue life of the cooled panel as influenced by the skin to manifold transition.
c. Stiffened Cooled Skin Fatigue Specimens* (see Figure 14)	2	Selected cooled panel configuration and materials including edge attachment design; loading adapters bonded and mechanically fastened.	Verification of structural integrity of edge attachment and stiffeners.
2. Additional Specimens for Testing by Bell			
a. Manifold End Plug Specimens (see Figure 34)	11	4.8 mm (0.188 in.) and plugs bonded into simulated manifolds with four different adhesives; all metal parts were 2024-T3 Aluminum alloy.	Selection of adhesive for bonding manifold end plugs.
b. Coolant Tube End Plug Specimens (see Figure 35)	8	Sections at coolant tubing with one end potted with each of three candidate adhesives and a pressure fitting at other end.	Selection of adhesive for potting tube ends.
c. Initial Pressure Test Specimens* (see Figure 33)	2	Selected cooled panel configuration and materials; included coolant passages and manifold.	Verification of pressure carrying capability.
d. Improved Pressure Test Specimens (see Figure 33)	2	Similar to 2c but a different fabrication/inspection sequence was used.	Verification of improved processing and demonstration of pressurization integrity.
e. Manifold Repair Specimen (see Figure 22)	1	Short section of manifold with pressure fittings; manifold to passage holes plugged with adhesive; three unset countersunk rivets and three blind rivets were bonded in place; heads were shaved flush.	Verification of technique to repair manifold after milling to remove excess adhesive in manifold to passage holes.
f. Joint Fatigue Test Specimens (see Figure 36)	15	Single fastener single and double shear configurations evaluated four fastener types and two nominal diameters.	Verification of corrective action to eliminate large deformation observed on stiffened cooled skin fatigue specimen.

*These specimens were cut from a single 0.61 x 1.22 m (2 x 4 ft) panel, see Figure 33, which incorporated crack arrestors.

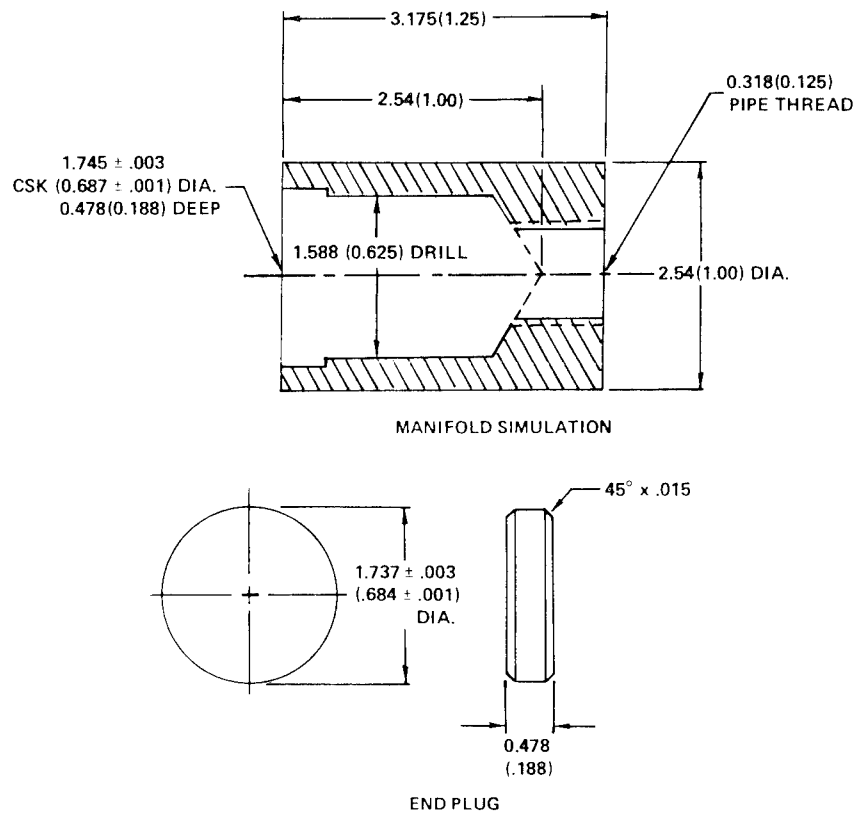


Figure 34. Manifold End Plug Test Specimen 2024-T3 Aluminum Alloy

The purpose of the manifold end plug and coolant tube end plug specimens, Figures 34 and 35, was to evaluate adhesives for bonding aluminum end plugs into the manifolds and for potting the ends of the coolant passage tubing.

Inasmuch as the coolant passage/ramp specimens and stiffened cooled skin fatigue specimens indicated the presence of leaks between the inner and outer structural skins four pressure test specimens were evaluated at Bell to investigate the nature of the internal leakage problem. The initial two specimens were cut from the same large panel as used for the Langley test specimens (see Figure 33). They were similar to the specimen shown in Figure 15, but did not have stiffeners or end loading plates. The two improved specimens were similar but were made especially for proof testing. While generally similar to the initial pressure test specimens, the last two incorporated different adhesive details for bonding the coolant passage tubing to the manifolds.

The manifold repair specimen, Figure 22, consisted of a 10 cm (4 in.) length of manifold with a pressure port bonded into one end of each plenum and an end plug bonded into the other. Three unset countersunk flush head aluminum alloy rivets were bonded into holes along one of the walls of one plenum. Three blind aluminum alloy rivets were bonded into holes in the wall of the other plenum. All rivet diameters were 4 mm (0.156 in.). This specimen was necessary because of the procedure required to remove adhesive from some of the holes which transition from the manifold to the coolant from the outboard manifolds to the coolant passage tubing. It was necessary to remove the adhesive by drilling through the outer surface of the manifold. The entry holes had to be plugged and the technique to be used, verified experimentally.

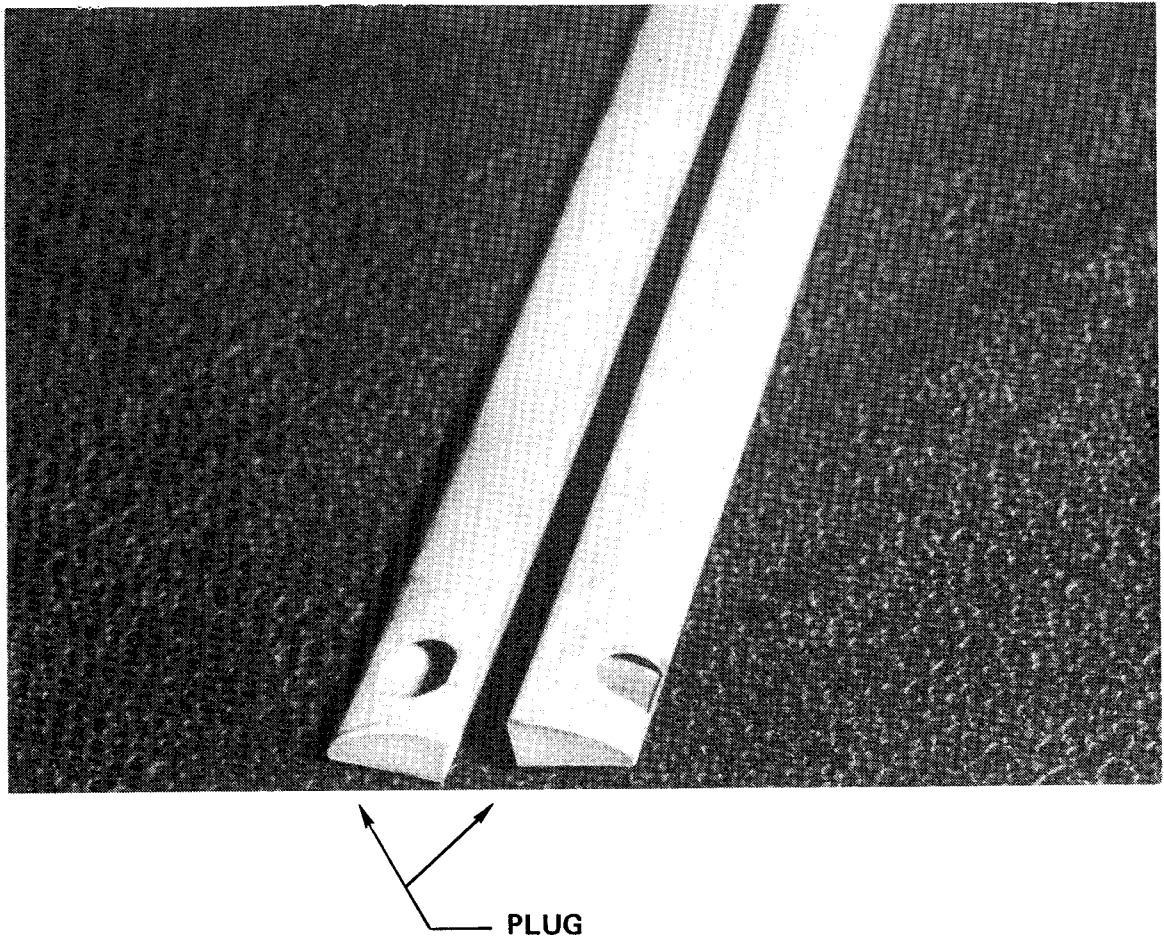


Figure 35. Coolant Passage Tube End Plug (Test Specimens Did Not Have Holes to Match Manifolding)

Of the 15 single fastener specimens illustrated in Figure 36, two were loaded to failure under increasing tensile loading and 13 were fatigue tested under tension-tension loading. Six fatigue specimens were single shear joints which utilized two sizes of high shear rivets and one type of steel bolt whose diameter was comparable to one of the rivet diameters. The two static and seven fatigue double shear specimens were used to investigate the relative performance of three types of rivets and one type of steel bolt whose diameter was comparable to one of the rivet diameters. The two static and seven fatigue double shear specimens were used to investigate the relative performance of three types of rivets and one type of steel bolt. Based on the experimental results 4 mm (5/32 in. dia.) Cherrybuck rivets applied in a double shear joint were found to provide the longest fatigue life.

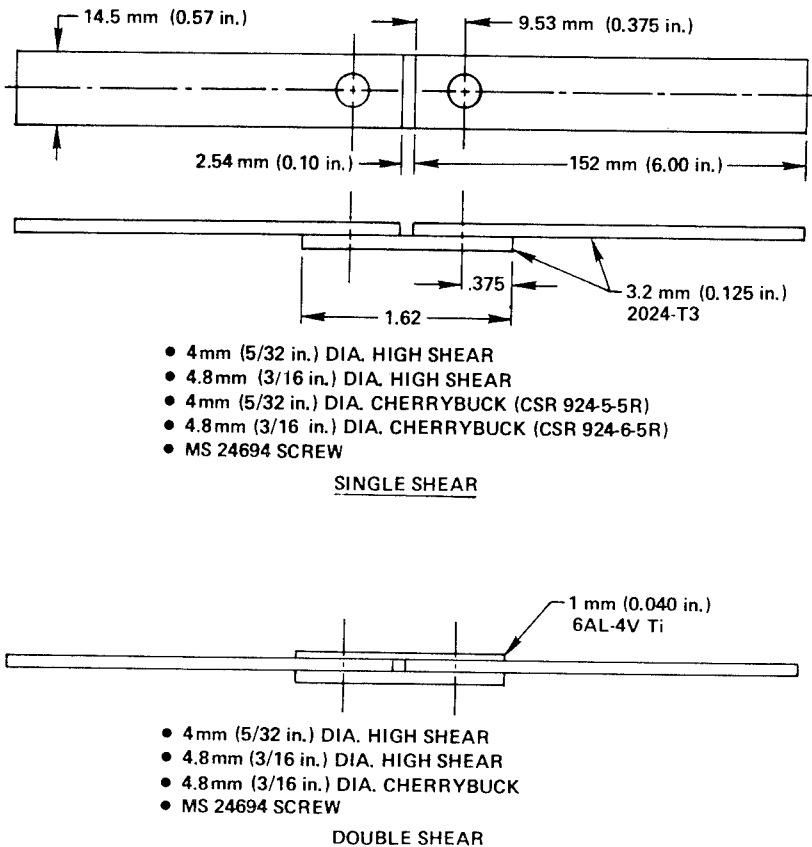


Figure 36. Joint Fatigue Test Specimens

Results

Bonded Skin Fatigue Specimens — The test specimens evaluated at NASA Langley Research Center served their purpose well in identifying strengths and weaknesses of the panel design. Results are summarized in the first three entries of Table XIII. The skin fatigue specimens, Figure 13 a, verified the structural integrity of the striped adhesive concept by successfully surviving 20,000 repeated load cycles (5,000 cycles \times a scatter factor of 4.0) of $2,268 \pm 2,118$ kg ($5,000 \pm 4,670$ lb), a stress level of $103,400 \pm 96,500 \frac{kN}{m^2}$ ($15,000 \pm 14,000$ psi), even though NASA had drilled a 3.2 mm (0.125 in.) diameter hole in the center of the specimen to simulate a rivet hole. The stress level used, corresponded to what would be expected from the $210 \frac{kN}{m}$ (± 1200 lb/in.) loading combined with the maximum tensile thermal stress and increased to account for the fact that room temperature testing was conducted whereas the final panel would operate at a temperature of 394K (250°F). Because there was no indication of damage after four life times, two sharp notches were introduced at the edge of the hole perpendicular to the loading direction. Failure occurred after an additional 7300 cycles; data of Reference 14 indicate a life of 8000 cycles at this loading if $K_t = 4.0$. There was no evidence of adhesive bond degradation in the form of delamination. After the second specimen survived 20,000 cycles of the same loading a flat notch was cut into the specimen surface. The bond line appeared to deter crack growth for several thousand cycles. Failure occurred after approximately 11,000 additional loading cycles. Visual inspection of the fracture area indicated no adhesive delamination. Ultrasonic inspection indicated a region of lateral disbond as a result of crack progression.

TABLE XIII
SUMMARY OF DEVELOPMENTAL TEST RESULTS

Type	Test Conditions	Results
1a. Bonded Skin Fatigue Specimens	Inplane loading to produce stress levels expected in test panel.	Notches introduced after 20,000 cycle requirement resulted in failure at 27,300 and 31,000 cycles.
1b. Cooled Skin Fatigue Specimens	Inplane loading to produce stress levels expected in test panel plus internal pressure.	Surface flaw introduced after 20,000 cycle requirement resulted in leakage after 24,500 and 86,000 cycles. One cycled 86,000 times without complete structural failure.
1c. Stiffened Cooled Skin Fatigue Specimens	Inplane loading to produce stress levels expected in test panel plus internal pressure.	Although the panel and substructure successfully completed the 20,000 loading cycle design requirement, excessive deformation at the edge attachment necessitated a double shear modification early in the testing and leakage was observed prematurely.
2a. Manifold End Plug Specimens	6 thermal cycles to 450K (350°F) to simulate fabrication sequence followed by pressure test to failure with GN ₂ while submerged in hot water.	Alumina filled Epon 828 selected based on test results and processing characteristics.
2a. Manifold End Plug Specimens	Exposure in ethyleneglycol-water at 366K (200°F) for 333 days without pressure; pressurized to 1.66 MPa (240 psi) every 90 days.	One failed at 510 MPa (740 psi) and one leaked at 166 MPa (240 psig) after the 333 day exposure.
2b. Coolant End Plug Specimens	Tube supported in fixture, except for potted tip, to prevent circularization: 6 thermal cycles to 450K (350°F) prior to being pressurized with GN ₂ to failure while submerged in water.	Alumina filled Epon 828 selected based on test results and processing characteristics.
2c. Initial Pressure Test Specimens	Pressurized at room temperature. Acoustic emission and holographic records obtained.	First sample leaked at fabrication defect at 1.24 MPa (180 psig), second sample failed at 4.14 MPa (660 psig).
2d. Improved Pressure Test Specimens	Same as 2c.	One failed at 2.62 MPa (380 psig). The other failed at 4.48 MPa (600 psig), verified fabrication procedures.
2e. Manifold Repair Specimen	Pressurized at room temperature	No failure at 7.58 MPa (1100 psig), verified repair procedure.
2f. Joint Fatigue Test Specimens	Tension-tension fatigue tests at 3 Hz.	Selected 4.2 mm (0.164 in.) Cherry buck rivets.

Cooled Skin Fatigue Specimens — The two specimens with coolant passages were pressurized to 1.10 MPa (160 psig) with light hydraulic oil during fatigue tests with an applied loading of 370 to 3733 kg (800 to 8200 lb), a stress level of $103,400 \pm 96,500 \frac{kN}{m^2}$ (15,000 \pm 14,000 psi), for 20,000 cycles. After the first specimen successfully completed this loading exposure a 12.8 mm (0.50 in.) surface cut was made between coolant passages. After an additional 66,000 cycles the crack had grown through both skin sheets to the edge of the coolant passages and leakage of oil was observed. Post test holographic inspection indicates a large debonded area extending axially as much as 25 mm (1 in.) on each side of the crack; visual examination indicated cracks in the tubing. The crack stoppers appeared to arrest crack growth for 200 to 300 cycles, a considerably shorter time than the 10,000 cycles indicated by the more lightly loaded $92,400 \pm 55,800 \frac{kN}{m^2}$ (13,400 \pm 8,100 psi) test panels discussed in Appendix H. After the second specimen survived the 20,000 cycles of loading, a deep surface flaw was cut into the surface

between coolant passages. Following 24,500 additional cycles, leakage of the pressurant was noted and testing was terminated. Post test inspections indicated no debonding in the vicinity of the crack and no cracks in the coolant passage tubing. The oil leak must have been caused by leakage at the tube end plug or at the tube to manifold bond.

Stiffened Cooled Skin Fatigue Specimens — These test specimens, see Figure 14, quickly indicated the inadequacy of the single shear edge attachment joint. After 90 and 2700 cycles, excessive motion at the edge attachment joint necessitated the addition of an aluminum strap to the first and second specimens, respectively, to convert the joint to a double shear arrangement. The first specimen was pressurized to 0.69 MPa (100 psig) and loaded to $\pm 3,723$ kg ($\pm 8,200$ lb), a stress of $\pm 103,400$ $\frac{\text{kN}}{\text{m}^2}$ ($\pm 15,000$ psi). After 4450 cycles there seemed to be an increase in audible noise emanating from the specimen. A bulge in the flat skin was observed after 11,500 cycles. A crack was noted from a rivet hole to a tube after 14,300 cycles, and at 16,000 cycles internal pressure decreased to 0. Testing was continued until failure occurred at 19,300 cycles through the first row of rivets off the manifold ramp and through the skin and stringer. Because of leakage in the first specimen the second specimen was not pressurized. The noise level seemed to increase at about 17,000 cycles but no cracks or other damage were observed at 20,000 cycles. At 23,200 cycles a rivet head popped off (the one through a stringer flange and the manifold ramp) and at 34,500 cycles cracks were observed at the first rivet through the skin and the same stringer flange; they eventually caused failure. After 35,200 cycles the rivet through the other stringer/ramp joint became loose. Failure occurred through the same row of rivets as for the first specimen but after 44,900 cycles.

Results of these tests led to a redesign of the panel edge attachment and to changes in the fabrication and inspection sequence for the deliverable test panel.

Manifold End Plug Specimens — During assembly of the stiffened skin fatigue specimens, which contained sections of the coolant manifold, it was necessary to bond plugs into the ends of the manifold plenums. Epon 934 was used initially but difficulty was encountered in obtaining a good seal. Eleven simplified specimens were fabricated using three adhesives in addition to Epon 934. Based on pressure tests at 333K (140°F) two adhesives were selected for further evaluation which consisted of six thermal cycles to 450K (350°F) followed by pressure testing to failure or 7.58 MPa (1100 psig) maximum. Although both adhesives met requirements the Epon 828/MPDA filled with 60 parts by weight of alumina was selected because neither cycled specimen failed when pressurized to 7.93 MPa (1150 psig) at 333K (140°F).

As a further evaluation of the selected system two specimens were exposed in ethylene glycol/water for 333 days at 366K (200°F). Proof pressure tests to 1.66 MPa (240 psig) were performed at approximately 90 day intervals including the end of the exposure. No leakage or failure was noted until after the entire exposure, then one failed at 5.10 MPa (740 psig) and one leaked at 1.66 MPa (240 psig).

Coolant Tube End Plug — Examination of panel fatigue and pressure specimens that showed internal leakage suggested that the precast Epon 934 end plugs for the coolant passage tubing had probably leaked even though they were bonded to the tube wall. Eight simplified tube specimens were fabricated to evaluate three adhesives in comparison to Epon 934. One sample of each type was tested to failure or 1100 psig maximum at 333K (140°F); the other was thermally cycled six times to 450K (350°F) before pressure testing. Both Epon 934 specimens leaked at less than ultimate

pressure. All three other adhesives sustained pressures in excess of ultimate. The alumina filled Epon 828 was selected because both specimens sustained 7.76 MPa (1125 psig) without leakage or failure.

Manifold Repair Specimen — Although only one specimen was tested it contained three identical repairs of the filled holes by blind aluminum alloy rivets and three with countersunk aluminum alloy rivets. The triplicate installations provided confidence in the repair when no failures or leaks occurred up to the limit of the pressure source, 7.58 MPa (1100 psig).

Joint Fatigue Test Specimens — Single and double lap fatigue test specimens of the type defined by Figure 36 were fatigue tested with a tension-tension loading equivalent to a completely reversed $280 \frac{kN}{m}$ (1600 lb/in.) panel edge loading (of which 79% is actually transferred through the splice in question). As shown in Table XIV, the Cherrybuck rivets gave superior performance in the double shear configuration and were selected for the test panel.

TABLE XIV
TENSION-TENSION FATIGUE TESTS OF RIVETED SPECIMENS
LOAD RANGE ALL SPECIMENS 45 TO 4464N (10 - 1000 POUNDS) MEAN LOAD
2232N (500 POUNDS) CYCLIC RATE 2 - 4 CYCLES PER POUND

Specimen Type	Rivet Diameter		Type Of Fastener	Number Of Cycles Sustained	Specimen Strap Materials	Comments Failure Mode
	mm	(In.)				
1. Butt Joint Single Shear	4.8	(0.189)	Huck	12,269	2024T3 Strap	Al strap started at rivet hole
2. Butt Joint Single Shear	4.8	(0.189)	Huck	11,315	2024T3 Strap	Al strap started at rivet hole
3. Butt Joint Single Shear	4.1	(0.163)	Huck	12,369	2024T3 Strap	Al strap started at rivet hole
4. Butt Joint Single Shear	4.1	(0.163)	Huck	7,682	2024T3 Strap	Al strap started at rivet hole
5. Butt Joint Single Shear	4.8	(0.189)	No. 10 Bolt	26,140	2024T3 Strap	Al strap not started at rivet hole
	4.8	(0.189)	No. 10 Bolt	28,153	2024T3 Strap	Al strap not started at rivet hole
6. Butt Joint Double Straps	4.8	(0.189)	Huck	75,215	2024T3 Strap 6Al-4V Ti Strap	Al strap and Ti failed
7. Butt Joint Double Straps	4.8	(0.189)	No. 10 Bolt	61,080	2024T3 Strap 6Al-4V Ti Strap	Ti strap cracked
8. Butt Joint Double Straps	4.8	(0.189)	No. 10 Bolt	40,000	2024T3 Strap 6Al-4V Ti Strap	Ti strap cracked
9. Butt Joint Double Straps	4.0	(0.156)	Hi-Shear	66,462	2024T3 Strap 6Al-4V Ti Strap	Ti strap cracked
10. Butt Joint Double Straps	4.0	(0.156)	Hi-Shear	107,950	2024T3 Strap 6Al-4V Ti Strap	Ti strap completely separated
11. Butt Joint Double Straps	4.2	(0.164)	Cherrybuck	149,696	2024T3 Strap 6Al-4V Ti Strap	Ti strap cracked
12. Butt Joint Double Straps	4.2	(0.164)	Cherrybuck	185,937	2024T3 Strap 6Al-4V Ti Strap	Joint completely separated. Ti strap cracked at 145,000 cycles

APPENDIX F FABRICATION OF TEST HARDWARE

A variety of specimens and a test panel were fabricated during this program. In a broad sense the basic fabrication processes were conventional; in a detailed sense close control of tolerances and coordination of configuration details among the elements, particularly of the cooled skin, were much more demanding than those normally encountered. Areas which required particular attention were fabrication of the thin-walled tubes and various aspects of adhesive bonding. Because the objective of specimen testing was to simulate configurational features and fabrication techniques to be used for the test panel, the fabrication steps for the detailed parts and assembly are described first. Comments of interest regarding the test specimens are provided later as appropriate.

Test Panel

The test panel consisted of an actively cooled skin and a substructure which are attached with mechanical fasteners. The cooled skin is assembled from two manifold blocks, a beaded inner skin, a flat outer skin, 40 coolant passage tubes, 38 L-caps, 38 cover disks, 2 seal sheets, 8 manifold end plugs, and 4 coolant fittings. All detailed parts to be bonded were acid etched and primed with Epon 952. The substructures consisted of 9 Z-stringers, 2 longitudinal edge channels, 3 transverse frames, 2 transverse edge splices (an extruded tee and a titanium splice plate at each end), and various types of spacers and clips. Assembly of the cooled skin with the substructure was done primarily with flush head aluminum alloy rivets; brazier head rivets were used for internal substructural elements and flush head titanium rivets were used for the transverse edge splices. Figures 15, 18 and 20 identify the details.

Manifold Block — The manifold block was machined from 2024-T3 aluminum alloy bar. Milling was the dominate process. The plenums were introduced with gun drilling techniques. The ends of the plenums were counterbored to accommodate the manifold end plugs. The planform surface was grooved to match the beads of the inner skin. Holes were drilled to permit interfacing between the plenums and the coolant passage tubing.

Manifold End Plugs — These were lathe turned from aluminum alloy rod. Grooves were milled into one face to provide a relief for matching the interface hole for the end coolant passage, see Figure 34.

Coolant Fittings — These were machined from conventional AN bulkhead fittings. Lathe turning removed threads from one end and shortened the modified end.

Beaded Inner Skin — This was formed into a female die using an hydraulic press. Oversized 0.5 mm (0.020 in.) sheet stock was used so that the edges of the sheet were formed around the die before significant pressure was applied to stretch form the beads. The 2024 sheet was formed in the heat treated condition and then allowed to age. After aging a second strike was made in the hydraulic press. The inner skin was trimmed to length but was left oversize in the width direction.

Outer Skin — This skin was cut slightly oversize from 2024-T3 stock purchased in the heat treated condition.

Coolant Passage Tubing – Round 3003 alloy tubing was cold drawn to the desired configuration, see Figure 35, and to the -H14 temper by the Precision Tube Company Inc. of North Wales, PA. Wall thickness was controlled to ± 0.13 mm (± 0.005 in.). Height, width, and contour were maintained within ± 0.05 mm (± 0.002 in.) except that the flatness of the long flat side was held to ± 0.013 mm (± 0.0005 in.). These close tolerances were required between the elements of the cooled skin.

This tubing was about 250 mm (10 in.) longer than needed for the panel assembly so that small portions could be cut from each end of each tube for contour checks. A jeweler's saw was used to minimize burr formation. A flat end mill was used to cut holes into the bottom and side of each tube at locations to mate with the interconnect holes from the manifold block. A drill fixture was used to position these holes accurately and to prevent damage to the opposite side of the coolant passage tubing.

Coolant Passage End Plug – End plugs were formed from alumina-filled Epon 828 adhesive. The desired depth of modified adhesive was placed in a container into which one end of the coolant passage tubing was inserted while the tubing was kept vertical. After a room temperature cure the tubes were separated from the cast adhesive block leaving a molded plug in the end of each tube. This process was repeated for the other end of the tubing. An oven cure followed. After the oven cure each end of each tube was given a low pressure leak test while submerged in water. No leaks were found in any tube.

Seal Skin – This 2024-T3 aluminum alloy sheet, see Figures 15 and 20, which covered the coolant passages in the manifold region provides redundant seal in the event of leakage past an L-cap, cover disk or tube end plug. It was cut oversize from sheet stock and then was chemically milled to achieve a taper of its thickness. The seal skin tapered from approximately 0.030 mm (0.012 in.) at one end to a feather edge at the other. Final trimming was done such that the thin edge of the part to be used was no greater than 0.05 mm (0.002 in.) while the thicker end was allowed to range between 0.25 and 0.30 mm (0.010 and 0.012 in.).

L-caps – These parts were machined in a picture frame configuration from sheet stock; inner and outer edges of the picture frame were chamfered, and then each picture frame configuration was cut into four L-caps. As a result of concern for internal leakage that was evidenced during the fatigue tests of samples at the Langley Research Center, it was decided to completely cover the L-slots (with the L-caps installed there was a half circle portion of the L-slot that was not covered, see Figure 20). Because the L-caps had all been produced, it was necessary to mill a recess on the nonchamfered surface to accommodate adhesive and a cover disk.

Cover Disk – The cover disks were chemically milled from thin aluminum alloy sheet stock. The etching pattern incorporated a small tab which connected each cover to a strip of sheet material so that after etching there were no loose detailed covers. After etching and before cleaning and priming the covers were cut from the tab with a sharp knife blade.

Subassembly of Manifold Blocks and Inner Skin – The manifold blocks were bonded to the inner skin with 0.13 mm (0.005 in.) of Epon 951 film adhesive placed along the tapered ramp of each manifold block. Tack rivets were used to hold the relative position of the skin and manifolds and to prevent a flattening tendency in the beaded skin. Adhesive squeeze-out at the inboard ramp/skin interface was removed by careful sanding. These areas were primed locally.

Installation of Coolant Passage Tubing – Several layers of Epon 951 film adhesive were placed in the outboard portion of the machined grooves in the manifold blocks. An excessive of silver-filled epoxy was extruded from a caulking gun into each bead of the inner skin. The subassembly was weighed after each deposition; the mass increase was compared to a target value. The as-deposited silver-filled epoxy was examined visually for uniformity. Slight additions were made at locations that seemed to be starved.

After each deposition was judged suitable, two coolant passage tubes were installed. Care was taken to match the interconnect holes at the L-slots; this properly positioned the holes that could not be seen because of the dimensional control used for the tubes and subassembly. Each tube pair was pressed into place with light roller pressure. No attempt was made to press the tubes flush with the lands on the inner skin but only to prevent the tubes from becoming dislodged from the adhesive. After all tubes were in place film adhesive was applied to the L-caps and the cover disks, see Figure 20. These detailed parts were carefully located in their proper positions. This unbonded subassembly was covered with bleeder cloth, a cover plate which extended between recesses in the manifold blocks, and a caul plate larger in size than the panel subassembly. Additional bleeder cloth was placed on both sides of this stack which was then vacuum bagged and debulked at room temperature with approximately 100 kPa (14.5 psi). The vacuum bag, bleeder cloth, and caul plate were removed so that the silver-filled epoxy squeeze-out could be removed. No solvent was used during this operation. A second debulking operation was performed in an autoclave at 339K (150°F) and 345 kPa (50 psig). Following clean-up after the second debulking operation this subassembly was autoclave cured.

Installation of Manifold End Plugs and Coolant Fittings – These elements were adhesively bonded in place using alumina filled epoxy adhesive. To minimize the load on the adhesive joints due to internal pressurization, steel drill rod was inserted into two holes drilled through the ends of the manifold block and into the end plugs, see Figure 14.

After the coolant fittings were bonded to the manifold block, holes were drilled through the hexagonal portion and steel drill rod was inserted at two locations. This drill rod reacted the torque when coolant lines were installed on the fittings.

Installation of Seal Sheets – Before the seal sheets were installed the small amount of silver filled epoxy squeeze-out was removed by sanding. The surface was cleaned and primed, then a low pressure leak test was performed and any leaks at the manifold end plugs, coolant fittings, and coolant tubing installations were repaired. Three sets of repairs were made before all leaks were sealed. The predominate location of leakage was at the joint between the L-cap and the side of the coolant passage where the bend radius of the tube sidewall prevented contacts with the L-cap. The L-cap should have been approximately 0.25 mm (0.01 in.) longer in this direction.

Alternate stripes of epoxy film adhesive and silver-filled epoxy paste were deposited on the manifold/inner skin subassembly in the region where the seal sheets would be installed. The film adhesive was applied first and tacked in place. The silver-filled epoxy was extruded from a pressurization caulking gun. The paste was thinned with four weight percent solvent to enhance flow. After the silver-filled epoxy was deposited, it was allowed to air dry for a minimum of one hour to evaporate the solvent.

After the seal sheets were installed, the subassembly was covered with a release film and an aluminum alloy slip sheet. Bleeder cloth was placed on both sides of this subassembly which was mated with a caul plate and vacuum bag material. The assembly was autoclave cured with the coolant passages vented to autoclave pressure so that good contact would be achieved between the long flat sides of the coolant passage tubing and the seal sheets.

Installation of Outer Skin – No particular preparation was required before installing the smooth outer skin. A light solvent wipe was used prior to installing the stripes of film adhesive. Care was taken not to remove the primer. The stripes of film adhesive were installed carefully and tacked in place. Beads of silver-filled epoxy were extruded in the same manner as described for the seal sheet installation. The extruded deposits were allowed to air dry for a minimum of one hour before the outer skin was installed. The outer skin was installed from one transverse edge of the panel with an action that gradually lowered it to the other transverse edge in a way that would expel air. As the outer skin was lowered the portion in contact with the inner skin subassembly was pressed down to flatten the extruded beads of silver-filled epoxy. Both sides of this assembly were covered with bleeder cloth. The stack was placed on heavy aluminum alloy caul plate, vacuum bagged and autoclave cured with coolant passages vented to autoclave pressure.

Installation of Substructure – The substructure was attached to the cooled skin by riveting. Before any rivet was initiated all of the detailed parts were predrilled and assembled with clip fasteners. Extruded T-sections and small reinforcing channels were riveted to each end of each Z-stringer to form subassemblies. The stringers, edge channels, and frames were riveted in proper sequence along with appropriate spacers and clips. Almost all of the riveting was done by squeezing rather than by bucking. The titanium cherry-buck rivets used for the transverse edge splices were squeezed in accordance with manufacturer recommendations.

Installation of Load Adapters – In order to insure a uniform distribution of loading across the test panel good fits are required for the bolts in the load path, see Figures 18 and 24. All holes for attachment of the links to the load adapters and test panel were jig-bored. Close tolerance AN17X series bolts were used for the assembly. The bolt shanks were measured and the hole size adjusted for the mean diameter. This was done to minimize the clearance that would be obtained if allowance had to be made for the normal tolerance for bolt diameter. As holes were bored at each location the appropriate load link was bolted in place. Each load link was numbered so that it could be installed in its proper positions if removal was necessary.

Test Specimens

A variety of test specimens were fabricated for experimental evaluations. These specimens represented specific details of the cooled-panel skin and assembly with the substructure. The fabrication procedures used were essentially the same as those used for the test panel as described above. Because some of the experimental evaluations were conducted to refine or select specific fabrication procedural details and adhesives it is more appropriate to discuss them in Appendix E. The critical fabrication aspects associated with adhesive bonding were verified on the test specimens before they were applied to the test panel.

APPENDIX G

INSPECTION OF TEST HARDWARE

The lack of technical data base for adhesively bonded actively cooled panels with discrete coolant passages made it essential to investigate inspection procedures that could be applied. Basic procedures were selected from among those generally used for adhesively bonded structures and those used for pressurized structures. They were modified to some extent by the requirements of the particular cooled panel configuration. The test specimens fabricated and evaluated prior to making of the test panel were inspected by the candidate techniques so that inspection standards could be refined. Visual, radiographic, holographic, thermographic, acoustic, ultrasonic, and eddy current techniques were evaluated on various test specimens. All but ultrasonic techniques were applied to the test panel. These conventional nondestructive techniques were supplemented by leak checks with gaseous nitrogen and hydraulic proof pressure testing. Post test observations were correlated with pretest inspection results. Correlation of results is discussed in Appendix E for purposes of clarity and to avoid repetition. The manner in which the fabrication and inspection operations were sequenced for the test panel is described here.

Test Panel

Detailed parts, subassemblies and the final test panel were subjected to dimensional, visual, radiographic, holographic, and thermographic inspections at various stages of fabrication. These inspections were supplemented by leak tests at modest gas pressure and proof-pressure tests as described in the subsequent subsections.

Detailed Parts — These were subjected to dimensional and visual inspection as appropriate. Particular attention was paid to the configuration of the grooves in the manifold blocks, the shape of the formed beads in the inner skin, the fit of the L-caps and disks in the manifolds and the characteristics of the coolant passage tubing. Wax moldings of the manifold grooves and beads were made for definition of dimensional characteristics on a comparator at magnification. These configurations were correlated with the tubing shape so that adhesive quantities required to attach the coolant passage tubing to the subassembly of the manifold and inner skin could be defined.

The tubing was purchased to a specification which incorporated the features of Reference 21. Mechanical properties were checked by measurements of ultimate and yield strengths and elongation. External surfaces were examined visually at 10X. The cleanliness of internal surfaces was examined by pulling black cloth through the tubing and inspecting for metal particles and by splitting a few lengths for visual examination. To make sure that the corners of the tubing had not experienced excessive cold work, sections of tubing were flattened with no evidence of corner cracking. Dimensional characteristics of the tubing were checked using metalographic sections. The most critical surface of the coolant passage tubing, the long flat side, was checked for flatness using a Taliysurf which provided a magnification of 100X in the horizontal and vertical directions.

After the coolant passage tubing was cut to length, the innerconnecting holes were milled, and the ends were potted. Each end of each tube was subjected to a low pressure leak test while the end being inspected was submerged in water. No leaks were detected. Unsupported samples of the tubing, with ends potted, were pressurized to failure. At about 516 Pa (75 psig) the test tubes began to deviate visually from their original cross section. Failure occurred at pressures in excess of 5.5 kPa (800 psig) by rupture at a corner (not always the same corner) well above the design burst pressure of 2.2 kPa (320 psig) for the panel.

Subassembly of Manifold Blocks and Inner Skin – This was subjected to visual inspection only. Particular attention was paid to squeeze out of the Epon 951 adhesive.

Installation of Coolant Passage Tubing – After the debulking operation but prior to cure, a radiographic inspection was conducted. One coolant passage hole in one tube appeared to be partially blocked with silver filled epoxy. The tube was raised locally and the unwanted adhesive was removed. Markings near the hole suggested that this tube had been touched by a gloved hand that was dirtied with the silver filled paste. After cure a second radiographic inspection indicated good distribution of silver filled epoxy; there was only one void area of significance, about 1.5 x 38 mm (0.06 x 1.50 in.). This defect was not evidenced in the radiographic inspection conducted after debulking; apparently there had been motion of the tubing during handling.

Coolant inlet and outlet fittings and manifold end caps were bonded to this subassembly so that it could be pressurized. A leak check was conducted at 172 Pa (25 psig) while the panel was submerged in water. Several leaks were found and repaired with alumina filled Epon 828 adhesive.

Holographic inspection was conducted in the region of the manifold blocks to ascertain the uniformity of bonding and to identify any anomalies that might suggest blockages in the coolant passage network, see Figure 37. In general, good uniformity was noted although slight differences in the depth of potting at the end of individual coolant passage tubes could be detected and some anomalies were found. The anomalies are suggestive of two plugged or partially plugged coolant passages and six possibly plugged transitions between the L-slot and the side hole in the coolant tubing. These indications can be seen in Figure 37 at the 9th tube from the left in the lower left photo and the 12th tube from the left in the upper left photo. The former indicates an anomaly although the particular tube is pressurized. The latter indicates the tube may be blocked at both ends because it does not appear to be pressurized. The anomalies at the L-slot/tube interface can be seen at the 2nd tube from the left in the lower left photo, the 3rd and 10th tubes from the right in the lower right photo, and the 2nd, 9th and 10th tubes from the right in the upper right photo. No corrective action was taken.

Installation of Seal Sheets – After the autoclave cure, which bonded the seal sheets to the inner subassembly, a low pressure leak test was conducted with gaseous nitrogen at 276 Pa (40 psig) with each end of the panel submerged alternately. No evidence of leakage was found. Holographic inspections were repeated. The results were the same as those obtained without the seal sheets.

Examination of the manifold tubing interconnect holes that could be seen from the coolant fittings indicated excessive adhesive squeeze out into these holes. The manifold end plugs were removed and these interconnect holes were examined with a boroscope. Almost all of the holes in the outboard manifolds indicated evidence of excessive adhesive squeeze-out. No evidence of adhesive squeeze-out had been expected at the holes from the inboard manifolds because of the L-slot configuration; none was found. It was postulated that the best repair for the adhesive squeeze-out would be made from the manifold side of the skin assembly. Such a repair would alleviate any indication of coolant passage blocking indicated by the holographic inspection. Therefore, inspection results were recorded and the assembly procedure continued. After the outer skin was bonded in place, holes were drilled through the manifolds and into the coolant passages as illustrated in Figure 22 and discussed on pages 26 and 27.

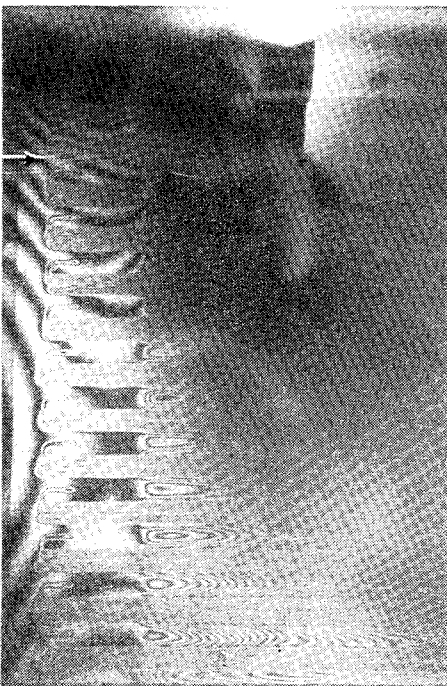
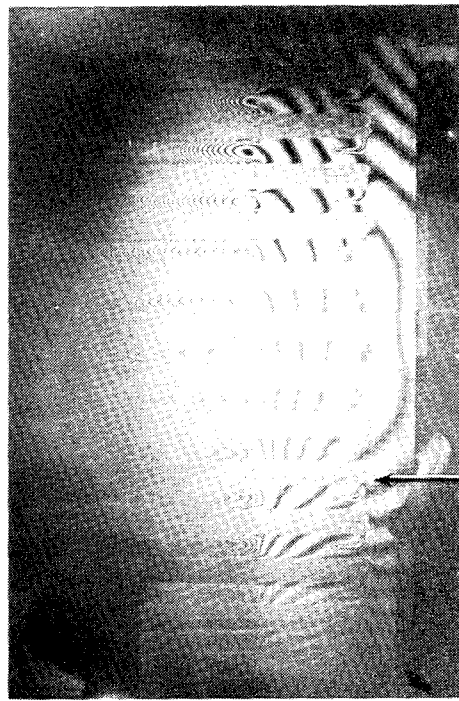


Figure 37. Holographic Inspection of Test Panel Cooling Passages

Installation of Outer Skin – After the outer skin was bonded to the inner subassembly, it was inspected radiographically and thermographically. The radiographic inspection indicated good distribution of the silver-filled epoxy in the stripes at the lands between coolant passages. It was difficult to assess the nature of the silver-filled epoxy stripes over the coolant passages because of the presence of the silver-filled epoxy bond lines which joined the coolant passage tubes to the beaded inner skin. Because the Epon 951 is transparent to X-rays no indication was obtained with regard to the stripes of this adhesive. The width of these stripes could be inferred from the extent to which the silver-filled epoxy flowed.

The thermographic inspection involved obtaining infrared scans of the panel surface while alternately flowing cold and warm water through the panel; water temperatures and flow rates were not at design conditions. These flow tests were performed after rework of the outboard manifolds. Despite the rework, large nonuniformities in the temperature scans were observed. After rework of the inboard manifolds, flow uniformity was improved substantially. Figure 23 illustrates the improved condition. Note that some of the coolant passages still appear to be partially blocked. Only one passage in each circuit has lower flow than the others to any significant degree. The flow through the edge tubes appear to be somewhat less than average. The majority of the coolant passages had uniform flow as evidenced by the general uniformity of temperature across the panel. Inasmuch as the differences in flow rates within the coolant passages could not be quantitized the effect on panel performance is uncertain. Under test conditions, the edges of the panel are likely to be somewhat hotter than predicted, and two streaks of higher temperature should be observed where the low flow is indicated by the infrared scans. However, because of the redundant nature of the coolant circuitry, the effects on performance should be small under normal operating conditions. With one coolant circuit inoperative, the effect will be more significant.

The final inspection on the actively cooled skin was a proof-pressure test to 1.65 kPa (240 psig), 1.5 x working pressure. Pressurization was applied in 0.28 kPa (40 psig increments) with about 15 seconds of hold at each increment so that acoustic emission data could be recorded. The proof pressure level was held for more than two minutes. The acoustic count was low and did not increase during the proof pressure hold.

Installation of Substructure and Load Adapters – Following these operations, a leak check was conducted with gaseous nitrogen at 0.69 kPa (100 psig). Three small leaks were found at coolant fittings and were sealed with adhesive. The proof pressure test to 1.65 kPa was repeated with a three minute hold at proof pressure. The acoustic count was low and did not change during the three minute hold at proof pressure.

Test Specimens

The various test specimens were subjected to inspections similar to those used for the test panel to inspect the particular design details exemplified in the test specimens. Not all specimens were subjected to all inspection techniques. Because the inspection results were compared to post test examinations of the various specimens, it is more appropriate to discuss the particular inspection techniques and results in Appendix E.

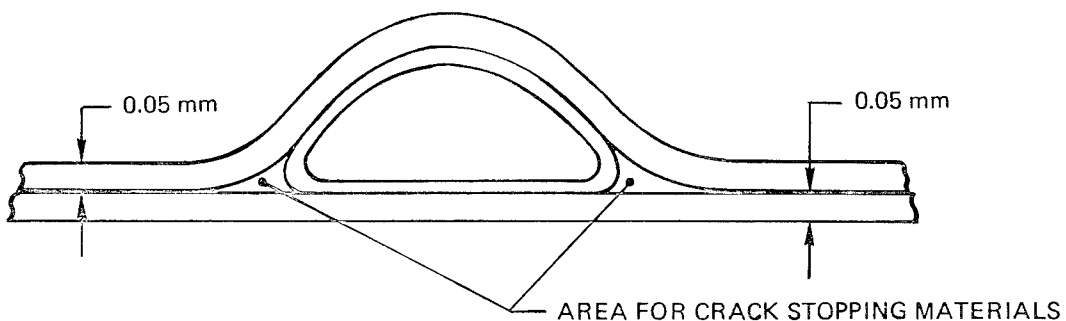
APPENDIX H CRACK ARRESTOR TEST DATA

One aspect of a cooled panel design that does not lend itself to analytical evaluation is the effect of a crack that is initiated between coolant passages. Nor is there test data available to substantiate crack stopping techniques that can be installed near a coolant passage to retard crack growth once it is started. Therefore, as part of an IR&D effort prior to the initiation of the NASA sponsored work, Bell Aerospace Textron conducted experimental evaluations of various crack stopper materials installed adjacent to the coolant tubes, to delay failure of a coolant tube by a crack.

Scratches, mechanical damage and holes for mechanical fasteners can initiate crack growth. A conservative estimate of crack growth behavior can be obtained by evaluating specimens with a through crack, which was used for the bulk of the testing. A limited number of tests were conducted with relatively shallow surface scratches.

Specimen Design and Test Procedure

As shown below the geometry required for the tubing and formed cover sheet for the panel provide an area adjacent to the tubing that is ideally suited for placing of the crack stopping materials which included: (1) 0.1 mm (0.004 in.) diameter boron filament, a high strength and high modulus of



elasticity material; (2) 0.15 mm (0.006 in.) diameter spring tempered stainless wire, a high strength material with a modulus of elasticity higher than that of the aluminum panel material; (3) 0.15 mm (0.006 in.) diameter copper wire, low strength and modulus but high ductility or (4) 0.75 mm (0.030 in.) diameter aluminum wire as crack stopping material. The test specimen configuration is shown in Figure 38. It is a tension-tension fatigue specimen containing two cooling passages parallel to the loading direction. Between the coolant passages, a center notch is formed by cutting with a jeweler's saw from a centrally located hole. One end of each coolant passage was sealed with epoxy. In order to detect the cracking of a coolant passage, the passages were filled with a red dye penetrant fluid. The tests were performed at a rate of three cycles per second. After installation of the specimens in the test unit, they were sprayed with a dye penetration developer solution, to facilitate detection of cooling tube failure.

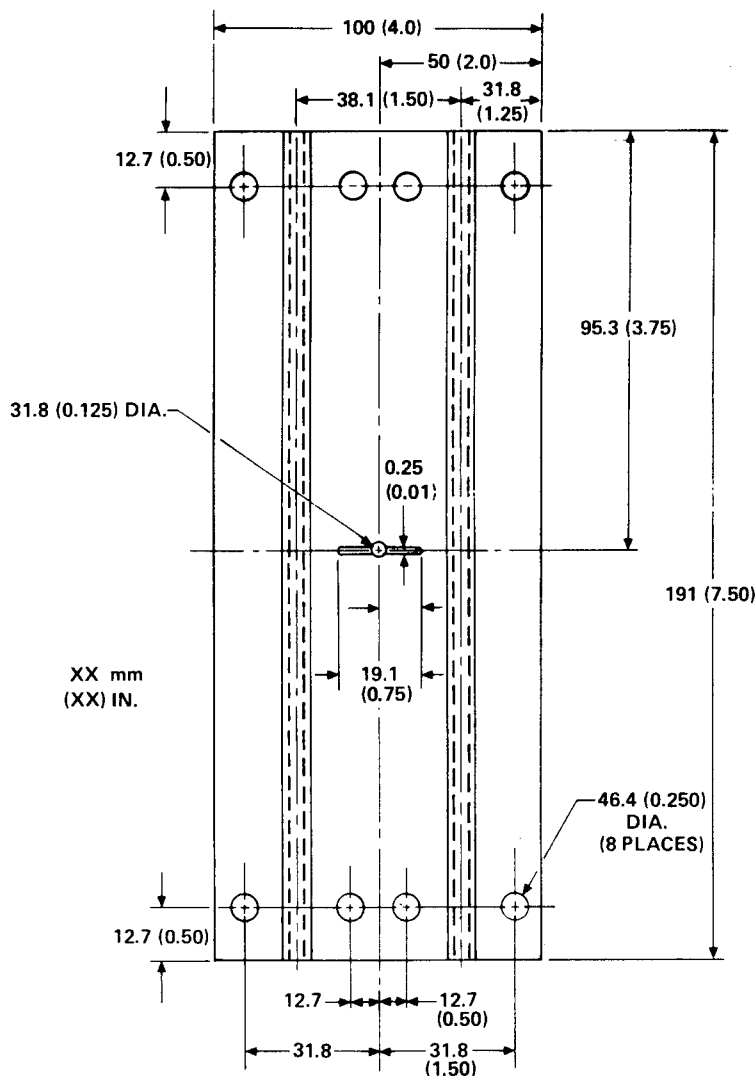


Figure 38. Crack Propagation Specimen, Center Notch

Crack growth was determined for each specimen by measuring crack lengths with a micrometer side comparator which has a telemicroscope magnification of 33X at 120 mm working distance and a direct readability of 1.25 μ m. After the start of the test, the slot ends were monitored closely using the comparator unit until crack initiation was observed. Crack length measurements were made periodically (250-300 cycles) by interrupting the test, loading the specimen statically to a level slightly less than the maximum cyclic load, and measuring the location of both ends of the crack. Then the cyclic loading was resumed. This was repeated until an indication of tube failure was obtained by leakage of the dye penetrant fluid contained in the tubes. Crack length was measured at the first tube failure and the test continued as before until failure of the second tube was indicated, and cracks became unstable. All crack length measurements were made on the formed skin side of the specimens but both specimen faces were monitored visually for unusual crack behavior and for tube failure indications.

Test Results

The cyclic load range for the crack arresting specimens were established by the cyclic loading of two unreinforced specimens. These specimens contained the coolant tube but no filamentary crack arrestors. These specimens established a maximum load of 1270 kg (2800 lb) and a cyclic load ratio $R = 0.25$ which produced a stress of 92.3 ± 55.8 kPa ($13,400 \pm 8,100$ psi) and life-time in the range of 5,000 to 10,000 cycles to tube failure. This life was quite short so that the various materials could be screened quickly.

In addition, it was desirable to determine if there was any modification in the fatigue life of 2024-T3 aluminum alloy when the two 0.5 mm (0.020 in.) thick sheets were adhesively bonded together. Therefore, three specimens were fabricated from 1.0 mm (0.040 in.) material with the center notch and three specimens from two 0.5 mm (0.020 in.) skins bonded together, also with the center notch. The specimens were cycled using the load range established from the control specimens. The results are shown in Figure 39. The slopes of the curves for both types of specimens appear to be quite similar up to 7000 cycles, after which crack growth became increasingly rapid and variations in behavior became quite large. On the average, the bonded specimens indicated longer life; but on the basis of the limited data, it is safe to assume no significant difference from the fatigue life of the single sheet material.

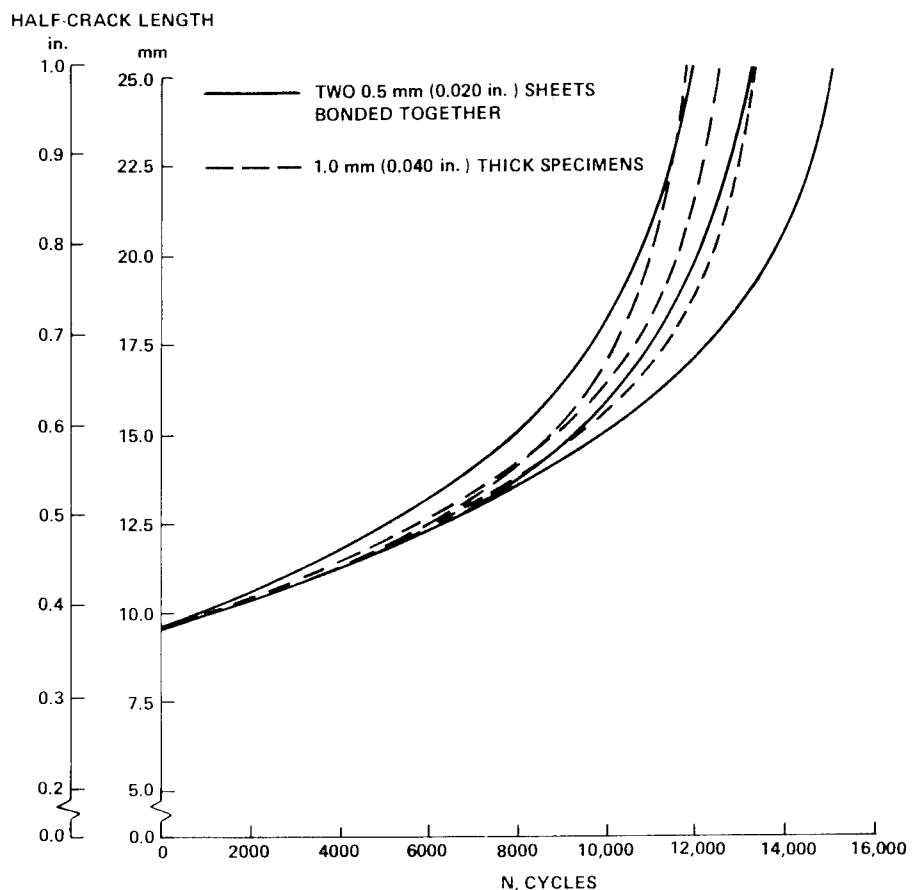


Figure 39. Crack Growth Behavior of Flat 2024-T3 Sheet 92.3 ± 55.8 kPa ($13,400 \pm 8,100$ psi)
(without coolant tubes or crack arrestors)

Figure 40 presents the results of life tests on specimens which contained crack arrestors. Note that the fatigue life of cooled panel specimens without crack arrestors is shorter than the life of the bonded sheet specimens. The small difference is within the scatter to be expected for aluminum alloy sheet. The use of the coolant tubes and the single 0.75 mm (0.030 in.) diameter aluminum alloy wire on each side of each tube increases the life expectancy by a factor of two over a panel containing no coolant tube or aluminum wire. The various crack arrestors increased life by from 85 to 230% while imposing a weight penalty of only about 3%.

Based on these results, the spring tempered stainless steel was selected for the panel design. Its lower cost and fewer number of wires, as compared to boron, and its superior performance compared to aluminum and copper warranted the choice. Considerable difficulty was encountered when installation of the crack stoppers was attempted on the test panel. Therefore, they were eliminated from the 0.61 x 1.22 m (2 x 4 ft) test panel.

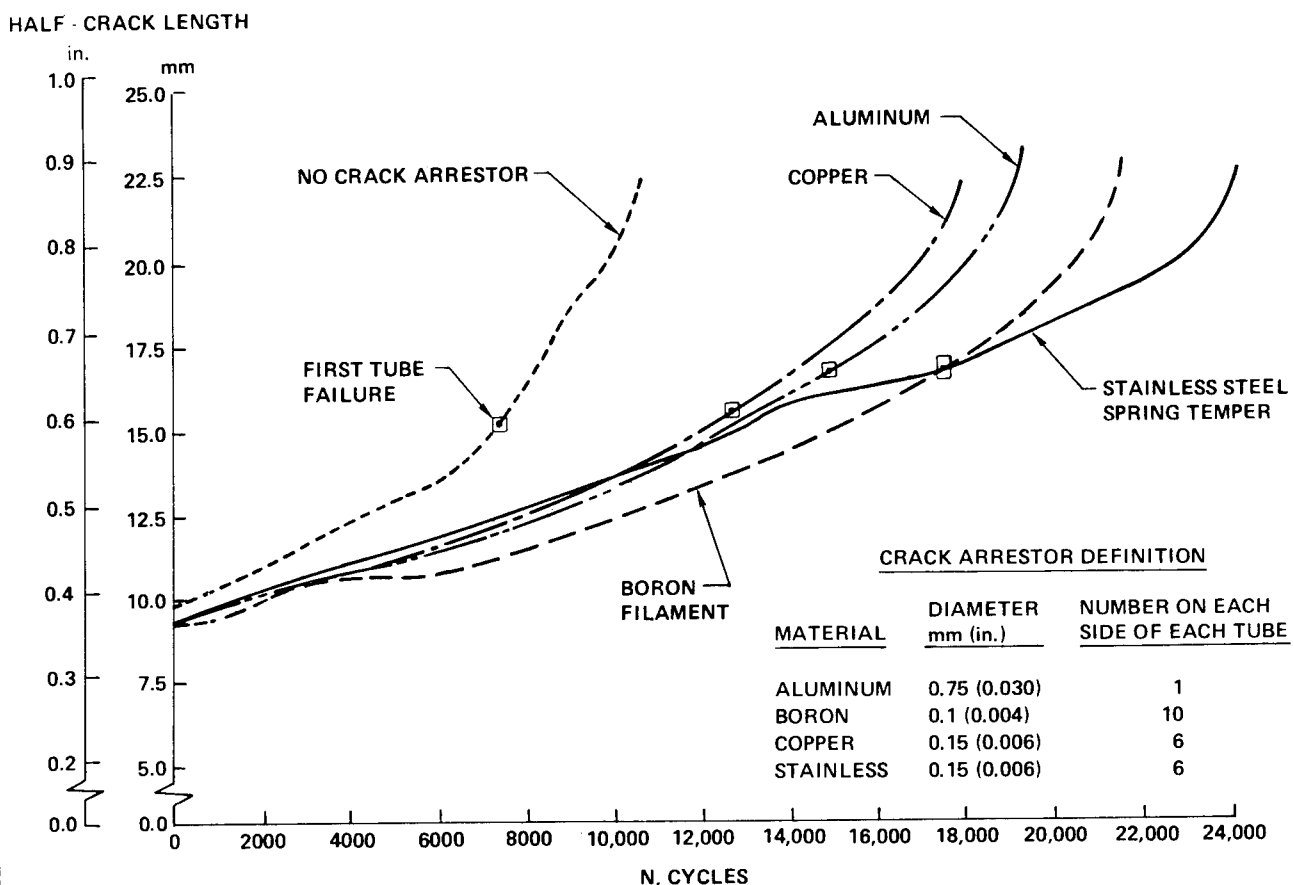


Figure 40. Crack Growth Behavior of Cooled Panel Specimens, Third Set/Second Series
 92.3 ± 55.8 kPa (13,400 \pm 8100 psi) Neglecting Load Inconsistencies

REFERENCES

1. Kelley, H.N., Wieting, A.R., Shore, C.P., Nowak, R.J., "Recent Advances in Convectively Cooled Engine and Airframe Structures for Hypersonic Flight," 11th Congress of the International Council of the Aeronautical Sciences, Sept. 1978.
2. McConarty, W.A., and Anthony, F.M., "Design and Evaluation of Active Cooling Systems for Mach 6 Cruise Vehicle Wings," NASA CR-1916, 1971.
3. Helenbrook, R.G., McConarty, W.A., and Anthony, F.M., "Evaluation of Active Cooling Systems for a Mach 6 Hypersonic Transport Airframe," NASA CR-1917, 1971.
4. Helenbrook, R.G., and Anthony, F.M., "Design of a Convective Cooling System for a Mach 6 Hypersonic Transport Airframe," NASA CR-1918, 1971.
5. Becker, J.V., "New Approaches to Hypersonic Aircraft," presented at the Seventh Congress of the International Council of the Aeronautical Sciences (ICAS), Rome, Italy, Sept. 1970.
6. Anthony, F.M., Dukes, W.H., and Helenbrook, R.G., "Internal Convective Cooling Systems for Hypersonic Aircraft," NASA CR-2480, 1974.
7. Ellis, D.A., Pagel, L.L., and Schaeffer, D.M., "Design and Fabrication of a Radiative Actively Cooled Honeycomb Sandwich Structural Panel for a Hypersonic Aircraft," NASA CR 2957, March 1978.
8. Dukes, W.H., et al, "Manufacturing Methods for Insulated and Cooled Double-Wall Structures," ASD Technical Report 61-7-799, Volumes I and II, May 1961.
9. Anthony, F.M., and Helenbrook, R.G., "Reusable Space Shuttle Vehicle Thermal Protection," NASA CR 123579, January 1972.
10. Heldenfels, R.R., "Structural Prospects for Hypersonic Air Vehicles," Paper No. 66-31, presented at the Fifth Congress of the International Council of the Aeronautical Sciences (ICAS), London, England, Sept. 12-16, 1966.
11. Shideler, J.E., et al, "Optimum Mass-Strength Analysis for Orthotropic Ring-Stiffened Cylinders Under Axial Compression," NASA TN D-6772, July 1972.
12. Elber, W., and Davidson, J.R., "A Material Section Method Based on Material Properties and Operating Parameters," NASA TN D-7221, April 1973.
13. Nowak, Robert J., and Kelly, H. Neale, "Actively Cooled Airframe Structures for High-Speed Flight," presented at the AIAA/ASME/SAE 17th Structures, Structural Dynamics and Materials Conference, King of Prussia, PA, May 5-7, 1976. (Also J. Aircraft, Vol. 14, No. 3, March 1977, pp. 244-250.)
14. Emero, D.H., and Spunt, L., "Wing Box Optimization Under Combined Shear and Bending," J. Aircraft Vol 3, No. 2, 1966.

15. "Metallic Materials and Elements for Aerospace Vehicle Structures," MIL-HDBK-5, Sept. 1976.
16. Kroll, W.D., "Aerodynamic Heating and Fatigue," NASA Memo 6-4-59W, June 1959.
17. Giles, G.L., and Anderson, M.S., "Effects of Eccentricities and Lateral Pressure on the Design of Stiffened Compression Panels," NASA TN D-6784, June 1972.
18. Gerard, G., and Becker, H., "Handbook of Structural Stability - Parts I Through VI," NASA TN 3781 through 3786, July 1957-1958.
19. "Glycols", F-41515A, Union Carbide Corporation, Chemical Division, New York, 1964.
20. Emerson and Cuming, Inc. - Product Bulletin 3-2-5A, "Eccobond Solder 58C," Revised November 1969.
21. Barzelay, M.E., "Range of Interface Conductance for Aircraft Joints," NASA TN D-426, May 1960.
22. Graff, W.J., "Thermal Conductance Across Metal Joints," Machine Design, September 15, 1960.
23. "Aluminum Alloy Tubing, Seamless, Drawn, Round 1.25 Mn - 0.12 Cu (3003-H14)," AMS 4067E Revised 7/1/76, Aerospace Materials Specification.
24. Batt, J.R., Jordan, S., and Gallo, A.M., "MAGIC III: An Automated General Purpose System for Structural Analysis, Volumes I, II, and III," AFFDL-TR-72-42, April 1972.
25. Kreith, Frank, "Principles of Heat Transfer," International Text Book Company, January 1966, pp 441-448.

1. Report No. NASA CR-3403	2. Government Accession No.	3. Recipient's Catalog No.	
4. Title and Subtitle DESIGN AND FABRICATION OF A STRINGER STIFFENED DISCRETE-TUBE ACTIVELY COOLED PANEL FOR A HYPERSONIC AIRCRAFT		5. Report Date February 1981	
7. Author(s) Frank M. Anthony and Robert G. Helenbrook		6. Performing Organization Code	
9. Performing Organization Name and Address Bell Aerospace Textron P.O. Box One Buffalo, N.Y. 14240		8. Performing Organization Report No. 7430-927001	
12. Sponsoring Agency Name and Address National Aeronautics and Space Administration Washington, D.C. 20546		10. Work Unit No.	
15. Supplementary Notes Langley Technical Monitor: Robert J. Nowak Assistant Technical Monitor: James C. Robinson Final Report		11. Contract or Grant No. NAS1-12806	
16. Abstract <p>This report presents the results of a program which iteratively optimized the design of a full scale 0.61 x 6.1m (2 x 20 ft) actively cooled panel for minimum panel mass. Design conditions and requirements were representative of those for a hypersonic transport. Details of the finalized panel design incorporated many design changes dictated by results from static and fatigue test specimens. A 0.61 x 1.22m (2 x 4 ft) test panel was fabricated and delivered to the Langley Research Center for assessment of the thermal and structural features of the optimized panel design. The panel concept incorporated an aluminum alloy surface panel actively cooled by a network of discrete, parallel, redundant, counterflow passages interconnected with appropriate manifolding, and assembled by adhesive bonding. The cooled skin was stiffened with a mechanically fastened conventional substructure of stringers and frames. A 40 water/60 glycol solution was the coolant.</p> <p>Structural considerations dominated in defining the minimum mass configuration, particularly structural/life requirements. Skin and stiffening elements were proportioned to maximize buckling resistance. Coolant passage characteristics were defined to limit panel operating temperature to 390K (240°F) which provided minimum equivalent thickness within practical design constraints. Based on measured weights for test panel details and subassemblies, the unit mass was 12.23 kg/m² (2.50 psf).</p> <p>Adhesive bonding permitted the use of an efficient structural alloy, 2024-T3, for the skin and substructure while a corrosion resistant alloy, 3003-H14, was used for the coolant passages. The high design heat flux 136 kW/m² (12 Btu/ft² sec) required the use of thin bondlines of high thermal conductance. Fabrication procedures were developed to permit the use of thin bondlines at critical locations despite the tolerances associated with machining and with sheet metal forming. High thermal conductance and structural strength were achieved by using alternate stripes of silver-filled epoxy paste adhesive and epoxy film adhesive.</p> <p>Low pressure leak testing, radiography, holography and infrared scanning were applied at various stages of fabrication to assess integrity and uniformity. By nondestructively inspecting selected specimens which were subsequently tested to destruction it was possible to refine inspection standards as applied to this cooled panel design.</p>		13. Type of Report and Period Covered Contractor Report	
17. Key Words (Suggested by Author(s)) Aluminum Actively Cooled Panel Counterflow Design Redundant Circuits Hypersonic Aircraft		18. Distribution Statement Unclassified - Unlimited Subject Category 39	
19. Security Classif. (of this report) Unclassified	20. Security Classif. (of this page) Unclassified	21. No. of Pages 87	22. Price A05